Analysis of post-mortem Magnetic Resonance Image data of the Human Brain for the diagnosis of Creutzfeldt-Jakob disease

Mark R Harding

A thesis submitted for the degree of Doctor of Philosophy.
The University of Edinburgh.
September 2002

Abstract

Despite its generally low annual global incidence rate, Creutzfeldt-Jakob disease (CJD) has become a subject of considerable interest in recent years. This is due to concerns that there may be a possible causitive link with Bovine Spongiform Encephalopathy and that this may forewarn of a future epidemic of CJD in Humans. Despite recent discoveries of CJD related abnormalites in lymph-node tissues, *in-vivo* diagnosis of CJD is difficult and relies on a series of clinical tests and observations to provide a probabilistic diagnosis of the disease. The confirmed diagnosis is currently only obtainable via biopsy or post-mortem histology. Medical imaging, specifically Magnetic Resonance Imaging (MRI), may offer a potential *in-vivo* diagnostic aid due to the reported presence of observable abnormalities in the MRI of CJD patients. To date research in this field has been hampered by a general lack of clinical data and the published work has been forced to consider exclusively the results of *in-vivo* MRI measurements. The National Creutzfeldt-Jakob disease Surveillance Unit in Edinburgh, U.K. has compiled a large and unique MRI dataset of post-mortem images of the Human brain from all deceased patients whose clinical presentation suggested CJD. Post-mortem confirmation of diagnosis is also held. This thesis describes the findings of an investigation to evaluate the potential of this post-mortem MRI dataset to provide diagnostically useful information in the task of assessing the CJD status of a patient. It uses image intensity analysis based tests to provide results whose performance may be compared to the accepted radiological methods of visual inspection of hard-copy data. By plotting distributions of statistical intensity metrics for specific regions of interest, known to have shown abnormalities in *in-vivo* MRI cases, the relationship between the MR image intensity for these regions and the ultimate patient diagnosis was determined. Additional work investigating methods for determining shape and intensity symmetry, which can help differentiate between disorders, is also described. Through the analysis of specific brain regions, it is shown that the MRI tests described display sensitivity to the condition of CJD. Future work is needed to investigate whether equivalent results can be produced by similar tests on *in-vivo* MRI data, when this becomes available. This could potentially offer a useful non-invasive pre-mortem test for CJD that would aid the task of clinical patient assessment.

Acknowledgements

I would like to thank the following individuals for their help and support in making this work possible.

- Dr. David Renshaw, my primary supervisor, for his continual support and advice throughout.
- Prof. James Ironside for providing support and advice on the medical implications of this study and for providing the main data used throughout this work.
- Dr. William H. Nailon for all his help above and beyond the call of duty and for sharing the already cramped corner of the CJD unit with me to provide me with an on-site base of operations when it was needed.
- Dr. Steve McLaughlin for his help and advice on statistical analysis techniques.
- Dr. Joanna Wardlaw for her help in reading MRI data and identifying regions of interest within the images.
- Prof. J.K. Best for providing access to the original data stored at the (late) City Hospital's MRI Unit.
- Annette Blane who provided useful information to permit the identification of WGH case numbers from City Hospital identifiers.
- The Computing Support Officers within this department who provided superb facilities and support throughout. Particular thanks are due to David Stewart whose help was always available, even when stressed and overworked.
- To the EPSRC for providing the financial grant that supported me and this work.
- To everyone in my research group and especially to those that shared an office with me for making the working environment as rewarding as it ultimately was. Notable mentions must go to Andy Connolly for his knowledge of dead (but) funny comedians, to Mark Glover for instilling fear in all those who might otherwise have thought to step foot in the office, to Emma Braithwaite for sage advice and the occasional friendly home-cooked

meal and to Robin Woodburn whose stories are always entertaining and whose experience and advice made a number of key decisions related to this work much simpler.

- To Alan Wilson, flatmate throughout the era of this project, whose knowledge of computers, planes and all matters related to a small Colorado mountain town helped make the hours spent not working a great deal more amusing and enjoyable.

- To my parents, Jenny and Brin, for their love, support and simply for helping me get this far through life. And, of course, for asking the most intimidating of questions; "What next Son?"

- To my sister Karen for her continual sense of humour and especially for her own unique thoughts on BSE and on the use of monkeys when testing for cross-species infectivity. Sadly, there was not time to follow up those threads of research but the memory of that discussion will last forever.

- To the rest of my family and to all my friends who assuredly suffered either occasionally or constantly as I worried about this work or exhibited other telling signs of work-related stress.

- And finally, rather more thanks than can be easily conveyed in a couple of sentences here to Gabriele Fischer for all her love, support and patience which kept me going throughout and which threatens to make a better person of me eventually. With patience. But I mentioned that already didn't I...?

Contents

List of figures

List of tables

Glossary

This glossary provides descriptions and meanings for various terms and abbreviations that appear throughout the thesis.

- **14.3.3 CSF Test** - This is a test of the Cerebrospinal Fluid (CSF) that looks for unusual (typically elevated) levels of the 14.3.3 neuronal protein.
- **Amyloid Plaque** - Fibril structures formed from peptides in numerous diseases including CJD. Typically 60-100 angstrom in width and of a variable length.
- **Astrocytes** - Large stellate-shaped cells, typically with many radiating processes.
- **Ataxia** - The inability to coordinate voluntary muscular movements; in common usage, unsteady gait.
- **Axial** - Orientation reference, typically describing a plane horizontal to the ground. (Plan view)
- **Bisymmetric** - Symmetric about an axis with both sides of the axis demonstrating the same properties.
- **Caudate Nucleus** - An upper brain structure.
- **Cerebral Cortex** - External layer of brain, principally composed of grey-matter tissues.
- **C.J.D.** - Creutzfeld-Jakob disease.
- **C.T.** - Computed Tomography.
- **Coronal** - Orientation reference, typically describing a plane vertical to the ground. (Front view)
- **Florid Plaques** - Plaques that are able to bind a staining agent such as the common bright red dye known as eosin.
- **Gliosis** - Scarring produced by astrocytes.

- **Hyperintense** - A stronger than usual response. In the case of a scan image, refers to an area of brighter than normal intensity.
- **Iatrogenic** - Refers to an illness caused by a physician or surgeon.
- **M.R.I.** - Magnetic Resonance Imaging.
- **Myoclonus** - Describes sudden, brief, jerky, shock-like, involuntary movements commonly seen during seizure.
- **Occipital Cortex** - Region of human brain primarily responsible for visual processing.
- **PrP** - Prion Protein.
- **PrP^{Sc}** - Prion Protein, Scrapie variant which is the PrP type seen in cases of Sporadic CJD.
- **Putamen** - Nucleus of the basal ganglia region of the Human mid-brain.
- **Sagittal** - Orientation reference, typically describing a plane vertical to the ground. (Side view)
- **Sporadic** - refers to the random distribution and appearance of the disease when used in conjunction with CJD.
- **Thalamus** - a structure in the Human mid-brain that receives impulses from all sensory areas except the olfactory and transmits them to the cerebrum.
- **Transmissible Causative Agents** - Any agent that can provide the mechanism by which a disorder in one specimen can pass to infect another specimen.
- **T.S.E.** - Transmissible Spongiform Encephalopathy. A family of diseases that includes Scrapie in Sheep, BSE in cattle and CJD in Humans. Transmissible implies it can be passed on from victim to victim, spongiform refers to the process of Vacuolation that commonly occurs in victims of a T.S.E. disease and encephalopathy informs that these diseases occur in and affect the function of the brain.
- **Vacuolation** - The process of creation of vacuoles.
- **Vacuoles** - Small holes in affected tissue that would not normally be present.

Chapter 1
Introduction

1.1 Theme of the thesis

The outbreak of Bovine Spongiform Encephalopathy (BSE) in the UK cattle population during the mid to late 1980s has had important consequences beyond those related directly to the agricultural community. Of perhaps greatest concern to society is the possibility of a follow on epidemic of Creutzfeldt-Jakob disease (CJD) in Humans. Apparent increases in the frequency with which this disease has been seen in the clinical environment may suggest a causality link to BSE entering the Human food-chain and this may then predict a greater increase in occurance frequency in the months and years to come.

CJD is a rare fatal transmissible illness that typically has an incidence rate of one person per million per annum. It affects the central nervous system (CNS) and is a debilitating degenerative disease. It is a particularly hard disease to diagnose due to a number of similarities the symptoms of the disease share with several other neurological disorders. The only method currently accepted for providing confirmed diagnosis of the disease is histological examination of a patient's neural tissue. In-vivo examination of neural tissue requires a neural biopsy which is both hazardous to the general health of the patient and has been shown in some cases to have negatively influenced a patient's condition following the biopsy procedure. Therefore, confirmed diagnosis is usually only possible post-mortem and this has serious implications for the patient, particularly with regard to the provision of suitable care for the patient who may be offered certain curative or comforting treatments if their condition is a disorder that is not CJD but yet is one that manifests with similar symptoms.

The quest to find acceptable pre-mortem indicators of condition for CJD is well underway and has opened up several promising avenues of investigation. Already, a carefully compiled template of clinical symptoms has been constructed allowing medical assessments of patients presenting with symptoms that might suggest CJD amongst a group of other neurological disorders to be more confidently made. Other studies into Lymph-node indicators and character-

istic Electro-encephalogram (EEG) signatures are providing more supporting means for medical personnel to make the correct and accurate diagnosis in potential CJD cases. However, at the current time, none of these alternative methods can provide an acceptable pre-mortem diagnostic test for CJD.

1.2 Motivation

A further alternative avenue of investigation that appears to promise a potential solution to the problem is Magnetic Resonance Imaging (MRI). Utilising the characteristic resonant properties of different materials when exposed to directed Radio Frequency (RF) radiation whilst located within a powerful electromagnetic field, MRI produces images that provide information on the spatial composition of those materials. Possibly due to the physical effects that CJD has on the neural and CNS tissues, MRI has been reported to demonstrate certain characteristic abnormalities in a number of CJD patients so far.

All abnormalities so far reported were observed from in-vivo MRI which suggests the potential for MRI to become a non-invasive pre-mortem diagnostic test for CJD. However, due to the small sample sizes observed it is not yet possible to ascribe any true significance to these results so far. Further tests on larger, statistically significant groups of patients will be required to properly assess the true potential of this method of investigation.

Within the U.K., any suspected case of CJD discovered in the clinical environment is reported to the National CJD Surveillance Unit (NCJDSU) which is located within the Western General Hospital of Edinburgh and is administered partly by the University of Edinburgh's Faculty of Medicine. The NCJDSU has been given the national remit to coordinate research into CJD and to monitor and report upon the state of the disorder within the United Kingdom. When a suspected case of CJD is reported to the NCJDSU the unit provides advice and guidance on how to best assess and treat that patient to provide them with the best possible care. Should the patient die and CJD is still considered as a possible cause, certain organs which include the brain are sent to the NCJDSU for testing in order to provide the confirmed diagnosis for or against CJD. Typically the entire brain is sent to the unit for testing and this allows for an MRI scan of the whole, or occasionally partial, organ to be made prior to dissection and histological examination.

As a result of its national status and its practice of capturing MRI scans of the organs before the brains are tested, the NCJDSU has accumulated a significantly large archive of post-mortem MRI of the Human brain captured from a sample of patients, all of whom were at least suspected to be suffering CJD even if the later diagnosis finally disproved this. Therefore, this archive offers the possibility to make a meaningful and significant investigation into the potential for post-mortem MRI to provide characteristic indication of CJD in Human patients and therefore to act as a diagnostic test for this condition. Since all existing observations regarding MRI have been limited to in-vivo MRI, such a study as is presented here offers novel and interesting results which should be of interest to the community at large.

1.3 Research Aims

Reported observations of abnormalities in CJD related MRI have been made by visual inspection of the hard-copy images by trained radiologists in a clinical environment. Such a technique is difficult to quantify and therefore this study proposes to examine the digital copies of similar images from the post-mortem MRI archive provided by the NCJDSU using image processing and analysis techniques that best reflect the decisions made when visual inspection is used. By testing a large sample of comparable images whose diagnosis has not yet been revealed, it will be possible to determine whether or not such images demonstrate any features that are characteristic of CJD to a statistically significant degree.

The results of these findings will provide valuable insight into the potential for using MRI as an alternative post-mortem indicator of condition and, if these findings do find MRI to be so indicative, it may then provide motivation for further study into the use of in-vivo MRI for determining and confirming diagnosis for CJD. If these findings do not show MRI to be an indicator of condition, it will have provided a valuable guide to other researchers in the field for directing future efforts and work.

1.4 Thesis organisation

The remaining chapters of this thesis are organised as follows:

Chapter 2 presents the medical background to the issues involved in this work which includes an explanation of the key features of the disease family of which CJD is a member as well as an in-depth view of CJD itself and the various diagnostic tests that are currently being employed in order to attempt to assess suspected patients. The process of medical imaging through the use of Magnetic Resonance imaging is described and the potential relevance of MRI to CJD is communicated.

Chapter 3 presents the image processing background to the techniques that have been employed in this work and describes the advantages such methods offer. The preparation of the MRI datasets is described and an account is made of how the data was converted from the original in-house hospital format to a format suitable for working with in this project.

Chapter 4 describes the tests that were performed on the data in the attempt to assess the ability of the data to indicate the CJD status of a patient and the results of these tests are presented along with a discussion of the value of the results and their implications.

Chapter 5 introduces several additional tests that were performed on the MRI data in order to investigate other properties of the data to help in determining other clinical assessments which may still have a relevence to CJD and these results are analysed and discussed.

Chapter 6 reports the conclusions of this work and summarises the findings that have been made in the course of the investigations described here. Future routes of further investigation are suggested and the success of this work in achieving its aims is stated.

Chapter 2
Medical Background

2.1 Introduction

Creutzfeldt-Jakob disease (CJD) is a Human specific disease and it is also a member of a family of related diseases called Transmissible Spongiform Encephalopathies (TSEs). The diseases in this family affect a diverse range of species including sheep, cattle, ungulates, felines and many others.

The various members of the TSE family are characterised by their unique brain pathologies. The transmission agents responsible for inter-species infection and cross-species infection are not yet fully understood although there is a growing consensus in the scientific community that TSEs may occur due to an accumulation of an abberant protein in the cells of the central nervous system.

This chapter discusses Creutzfeldt-Jakob disease, describing its background and focussing on important issues including the different strains of CJD that are currently known and the difficulty CJD presents for pre-mortem diagnosis which is a significant motivating factor in this work.

2.2 Creutzfeldt-Jakob disease

Creutzfeldt-Jakob disease (CJD) is a rare, fatal degenerative disorder of the central nervous system that is specific to Humans and occurs with a sporadic frequency of approximately one case per million of the global population [1]. It was first reported in 1920 by H.G. Creutzfeldt [2] and then soon after in 1921 by A. Jakob [3]. It was later discovered that the case reported by Creutzfeldt in 1920 did not actually involve CJD as it is described today nevertheless the disease was named after these two initial publishers.

There are three major categories of CJD that are predominantly defined by the route of transmission although subtle differences in the symptoms of each type can be perceived.

- **Sporadic CJD** - appears even in the absence of the victim being exposed to any known risk factors. This is the most commonly seen type of CJD accounting for approximately 85% of all cases worldwide.
- **Familial CJD** - is the inherited form of the disease and it occurs in victims who normally have a family history of the condition and/or test positively for a genetic mutation associated with familial CJD. Familial CJD accounts for approximately 10% of cases of CJD worldwide.
- **Iatrogenic CJD** - or *acquired* CJD appears after the victim has been exposed to a known risk or hazard which includes exposure to infected brain or central nervous system tissues during medical procedures and/or operations. This type of CJD is extremely rare and only accounts for around 1% of all cases that occur.

Victims of CJD exhibit common symptoms and the most characteristic of these is rapid and progressive dementia. Initial signs include personality variations, impaired memory function and judgement and impaired vision. Other symptoms may include depression, imsomnia and unusual sensations. As the illness progresses, the severity of the dementia becomes more extreme and the patient normally becomes ataxic, often exhibiting myoclonus and further sensory disruption including complete blindness. The patient will most commonly end up in a coma unable to move or speak and may fall prey to pneumonia or other infections which can lead to death [4]. The onset of symptoms for CJD typically occur in people of age 50-70 years and the duration after onset is usually less than 12 months. The incubation time for CJD is not known precisely but it is thought to be long with periods as long as 35-40 years in some cases of Familial CJD and as short as 18 months for cases of Iatrogenic CJD.

There is no evidence to suggest that CJD is a contagious disease and it cannot be transmitted through the air or by casual contact. Direct contact with tissue from the brain or with cerebro-spinal fluid (CSF) should be avoided however because there is a high transmission risk associated with handling these materials.

CJD was initially shown to be a transmissible spongiform encephalopathy in 1966 when it

was transmitted to a group of chimpanzees through innoculation [5]. Sporadic CJD has also been spread through the use of improperly disinfected surgical instruments and through certain transplant operations, especially Cornea transplants [6]. Other Iatrogenic transmissions have occured following a dura-mater graft, from the use of insufficiently-disinfected silver electrodes and from the use of infected pituitary human growth hormone.

The actual mechanism through which CJD is transmitted is not fully known although it is believed to be dependent upon an abberant form of the commonly occuring Prion Protein (PrP^{c}) known as the *Scrapie Isoform* of the Prion Protein (PrP^{Sc}). Scrapie, along with Bovine Spongiform Encephalopathy (BSE), is a member of the same family of diseases as CJD which are referred to as Transmissible Spongiform Encephalopathies (TSEs). TSEs are fatal diseases that share certain common characteristics which include:

- Long incubation periods ranging from several months to many years.
- Rapid and progressive dementia upon clinical onset.
- Common pathological identifiers, brain cell vacuolation, neuronal loss and gliosis.
- Transmissible causative agents.

2.3 Variant CJD

In March 1996 a new variant form of CJD (vCJD) was reported [7] which showed distinctive pathological features in its victims, the most recognisable of these being florid plaques visible in the histology of certain regions of the brain [8]. With the BSE epidemic that was also present in the UK cattle population at that time much speculation was made of the existence of a connection between the increased presence of BSE and the emergence of vCJD. The most convincing evidence to link BSE to vCJD came from the transmission studies where laboratory mice were inoculated with neural tissue collected from victims of vCJD. In this study, it was noted that after inoculation the mice suffered the same pattern of TSE disease characteristics that were formerly believed to be unique to those produced when the mice were inoculated with BSE infected neural tissue from cattle [9].

The duration after onset until death of vCJD is often comparatively prolonged compared to

sporadic CJD and onset appears to occur at a much younger age. The unusual formation of plaques mentioned before in cases of vCJD demonstrate widespread distribution throughout the cerebral cortex, particularly in the occipital cortex. Earlier studies have suggested that similar plaques can be detected in the lymphoid tissues of Scrapie infected sheep before the clinical onset of the disease occurred [10]. If the link between vCJD and BSE is later confirmed then the possibility of developing a reliable premortem test for vCJD through the examination of human lymphoid tissues is quite realistic. The most pronounced spongiform changes occur in the basal ganglia and the thalamus with notable astrocytosis of the thalamus also present.

2.4 Diagnosis of CJD and vCJD

The attending medical examiner has numerous sources of information to draw upon in order to affect the diagnosis of a patient who presents with symptoms that possibly suggest CJD. Firstly, there are the symptoms themselves which encompass the physical effects the disorder has had on the patient plus the more subtle symptoms that manifest themselves as behavioural changes or altered mental conditions. Next, there are the results of any relevant clinical tests and in cases involoving neurological disorders and potentially CJD, these include Eletroencephalogram Tests, 14.3.3 Cerebro-spinal Fluid Tests and the medical imaging based tests such as Computed Tomography (CT) and Magnetic Resonance Imaging (MRI) scans. The final source of information is the results of any tests or examinations made post-mortem via autopsy.

Patients with CJD usually present initially with neurological problems such as changes in behaviour and attitude, memory problems, coordination difficulties and sensory abnormalities. As the illness progresses, dementia becomes rapidly severe and the patient often suffers myoclonus (involuntary body movements), ataxia (walking difficulties) and pronounced sensory disruption that can often include blindness. The final stage is usually coma combined with another complication such as infection or pneumonia.

Currently, there exists no single diagnostic clinical test for CJD. Although CJD is itself a fatal condition, if a patient presents with CJD-like symptoms yet actually has a different disorder then it may be possible to treat that other condition and even cure the patient. If the patient does have CJD however, then the clinician is likely to prescribe treatments designed to ease the discomfort of the patient through their decline.

2.4.1 Neuropathological diagnosis of CJD

The only way to confirm a diagnosis of CJD is by examining the neural tissue to look for the characteristic markers of the disease such as the more common 'Scrapie' variant of the Prion Protein, PrP^{Sc}. This tissue can either be harvested by biopsy whilst the patient is alive or through autopsy after death. The brain biopsy is usually discouraged because of the risks to the patient. Additionally, the section of brain sampled by the biopsy may not be infected even though other parts of the patient's brain are due to the patchy infection pattern often seen in the frontal cortex.

Whether the neural tissue is examined *in-vivo* via biopsy or post-mortem, the characteristic markers which define the disease are effectively the same. There are four key features that TSEs exhibit:

1. **Spongiform change** - where vacuoles form in the neural tissue and give the affected areas a 'sponge-like' appearance. In CJD, the areas that show the greatest spongiform change are usually the Basal Ganglia and the Thalamus. Figure 2.1.

2. **Astrocytosis** - where large numbers of astrocytes are seen to accumulate within regions of the brain. Figure 2.2.

3. **Neuronal Loss** - where the individual neurons die off or become smaller. In TSE diseases, neuronal loss is often quite severe and can be clearly seen in affected tissues.

4. **Amyloid Plaque Formation** - where PrP^{Sc} deposits are seen within regions of the brain. The plaque formations of vCJD are quite different from those of sporadic CJD making it easy to differentiate the two strains of the disease. Plaques caused by vCJD typically have a dense eosinphillic centre (eosin is a bright red dye that is often used to stain tissue samples prior to viewing under a microscope) and a pale periphery and are often surrounded by a zone of spongiform change. Such characteristics are not found in the plaques caused by Sporadic CJD. Figures 2.3 and 2.4.

Spongiform change is the most consistent abnormality in relation to Human TSEs and the changes can occur in any area or layer of the cerebral cortex. Also, in cases where neuronal loss is severe, there can be a spongiform-like change as a result of the neuronal loss which further amplifies the effect.

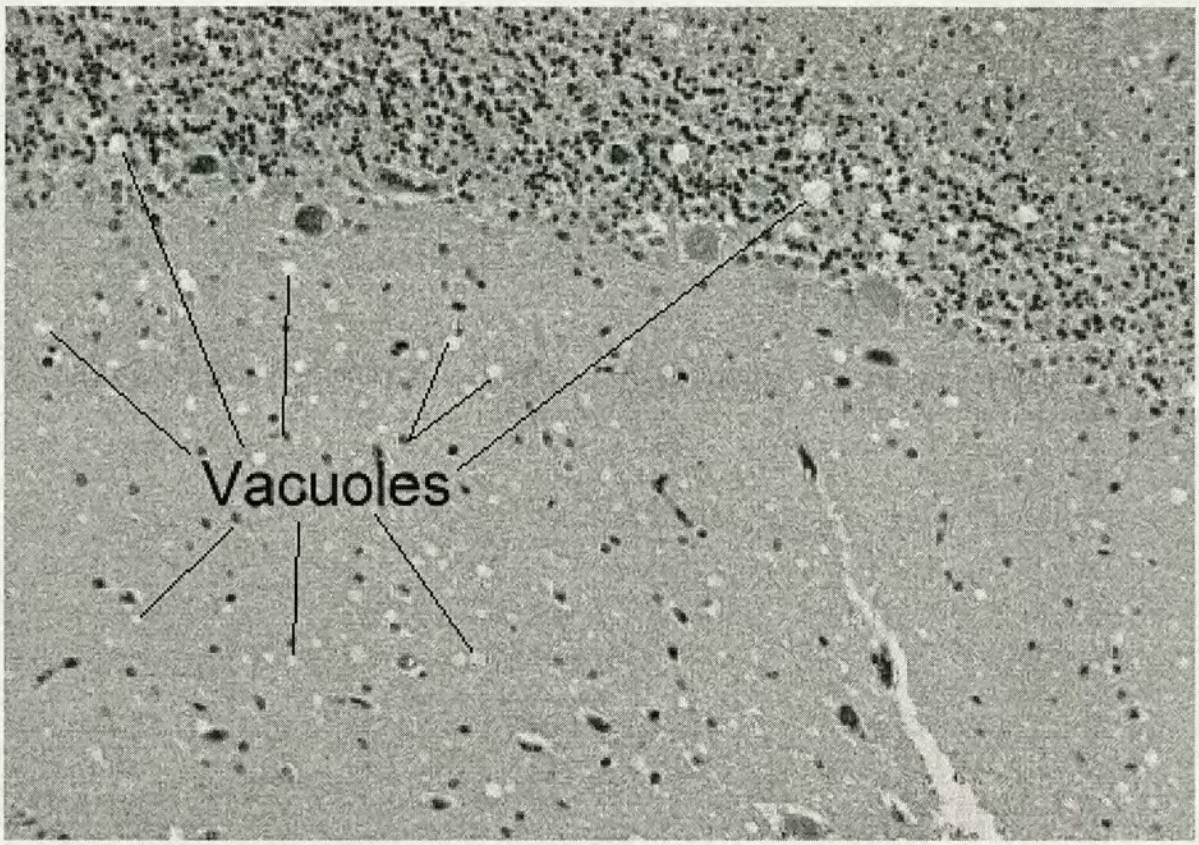

Figure 2.1: Spongiform Change: *CJD has been observed to caused small holes, known as vacuoles, to appear in affected neural tissues. This process is commonly referred to as Spongiform Change.*

The occurance of plaques is related to the Prion Protein (PrP) Genotype which is affected by the codon 129 polymorphism. At codon 129 in Humans, there is a polymorphism between Methionine (M) and Valine (V). At this codon point, an individual can have one of the following combination-pairs of Methionine and Valine; either M-M, M-V (which is equivalent to V-M and therefore always simply referred to as M-V) or V-V. Plaques appear to be seen more often in patients with either M-V or V-V combinations at this codon point than for patients with the M-M combination.

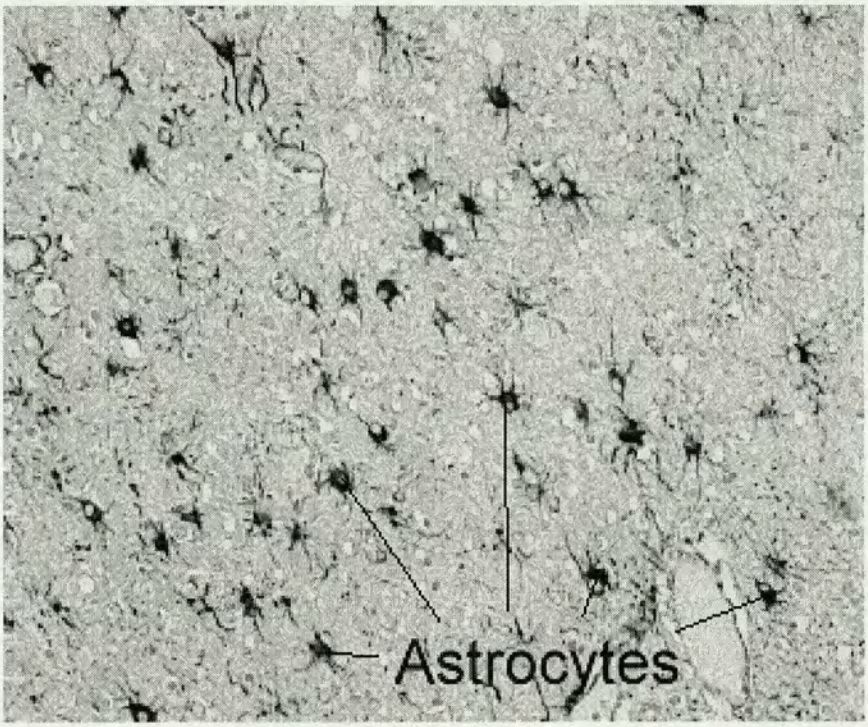

Figure 2.2: Astrocytosis: *Illustration of the enlarged astrocytes that occur through the process of astrocytosis in typical cases of CJD. The astrocytes, visible here as the dark objects above, appear larger than they would in a healthy subject.*

2.4.2 Clinical diagnosis of CJD

There are certain clinical features that can guide the clinician to a diagnosis of CJD and one of the most indicative of these is the Electroencephalogram (EEG) test. The EEG test involves inserting silver electrodes below the scalp of the patient in order to measure the electrical activity of the brain. In about 60% of cases of CJD a charateristic waveform commonly described as a periodic tri-phasic sharp wave complex is seen and this is illustrated in Figure 2.5.

Abnormal EEG readings such as these are not considered diagnostic of the disease although they are a characteristic feature of CJD. Also note that the EEG test has not been seen to produce similarly characteristic results in patients with vCJD.

Another test, called the 14.3.3 CSF test, involves taking a sample of the cerebral spinal fluid (CSF) [1] and then measuring the concentration of the 14.3.3 protein within the sample. Some

[1]The CSF sample is usually taken by performing a *lumbar punch* which can cause additional discomfort and stress to the patient.

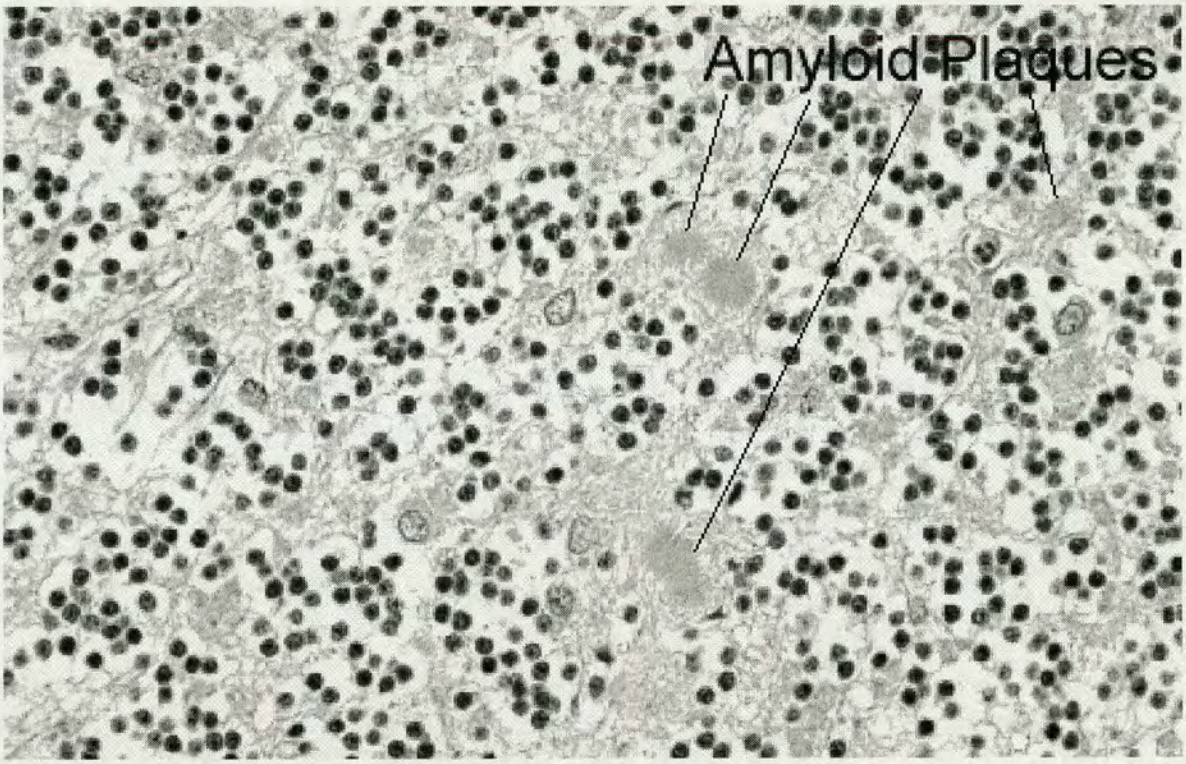

Figure 2.3: Amyloid Plaques: *Example of the formation of amyloid plaques in the cerebellum as seen as a result of CJD. Such plaques would not normally be seen in a healthy patient.*

cases of CJD have demonstrated increased 14.3.3 levels in the CSF and this again offers a charateristic feature, but not a diagnostic test, for CJD.

All of the tests mentioned so far are invasive and can therefore cause stress and discomfort to the patient. Typically, a clinical assessment is made by aggregating many different observations of the patient together. These observations include the results of any tests performed plus the presentation symptoms such as dementia, myoclonus, ataxia and any other relevant feature. Based on a criteria of combined factors, patients are normally diagnosed as either being 'probable', 'possible' or 'not' CJD patients. Upon death, the final diagnosis is made from the results of the pathology tests.

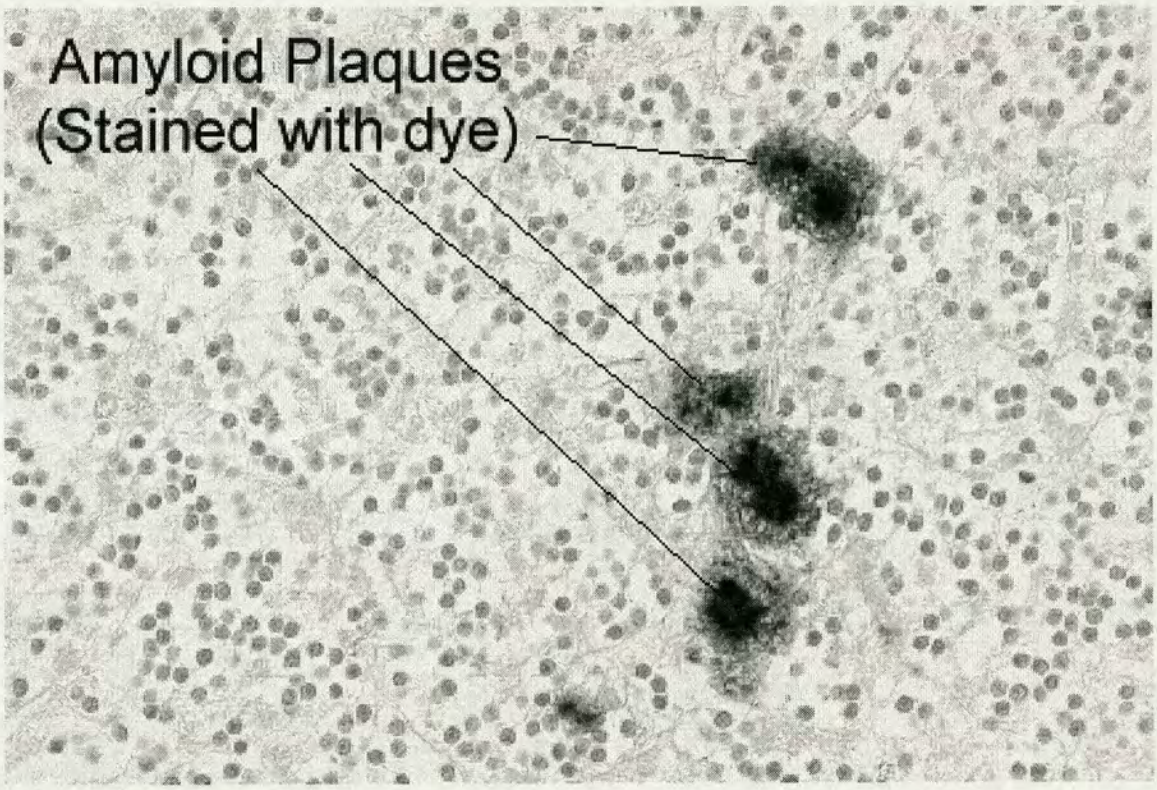

Figure 2.4: Amyloid Plaques: *Example of how staining the PrP causes amyloid plaques to become visible on the tissue samples. This makes the viewing of the plaques easier under a microscope and can also aid automated image processing tasks.*

2.5 Medical Imaging

Ideally, it would be possible to diagnose the patient's condition using a single, simple, reliable non-invasive test. Currently there is no such test. However, the field of medical imaging offers some potential avenues of investigation through both Computed Tomography Imaging and Magnetic Resonance Imaging. Both of these imaging systems can produce complex detailed information on the internal state of an object by utilising X-Rays or radio-frequency radiation and using a computer to interpret the transmitted/radiated output signals to produce an image of the object internals.

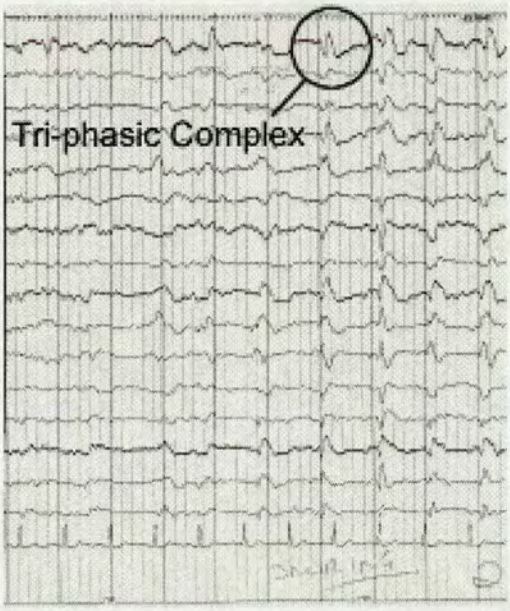

Figure 2.5: Clinical Tests - EEG: *Output of an EEG test exhibiting the characteristic generalised tri-phasic periodic sharp wave complex which can be indicative of CJD. The three phases are difficult to see clearly in this figure but one of the clearest examples of the tri-phasic complex is highlighted above.*

2.5.1 Computed Tomography Imaging

Computed Tomography (CT) Imaging is based upon the same principal as the more commonly known X-Ray imaging which is commonly used to assess breaks and fractures in bones and other hard tissues. Basically, X-Rays are passed through the body and are either absorbed or attenuated by the different tissue types within the body. This creates a profile of individual beams which are registered on X-Ray sensitive film creating an image. In the case of CT, the X-Ray source is rotated around the patient and in place of X-Ray sensitive film, a curved detector measures the profile for each axis. Figure 2.6 illustrates the basic setup used in CT Imaging.

The X-Ray source rotates around the patient and for each 360^o rotation, approximately 1000 profiles are sampled. Each of these profiles are subdivided into about 700 channels which feed into the controlling computer that then back-projects to create a single two-dimensional 'slice' image. By collimating the X-Ray beam, using lead shutters in front of the source and detector, the slice thickness is controlled and is normally set to lie within the range of 1-10mm.

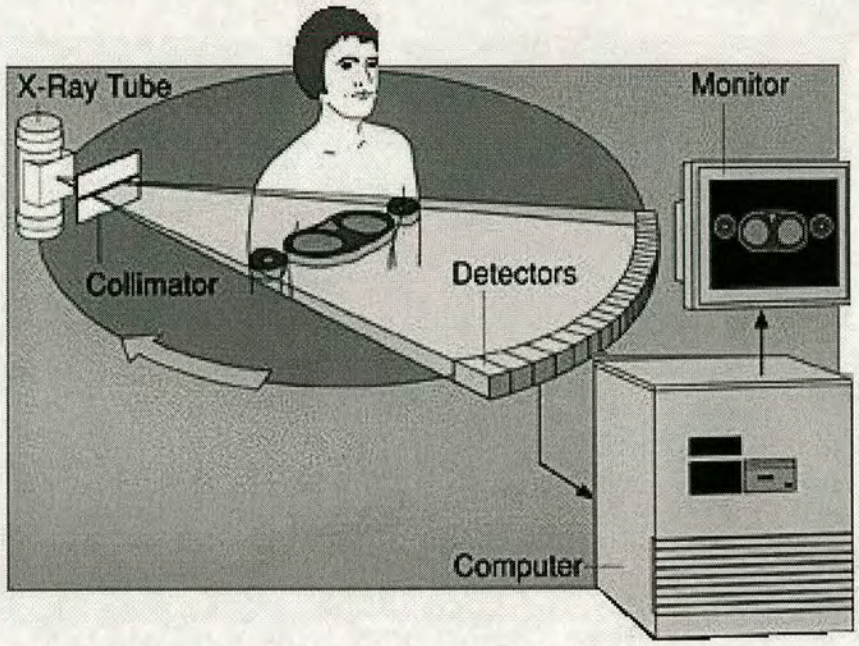

Figure 2.6: *Relationship of X-Ray source, patient and X-Ray detector used in CT Imaging.*

Although CT Imaging is incredibly useful in many applications, it has not been shown to be a particularly sensitive imaging technique for CJD and studies comparing Magnetic Resonance Imaging (MRI) and CT Imaging in CJD have favoured MRI as the more useful test in each case[11–13]. Such results are not surprising because X-Ray imaging is suited to the imaging of hard tissues such as bones, fiberous and cancerous masses. Since the brain is composed of soft tissue, X-Ray imaging may only be expected to be of significant use if it were expected that CJD would cause a build-up of hard tissue structures within the brain and to date no such observations for CJD have been made.

2.5.2 Magnetic Resonance Imaging

Magnetic Resonance Imaging (MRI) offers several benefits over Computed Tomography Imaging. CT uses ionising radiation to scan the patient which can be harmful if the patient's exposure is not controlled. Also, CT is bound by the physical limitations of the device which means that it can only produce images in the plane of the scanner; either axial or semi-coronal.

Figure 2.7: *A typical MRI showing a sagittal image of the Human head.*

By contrast MRI utilises the effectively harmless phenomena between the hydrogen nucleus and electromagnetic radio-frequency radiation, in the presence of a strong magnetic field, to scan the patient and reconstruct image slices not only from the three major planes (axial, sagittal and coronal) but also oblique slice images too. Figure 2.8 shows a patient being prepared to enter into a full size MR scanner prior to imaging.

The technique of MRI relies on the properties of the magnetic dipole moment inherent in many nuclei and parallel to their natural spin axis. Although typically random in orientation, in the presence of a static magnetic field these moments will align with the orientation of the applied field to produce a macroscopic nuclear magnetisation. In this situation, if the subject being magnetised were then exposed to radio-frequency electromagnetic radiation (EM) of a specific frequency known as the *Lamor* frequency (equation 2.1) then the nuclei experience a restoring torque that forces the spins of the nuclei to precess around the axis of the magnetic field.

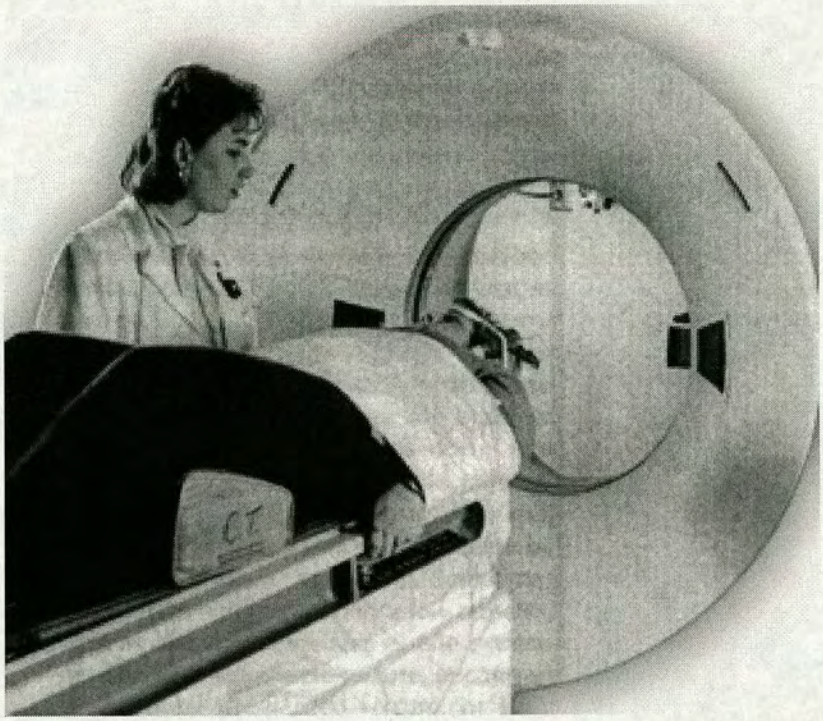

Figure 2.8: *A patient being prepared to enter a typical full-size MRI scanner prior to being imaged.*

$$\omega_L = \gamma B_0 \tag{2.1}$$

Where:

ω_L is the *Lamor* frequency.

γ is the magnetogyric ratio of the nuclei.

B_0 is the strength of the static magnetic field.

The precession of the nuclei is governed by the magnetogyric ratio which is a constant dependent upon the nucleus. When the applied EM radiation is removed the nuclei revert to precessing around the field axis and in doing so they emit a signal themselves. This return signal is called the *spin echo* and the phenomena through which it is emitted is called *resonance*. It is directly related to the Lamor frequency which is a function of the nuclei themselves.

If an additional small transverse magnetic field (B_1) is applied to the nuclei, creating a magnetic field gradient, then the resonant Lamor frequency of each nuclei will be slightly shifted which then allows spatial information to be determined from the spin echo return signal for each nucleus. By switching B_1 on for a short time of set length, the magnetisation of the nuclei will precess through an angle of 90^o into the transverse plane.

If the transverse field B_1 is then removed, the magnetisation of the nuclei will return to precessing around the static field B_0 and the rate at which it does so is governed by the first magnetic relaxation time T_1 which is also variously called the *longtitudinal*, the *thermal* or the *spin-lattice* relaxation time. As this occurs an electric current known as *Free Induction Decay* (FID) signal, is induced in the detection coil of the MRI scanner. The time for the magnetisation to completely return to precessing around the static field B_0 is governed by the characteristic relaxation time $T2$ which describes the rate at which the initially coherent nuclei dephase in relation to each other. Such dephasing is the result of small inhomogeneities in the magnetic field which are experienced by the individual nuclei depending upon their spatial location. Dephasing is also caused by the dipolar fields that occur between neighbouring nuclei. The dephasing caused by the field inhomogeneities is coherent in nature where as the dephasing caused by the dipolar fields is incoherent in nature and this difference makes it possible to separate the two dephasing contributions.

If a second radio-frequency pulse is applied to the nuclei then the magnetisation orientation is inverted by 180^o. Following this, the coherent dephasing effect caused by field inhomogeneities is cancelled. However, the dipolar field dephasing effect continues at the same rate as before. Therefore, although the field inhomogeneities are cancelled out, it is not possible for the field to completely rephase after each subsequent 180^0 pulse and the echo train produced as a result of these continued pulses will decay exponentially with time constant T_2.

Thus, by implementing a magnetic field gradient to alter the resonant frequencies of the nuclei within a subject being scanned, the resonant frequency measurement becomes a direct probe of its location and the amplitude of the returned spin-echo signal provides a measurement of the local density of atoms containing the specified nucleus in that region. If three orthogonal field gradients are applied simultaneously then a 3D image of the subject can be produced.

By analysing various quantities such as the value of the time constants T_1 or T_2 the images produced can be weighted to visualise different characteristics of the subject. For example, the T_1 time constant reflects the relationship between a molecule's natural vibrational motions and the resonant Lamor frequency of that molecule. When both are similar then T_1 relaxation is efficient and occurs rapidly. The water molecule (H_2O) is a small molecule and moves too rapidly to allow efficient T_1 relaxation to occur and protein molecules are generally larger and move too slowly to allow efficient T_1 relaxation to occur. However, a typical liquid-form cholesterol molecule moves at a similar vibration frequency to those frequencies used in MRI and efficient T_1 relaxation therefore occurs. As a result, on a T_1 weighted MR image areas containing mostly water molecules or solid-form cholesterol molecules appear dark whilst areas containing high densities of liquid-form cholesterol molecules appear bright.

In contrast, paramagnetic substances with a high magnetic susceptibility quickly lose conherence and therefore have a short T_2 relaxation time. Substances with such susceptibility are those with high proton densities, such as water (H_2O) and on a T_2 weighted MR image such substances often appear brighter than the background therefore aqueous regions are often best viewed on T_2 weighted images than on T_1 weighted images. Figure 2.9 illustrates the basic differences in character between T_1 and T_2 weighted MR images.

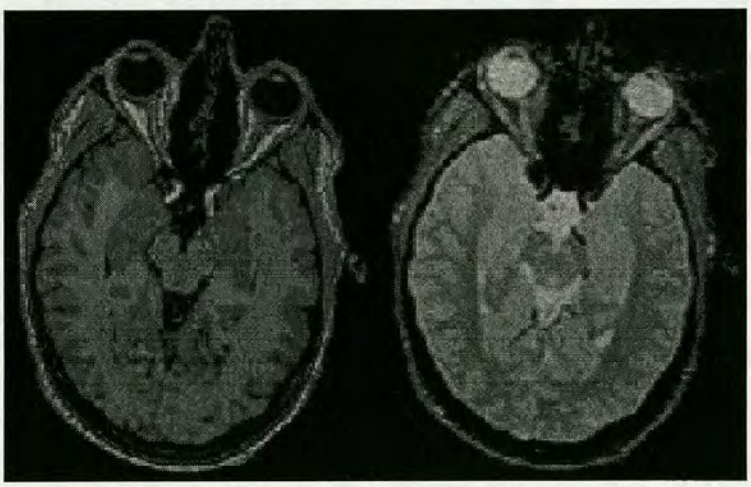

Figure 2.9: *Comparative eye-level axial MRI T_1 (left) and T_2 (right) scans of the Human head demonstrating the different characteristics highlighted by each imaging modality.*

To summarise, when the T_1 relaxation time is short and both the mobile proton density (PD) and the T_2 relaxtion time are high then the spin-echo MR signal received is the greatest. If the

T_1 relaxation time is long and the PD is small then the spin-echo signal is much weaker [14].

2.6 Using MRI to detect CJD

When a patient displays abnormal neurological symptoms and the clinician is attempting to make a diagnosis, an MRI of the patient's brain is often taken because it has proven to be a useful tool in revealing various disorders ranging from Alzheimer's disease to stroke to Cerebrovascular disease[15]. Therefore, as MRI became more widely available to clinicians as a diagnostic tool for use in the assessment of neurological disorders it naturally became used more often when assessing patients whose ultimate diagnosis proved to be CJD.

Some of the earliest findings from using MRI to assess CJD patients reported the discovery of bilateral signal abnormalities visible in the Basal Ganglia region of the brain when viewing proton density (PD) and T_2 weighted MRI [16]. Specifically, these signal abnormalities were bisymmetric hyperintense signal responses from regions within the Basal Ganglia including the caudate nucleus, the putamen and the thalamus. In the following months and years these findings were generally supported by further similar findings [17–22]. There was some variation in the hyperintense abnormalities reported by different clinicians. Most reports described bilaterally symmetric hyperintensities but occasionally this varied with some investigations reporting asymmetric findings [23, 24] or unusual hyperintensities [25]. The general conclusions from the majority of these reports suggested that, although not diagnostic in its own right and that the absence of such abnormalities did not rule out a diagnosis of CJD, seeing such abnormalities in the appropriate clinical setting may be a specific finding of CJD or may otherwise help to differentiate CJD from other disorders [26].

Occasional investigations did report findings that opposed the growing mass of opinion [11] but in general the limitations of the equipment used, such as low field strength MRI scanners, and the possibility that the genetic variations in the subtype of CJD being diagnosed may cause different findings for Iatrogenic and Sporadic CJD were usually ascribed as a possible cause. This was a rational explanation of the findings and represented the most accepted understanding of the field although the major limitation to all the studies performed was the lack of quantitative results. CJD is classified as a rare disease with respect to the global population and therefore the most difficult problem to overcome was that of making intelligent conclusions based upon the very limited amount of data available.

The first really supportive results for supporting the MRI abnormalities in CJD hypothesis came from the work published by Finkenstaedt [27] in 1996 where the MR findings from 29 prospective CJD patients was discussed. From the 29 patients whose MRI were examined, 23 patients (79%) showed the characteristic signal abnormalities previously mentioned in the earlier works for T_2 weighted MR images. No unusual signal changes were recorded for the equivalent T_1 weighted MRI and additional findings were discussed including the notable volume loss in patients whose illness duration was greater than four months.

From all of the results discussed, the common theme is the hyperintense signal abnormality visible in the T_2 MR image. As mentioned before, the T_2 MRI demonstrates proton-dense substances with higher intensities such as areas containing plenty of fluids. The areas on the MRI which produce an abnormally high signal response correspond to those areas which most often appear to be worst affected by the pathological effects of CJD which are principally spongiform change and cell gliosis. Although no supporting work has yet proved the case, the most likely explanation for the hyperintense signal response is that the holes left in the brain by the spongiform change have filled with fluid, which will likely be proton-rich due to the high water content, and that is what is visible as the comparatively bright region on the MRI.

2.7 A unique post-mortem MRI dataset

Since its creation in 1994, the National CJD Surveillance Unit (CJDSU) in the United Kingdom has been compiling a dataset of post-mortem Magnetic Resonance Images of the Human brain taken from deceased patients whose clinical presentation was suggestive of CJD. Upon death the patient's brain is removed and fixed in a solution of formalin over a period of several weeks to allow the brain to be properly preserved for future study.

Through this process the structure and shape of the brain are altered from its *in-vivo* state since immersion in the formalin solution will effect chemical changes to occur throughout the brain. In addition, the removal of the brain from the supporting structure of the patient's skull causes some physical deformation of the brain to occur.

The full implications of the chemical changes that occur in the brain as a result of fixation

are not completely understood and it is important to recognise early on that the results of tests performed on fixed post-mortem brains may yield different results to those performed on an *in-vivo* brain.

The amount of physical deformation that the brain will undergo can be related to a number of factors that vary from patient to patient. Such deformations are a product of handling the brain outside of the supportive skull structures and are an unavoidable factor. Careful handling may help minimise these deformations but is unlikely that it will be possible to erradicate them this way. There are also other contributing factors that may cause further deformation to occur. For example, if a patient had suffered significant atrophy of the brain prior to death then the internal tissues of the brain would be able to offer less support once the brain was removed from the skull and therefore more deformation would be likely to occur as a result.

These factors are important to consider because they have direct relevance to any potential tests that one may wish to perform upon the post-mortem brain and how the results of any such tests may be related to the pre-mortem brain if such extrapolations are at all possible.

Once the brain has been properly fixed it is then sent to be scanned in an MRI scanner before it is passed on to a neuropathologist for dissection and histological examination. This is a required action in the case of CJD where post-mortem histological assessment is currently the only accepted method for reaching a confirmed diagnosis of CJD.

In order to scan a brain, the brain is placed in a support vessel containing Formalin which itself is then placed within the MRI scanner. When scanning a live patient the scanning time has to be optimised to minimise the effects of patient motion which may result in blurring in the images. Such motion includes both the gross physical movements of the patient and the more subtle motions caused by other factors such as the flow of blood through the vessels of the patient. Therefore, the scanning time for a live patient will typically be measured in minutes. However, the potential for such motion artefacts when scanning post-mortem brains has effectively been removed and it was possible therefore to scan these brains for much longer. In this case, all brains were scanned for approximately one hour. This allowed better focus and resolution in the output images to be achieved because the signals produced by the brain in response to the scanner environment could be averaged over a greater length of time.

For the brains scanned by the CJDSU, two modalities of MRI data were recorded for each scanned brain; T2 and Proton Density (PD). Therefore, the gross dataset compiled by the CJDSU comprises roughly six years worth of PD and T2 MRI scans of the post-mortem brains of potential CJD victims. It is important to emphasise here that due to the requirements of following standard research procedures for medically invested research, the exact diagnoses of the individual patients was not revealed along with the data such that all tests performed throughout the course of this investigation may be done in a blinded and therefore unbiased manner.

For the first five years of the CJDSU's existence, all MRI scans were performed on a 1.5T Siemens scanner located in the City Hospital of Edinburgh. However, due to the closure of this hospital at the end of 1998, the scans made since that date were made on an Elscint 2T scanner located in the Western General Hospital of Edinburgh.

Although each MRI scanner works from the same basic principals, slight differences in the individual specifications, geographical locations and environments can introduce small differences which ultimately mean that it is not possible to directly compare the images of one scanner with those of another. In certain circumstances, when 'phantom [2]' images are made on both scanners then it is possible to make adjustments to allow the images of one scanner to be compared with those of another. However, in the present research, no 'phantom' images were made and therefore the point at which the scanning was switched from the original scanner to the newer scanner provides a natural and necessary break of the overall dataset into two distinct subsets of data. In fact, two separate collections of data from each scanner were made and that provided the opportunity to make another natural split of each 'scanner' subset into two further subsets for convenience when testing later. Therefore, the 'gross dataset' can be considered to be comprised of the following four subsets:

Dataset 1 = 85 patients scanned on **Scanner 1***
Dataset 2 = 15 patients scanned on **Scanner 1***
Dataset 3 = 19 patients scanned on **Scanner 2***
Dataset 4 = 11 patients scanned on **Scanner 2***

[2]Phantom images are images created by scanning when no objects are placed within the scanner, therefore providing a report of the scanner's unique characteristics.

*Where **Scanner 1** refers to the original 1.5T Scanner located in the City Hospital of Edinburgh and **Scanner 2** refers to the newer 2T scanner located in the Western General Hospital of Edinburgh. The scanning protocols were consistent for all four datasets and the separation of data from the same scanner into multiple datasets merely represents the fact that two collections of data were made from each scanner on dates several months apart. Later on, when the testing of these datasets is discussed, datasets 1 and 2, representing all data from Scanner 1, will be amalgamated into a single dataset to provide the largest possible population for testing. A similar amalgamation will also be performed for datasets 3 and 4 which represents all data from Scanner 2.

Since datasets 1 and 2 were produced on a common scanner it would be possible to either consider them separately for testing and then compare the results or alternatively to integrate them together into one larger dataset and test that instead. The same possibilities are true for datasets 3 and 4. Datasets 1 and 2 may not be directly compared or integrated with datasets 3 and 4 however since they were produced by different scanners.

2.8 Summary

We have seen in this chapter that CJD is part of a family of related diseases known as Transmissible Spongiform Encephalopathies (TSEs) and that although not fully understood, the transmission mechanism for these diseases is most likely to be dependent upon an aberrant protein called the prion protein (PrP^{Sc}). We have seen that these TSEs share common characteristics and that they are all fatal after onset although with very long incubation times it may be possible to carry these diseases throughout life without experiencing the onset of symptoms.

The diagnosis of CJD has been shown to be a difficult task and the only currently accepted method to provide definative conclusion is either biopsy or autopsy. Despite this, Medical Imaging techniques have been introduced and the potential of Magnetic Resonance Imaging for use in a diagnostic capacity has been reported. Although the current body of work in this field has only reported on findings for *in-vivo* patients, it is hoped that there is enough promise in these results to make the application of MRI to post-mortem brains an acceptable approach to the task in hand.

Chapter 3
Image Processing Background

3.1 Introduction

MRI scanners are used to scan three dimensional objects and they therefore produce three dimensional volumetric data sets as output. These datasets are then typically transformed into sequences of two dimensional images which are then stored and can be printed onto photographic plates to provide hardcopy material for use by radiologists for the purposes of analysing the data. Radiological analysis of this data in the clinical environment is effectively limited to visual inspection of the hardcopy images. This chapter will describe non-visual statistical techniques that may be applied to such images to provide an alternative method of analysis for these images.

The first part of this chapter describes how the MRI data used in this study was acquired and then follows on to describe how the MRI data was prepared for this study. The next part of the chapter details the segmentation procedures adopted throughout for selecting Regions Of Interest (ROIs) from an image for later analysis and then discusses the statistical analysis methods that are to be used to analyse the ROIs. The description of a simple test that was designed to test the robustness and sensitivity of the chosen method of segmentation follows and the chapter then closes with a report of the results of running that test on one of the MRI datasets followed by a brief chapter summary.

3.2 Acquisition of the MRI Scan Data.

The MRI scan data used within this study was sourced from two different suppliers, although both sets were generated for and on behalf of the National Creutzfeldt-Jakob Disease Surveillance Unit in Edinburgh, UK. The first supplier was the MRI Unit of The City Hospital, Edinburgh. This Hospital has since been closed and demolished and subsequent scanning requirements were thereafter fulfilled by the Department of Clinical Neuroscience of the Western

General Hospital, Edinburgh.

Each supplier used a different scanner which, due to the characteristic variations between scanners, means that it would not be possible to combine the two data sets into a single homogeneous data set. However, the same technician was responsible for creating both sets of data and by adhering to the same protocols for every scanning event, each individual patient case of a given data set from one supplier could be considered suitable for comparison against the other patient cases within that supplier's data set. This effectively therefore provided two independent datasets to which similar analysis techniques might be applied.

For the case of each supplier, the data sets were comprised of a number of individual patient cases. For each patient case, one or more scans were made of their post-mortem brain and these were then collated to form a mini data set representing one individual.

The image data sets from both suppliers were collected using the same basic protocols throughout to provide the maximum possibility for the production of comparable images. In each patient case, the brain was surgically removed from the human skull and was then fixed in a formalin solution for a period of two to three weeks. Once properly fixed the brain could then be imaged.

The fixed brains were stored in bags containing a formalin solution and these bags were contained within a simple plastic bucket. The first supplier used this bucket to hold the bag and provide suspension for the brain whilst in the scanner.

The second supplier utilised a custom made cage (see Figures 3.1, 3.2 & 3.3.) to provide similar suspension to the brain. In each case, the aim was to avoid letting the brain rest on a surface such that its full weight would potentially deform the shape of the brain further.

The scanner settings used in the acquisition of the scan data were also standardised across all the patient cases in the two datasets. For each scan event, the scanner protocol settings as shown in Table 3.1 were used.

For each scanning event, the settings used will image a square field of view of height/width 230mm. This field of view is divided into pixels with an approximate dimension of 0.898mm square to provide the desired image dimension of 256x256 pixels. Each field of view is acquired

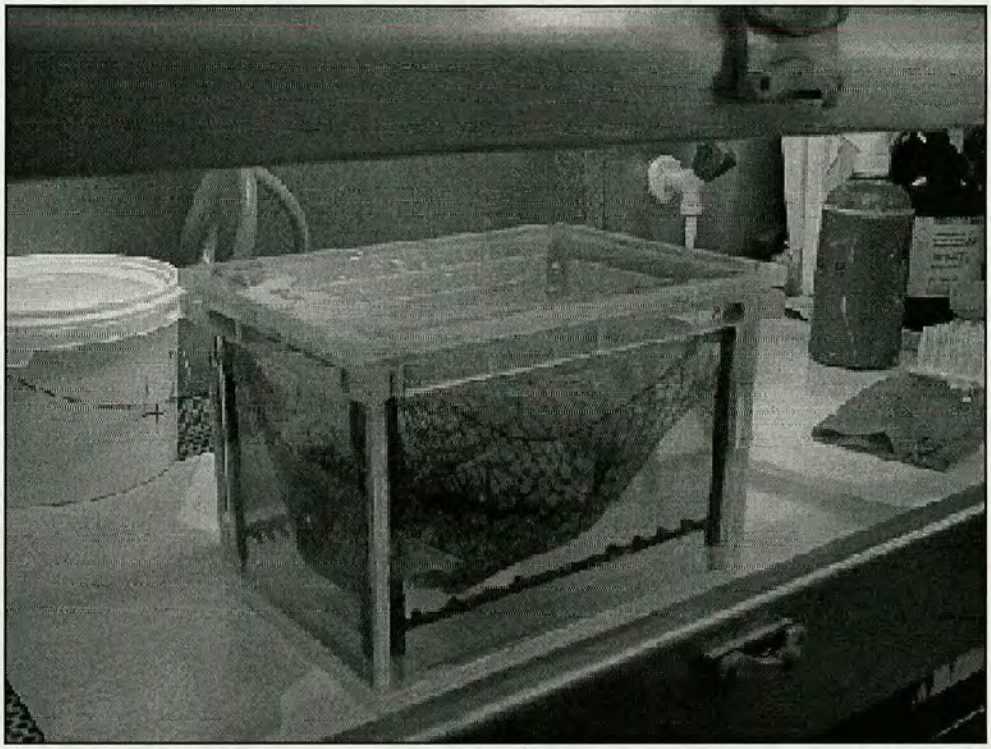

Figure 3.1: *The custom-made brain suspension cage. (Angle View)*

15 times and then averaged and the resultant images at 20ms (PD) and 90ms (T2) are exported. Each pixel value represents the signal intensity for the area encompassed by the pixel and extended through a depth of 5mm into the material. The plane separation of 0mm means that each image-slice directly ajoins its neighbouring slices such that no volume of the material between the first and last image-slices is not represented. On average, the number of planar images required to encompass the volume of the patient's brain was 19 and the time taken to scan this volume was 1.5 hours.

3.3 Preparation of the MRI Scan Data.

The three dimensional volumetric data produced by scanning a patient is recorded on the scanner's storage facility for onward conversion into usable data analysis formats. Due to the existence of a non-disclosure agreement between the scanner manafacturers (SIEMENS, GMBH) and the City Hospital, Edinburgh it was not permitted for the hospital to provide the scan data for this study in its native scanner format. Therefore, the data was first converted by the scanner systems into the ANALYZE image database format (MAYO FOUNDATION) before it was

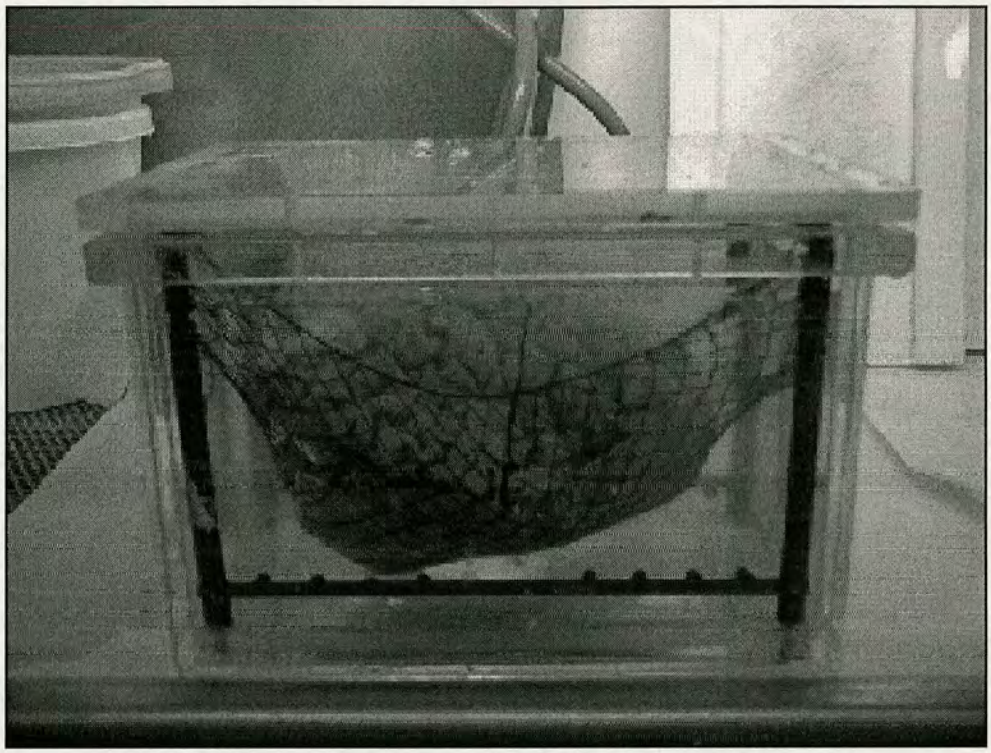

Figure 3.2: *The custom-made brain suspension cage. (Side View)*

handed over.

Once converted to the ANALYZE format, each patient scan comprises a sequence of 12 bit greyscale images, 256x256 pixels in dimension based upon the selected scanner settings which were described previously and are listed in Table 3.1.

The ANALYZE image format bundles a sequence of images into two connected files: A database file containing the raw image data and a separate header file which describes the content of the database file. This arrangement is suitable when the image handling and analysis will be carried out using the ANALYZE application but when the ANALYZE application is not available for such use, as was the case here, it is more practical to convert the data into another image-data format which can be more readily manipulated.

A set of utility programs was written to read in the ANALYZE image database files and convert them to a sequence of individual Portable Pixmap (PPM) image files based upon the descriptive information provided in the associated ANALYZE image header files. The interpretation

Figure 3.3: *The custom-made brain suspension cage. (Plan View)*

of these header files was made based upon the information provided in the ANALYZE image file-format specifications provided by the MAYO FOUNDATION.

Although there is a Portable Greymap (PGM) image format defined for the storage of greyscale images the PPM format, which is intended primarily for RGB (red, green and blue) component colour images, can instead hold three separate greyscale images by using each of the three component bands to store one greyscale image each. (Naturally, the three greyscale images must conform to the same dimensions and maximum pixel intensity values.) To afford the possibility of using the PPM image in this manner later on to store one greyscale image and up to two additional mask images related to the greyscale image the PPM format was selected as the target format when converting the supplied ANALYZE format image data.

The PGM and PPM image formats are part of a collection of complimentary image formats that also includes the PBM or Portable Bitmap format. They are all integral parts of the PBMPlus toolkit of image manipulation utilities that was released on the 10th December, 1991 and is now freely available for download from numerous internet imaging and software sites.

Scanner Parameter	Parameter Value
Relaxation Time (TR)	2200ms.
Image Capture Times	20ms (PD) & 90ms (T2).
RF Field Angle	90 Degrees.
Matrix Size	256 x 256.
Acquisitions	15.
Field of View	230mm square.
Plane Depth	5mm.
Plane Separation	0mm.
Avg. Scan Time	1.5 Hours.
Avg. # Planes	19.

Table 3.1: *MRI Scanning Protocol: Scanner Parameter Settings.*

The original PBMPlus toolkit included a 'README' document which stated that: *PBMPlus is a toolkit for converting various image formats to and from portable formats, and therefore to and from each other. The idea is, if you want to convert among N image formats, you only need* $2*N$ *conversion filters, instead of the* N^2 *you would need if you wrote each one separately.*

Although a detailed description of the PPM file format structure would be inappropriate here, a basic overview of the main features of the format is pertinent. It can be noted that all variants in the PBMPlus family of portable image file formats follow the same basic convention. The first element of the file is a magic number that identifies the file format type. The next elements of the file, separated by whitespace, are the image width and height in pixels and the maximum colour component value. All the values described so far must be provided in ASCII decimal format. Finally, following another whitespace separation from the earlier information, the individual pixel values are listed sequentially separated by whitespace and working across the image (left to right) and down the image from top to bottom. For the special case of a PPM image where a pixel must describe the image colour at that location, the pixel colour is given as three whitespace separated component intensity values for Red, Green and Blue (RGB) respectively.

In each PBMPlus portable format, the pixel value data may be provided as either decimal ASCII values or as RAWBITS binary data. However, if provided in the RAWBITS format the maximum component value permitted is 255 which represents an 8 bit data resolution. Since the MRI data considered in this work has a 12 bit resolution, all PPM images generated here are of the ASCII variant to ensure that the full bit-resolution of the component pixel values may

be preserved.

Following the initial data preparation process, the converted MRI data sets were comprised of multiple PPM image sequences where each sequence represents a single patient scan and each of the individual images within a sequence represented a single slice of scan data mapping to a volumetric slice through the patient's brain.

3.4 Segmentation of the MRI datasets.

The next stage in preparing the image datasets for processing involves the identification and selection of the important Regions Of Interest (ROIs) within the individual images. This will allow just the data corresponding to regions that have been connected in previous studies using in-vivo data with indicator potential to be examined. This process of identification and selection is called segmentation.

3.4.1 Methods of Image Segmentation

Segmenting images is perhaps one of the most important tasks that is required to be performed on an image in order to be able to extract the required information from the image in question. Numerous different techniques exist for segmenting an image and a brief overview is given below.

- **Thresholding** - Segmenting an image via thresholding is one of the oldest and most common forms of segmentation. It is computationally cheap to perform and therefore fast and is widely used. This method converts an image into a binary image using rules shown in Equations 3.1 and 3.2. The simplicity, speed and effectiveness of thresholding makes it a very popular tool and because of this a large range of different thresholding techniques exists [28] today in common usage. For the purposes of this work however, the average intensity of the regions of interest are too similar to many other areas of the image making segmentation via this technique more difficult than it ideally should be.

$$t(i,j) = 1 for f(i,j) \geq T \quad (3.1)$$

$$= 0 for f(i,j) \leq T \quad (3.2)$$

- **Edge Detection** - These segmentation techniques use operators to detect borders between regions in an image where the borders represent discontinuities in the grey level or colour (or other metric) of the image pixels. It is usual to require to combine several edge detection steps together to convert individual edges into coherent chains of edges to ultimately form acceptable region edges. Various techniques including edge image thresholding [29], edge relaxation [30] and border tracing all have strengths but common to all these techniques is a sensitivity to image noise which can cause false edges to be detected.

- **Region Growing** - Is a method for directly constructing regions unlike the edge detection method described above which instead finds borders between regions. The advantage of this direct approach comes when dealing with noisy images where the edges between regions are hard to detect. Thus, more important to these techniques, is the homogeneity of the regions. Various criteria for determing the homogeneity of a region exist and can include intensity (grey levels), textural features or semantic models [31].

Many other edge-detection methods exist including techniques based upon active contour models and alternative clustering based approaches. Previous investigations have examined the suitability of various segmentation techniques [32] to MRI applications and in some instances it has proven possible to achieve successful fully-automated segmentation solutions [33]. However all these various techniques required the use of *a priori* knowledge in order to successfully segment regions of the Human brain and this is commonly the biggest cost-overhead involved. Due to the limited budget of time available to this project, it was not possible to explore the effectiveness of automated segmentation techniques here. It was therefore decided that the most expeditious method to use here in order to minimise the time taken would be to manually segment the regions of interest (ROI) by hand since it would be necessary in any case to identify the ROIs manually.

3.4.2 Segmentation of the Images

For each set of data relating to a single patient, two different sequences of images were produced by two different imaging modalities, namely: Proton Density (PD) weighted images and T2 weighted images as illustrated in Figure 3.4.

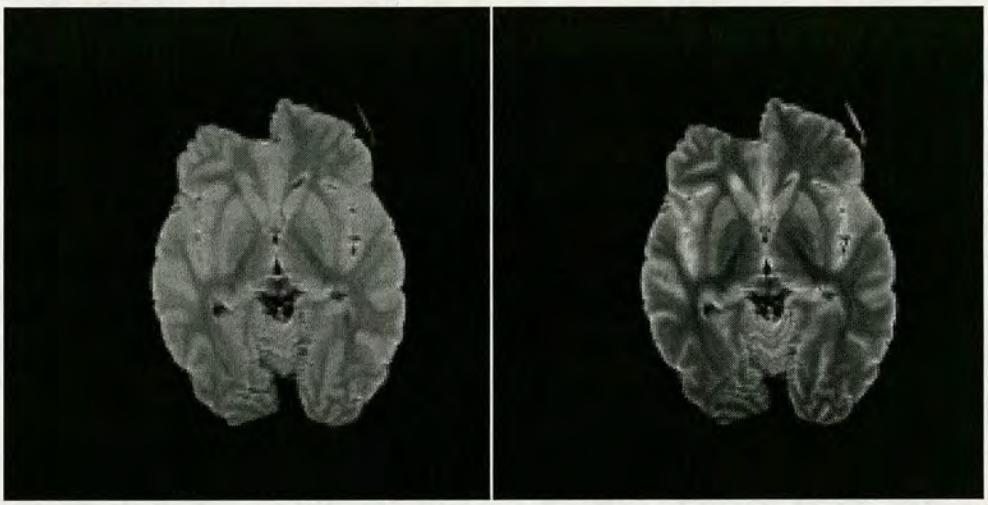

Figure 3.4: *A typical PD weighted MRI (left) and a typical T2 weighted MRI (right) of the same brain region in each case.*

Previous work [34] has suggested that T2 weighted images have the potential to display characteristic abnormalities in CJD related cases and therefore the intial attempts at segmentation of the MRI datasets looked primarily at the T2 image data. The earlier work suggested that the regions most likely to provide a characteristic response were the Putamen and Thalamus regions therefore these regions of the brain were selected to be the ROIs for our MRI datasets.

When a radiologist examines the hard-copy MRI scans for any given patient their expert judgement is used to identify and compare image ROIs by visual inspection alone. Therefore, to provide the closest approximation to real world conditions, visual inspection was chosen as the mechanism by which segmentation would be performed here. In addition, the ability to accurately identify and segment an ROI that represents a specific brain structure is still difficult to do and is itself the subject of a large body of on-going research that is seeking to develop the tools and a sufficiently accurate and workable brain atlas to permit the tools to perform to an acceptable level. Therefore, manual selection of the ROI by visual inspection was also the most expeditious solution available that was expected to perform to the required level.

For every single patient case in the datasets, an initial observation of the slice images was made to identify the image slice in each patient set that best represented the ROIs. This image slice was then selected as the slice to perform the segmentation procedure on. This procedure would involve opening the image in a standard image editing package, in this case Paint Shop Pro Version 5 (PSPv5) and manually segmenting the ROI using the freehand region selection tool to finally create a mask image corresponding to the ROIs that could be used to segment either of the PD or T2 images from which it was made.

Since the large majority of existing work had identified the T2 modality MRI as the one that exhibited the strongest characteristic response with respect to CJD, the initial plan was to use the T2 images to create the set of desired mask images.

However, the darker (less intense) property of the T2 modality image, plus the more limited response that grey-matter structures such as the Putamen provide in the T2 format, meant that the identification of the ROIs in the T2 images was often extremely difficult. Ultimately, the consequence was a set of poor quality mask images that did not provide sufficient acceptable confidence in their validity to allow them to be used further.

Further discussion with a radiologist familiar with MRI hard-copy data sought to improve the understanding of how a radiologist can identify such ROIs by visual inspection and this yielded useful information that allowed the segmentation process to be improved. One of the useful properties of hard-copy MRI data for a radiologist is that the PD and T2 images for corresponding scan slices are arranged side-by-side on the photographic plates. This allows a radiologist to make quick comparisons of a chosen region between the two imaging modalities. More significantly, in the case where it is necessary to identify a specific region of the brain in one image it is often possible to view and identify that region more easily in the corresponding image of the other modality.

This is certainly the case for grey-matter structures such as the Putamen and Thalamus which we are concerned with here and, following our discusion with the radiologist, it was decided to attempt to use the PD images for the creation of the mask images. Any mask image created from a PD image would of course be applicable to the corresponding T2 image because the two

images simply represent the same volume information in two different modalities.

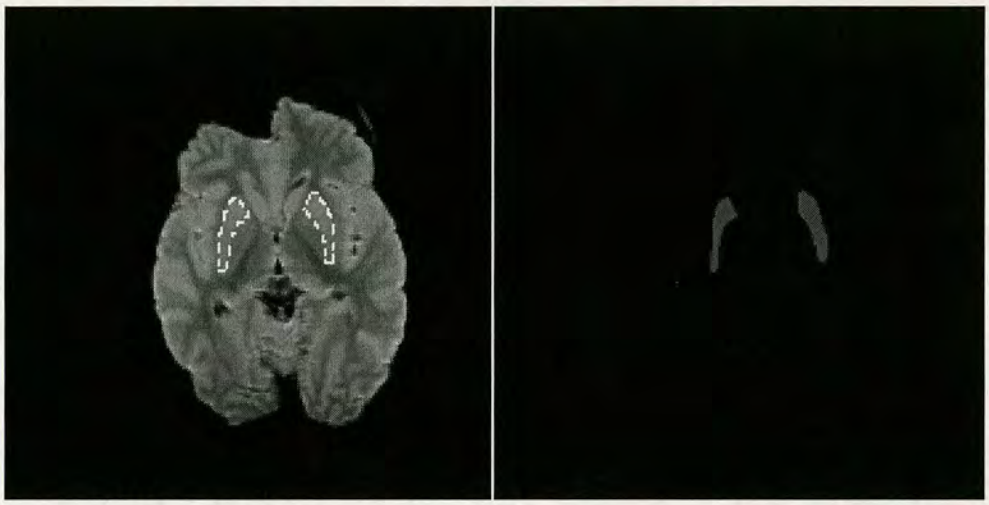

Figure 3.5: *Segmentation: A typical PD weighted MRI (left) and a simple mask image (right) indicating the Putamen region of the brain.*

The revised segmentation method yielded a much improved set of mask images which could then be confidently used to segment the PD and T2 images of the patient datasets. A typical mask image that was created in this manner is shown in Figure 3.5 along with the original PD image from which it was created. It is possible to note from the image that the ROI, which in this case is the Putamen, is visibly brighter than the regions directly surrounding it. In further follow-up discussions with the same radiologist it was revealed that these darker surrounding structures represent white-matter regions of the brain and these typically provide good contrast with the grey-matter structures which appear brighter here but, importantly, they are typically of a very consistant dark nature. Therefore, when a radiologist is attempting to decide if a grey-matter region appears to exhibit unusual intensity it is often the intensity difference between the grey-matter and white-matter regions that helps them to make that decision.

It was therefore decided that an additional ROI should be identified that represented an area of white-matter within the brain that a radiologist might refer to when examining an ROI such as the Putamen or Thalamus. The most immediately adjacent white-matter region to these two grey-matter ROIs and the most likely candidate for this role was agreed to be the Internal Capsule region. As a result, the entire set of mask images was modified to include the possibility of also segmenting a portion of the Internal Capsule to allow the contrast between the grey-matter and white-matter regions to be considered.

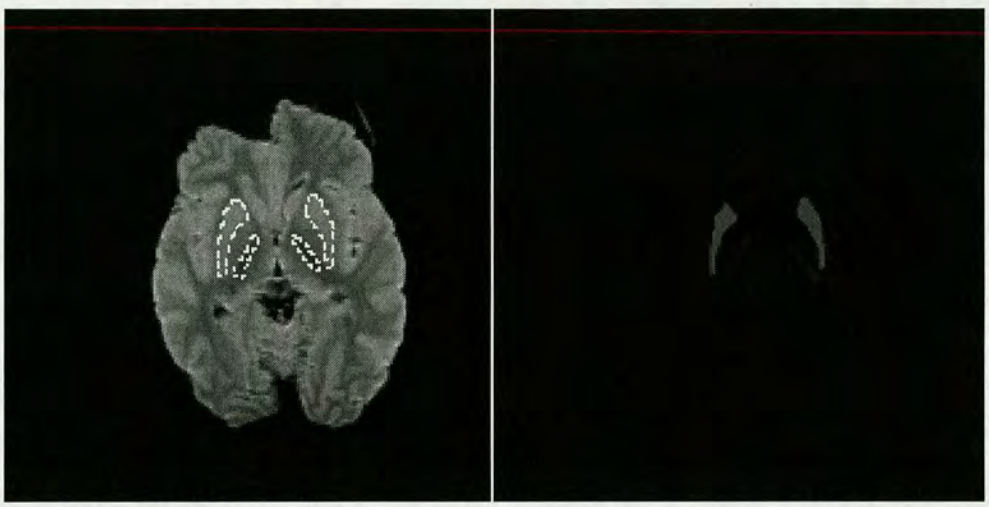

Figure 3.6: *Segmentation: A typical PD weighted MRI (left) and a contrast mask image (right) indicating the Putamen region of the brain (outer segments) and a portion of the Internal Capsule (inner segments) which is selected here to act as a region of contrasting intensity to the Putamen segments.*

A typical "contrast" mask image can be seen in Figure 3.6 once again along with the original PD weighted MRI from which it was created.

3.5 Image Processing Methods.

Once a set of prepared segmented images has been created the next logical step is to determine an effective strategy for processing the images in order to reveal the characteristic properties that the images may contain. In this respect, the methods adopted so far in this investigation have been strongly influenced by the clinical practices involved when a radiologist examines standard hard-copy MRI data.

There are many possible image analysis avenues of investigation that might be explored. Basic image intensity analysis techniques which observe characteristics related directly to the intensities of an image's pixels are an obvious starting point and may, where appropriate, be followed by the application of textural based analysis techniques [35] which range from simple statistical analyses of the image histogram properties to higher order metrics that seek to optimise features of an image that cannot be so easily determined by the human eye [36]. Additional paths such as the use of fractal based analysis techniques [37] which measure the degree of irregularity within

a region may offer further benefits to those that follow them. Common fractal approaches when considering medical images include *fd* (fractal dimension), *fBm* (fractal Browian motion) and, more recently, FIFS (Fractal Interpolation Functions) [38, 39] which attempts to avoid some of the noise-sensitive characteristics of the *fd* and *fBm* methods.

The mechanism used in the clinical environment is simple visual inspection and this method is keyed to simple intensity analysis methods more than to any other technique. In addition, since our original images are a mere 256x256 pixels (a total of 65536 pixels) in dimension with a segmented ROI that is typically far smaller, being an average of only 100 pixels in area, there are therefore relatively few pixels in an ROI to consider. Furthermore, the intensity values across these ROIs change with relatively low frequency which thus indicates that textural content will, at best, be low. As a result of this, it is highly unlikely that the higher order textural analysis methods will be able to yield suitably rewarding results when applied to the MRI data considered here. Furthermore, since fractal based techniques are targetted towards measuring the degree of irregularity in surface texture, the probable lack of texture within the selected ROIs of these images suggests that fractal measures will also prove to be ineffective.

Thus, for the purposes of this work, and in order to best approximate the real-world clinical practices, the methods of image analysis that will be used predominantly will be intensity analysis methods that may help to pick out statistically significant characteristics that the real-world visual inspection method is discerning. Limited time for experimentation with various techniques also prevents a more complete examination of alternative techniques within the scope of this project.

3.5.1 Intensity Analysis Image Processing Methods

Intensity analysis methods of image processing are based upon the examination of the values of the pixels within an image and their variation and distribution. Properties related to the values of the image pixels, their variation and distributions can be observed through various statistics that can measure various pixel intensity characteristics of an image.

Perhaps the simplest image intensity tool is the pixel intensity histogram which most commonly takes the form of a simple bar-chart where there is a bar for every unique pixel intensity value within the image and the height of the bar represents the number of occurances of that

unique pixel intensity value over the entire image. Usually the bars of the chart are ranked in ascending order so that it is possible to view the distribution of the pixel intensity values within the image.

In a similar manner, the most common and perhaps the simplest statistical measure is the mean pixel value. This is the "average" value calculated as the result of summing all the pixel values together and then dividing the total by the number of pixels being considered. ie: Considering either an image or an ROI where the total number of pixels is N and the intensity value of any individual pixel is r_i then the mean μ of all the pixel intensity values is given by Equation 3.3 below:

$$\mu = \frac{1}{N} \sum_{i=1}^{N} r_i \tag{3.3}$$

The mean is often regarded in practice to be one of two of the most important measures of a distribution. The other important measure is the variance which provides a metric that describes how dispersed from the mean the individual pixel values within the distribution are. Assuming the same shorthand as before, the variance σ^2 is defined by Equation 3.4 below:

$$\sigma^2 = \frac{1}{N} \sum_{i=1}^{N} (r_i - \mu)^2 \tag{3.4}$$

The variance is often considered in a more "standardised" form known as the standard deviation σ which is simply the square root of the variance as shown in Equation 3.5 below:

$$\sigma = \sqrt{\sigma^2} \tag{3.5}$$

Like the variance the standard deviation describes a similar property of the data. ie: How clustered the data is around the mean value of the data. However, the standard deviation is keyed to the distribution of the data in such a way that it is possible to predict the amount of data

that lies within a certain distance of the mean value. For example, for datasets that are normally distributed, if the distribution of data around the mean is plotted onto the axes of a simple chart, then some 68% of all the data will lie within one standard deviation from the mean. Expanding the range to two standard deviations from the mean will account for approximately 95% of the data and roughly 99% of the data falls within three standard deviations from the mean. A simplistic overview of a normally distributed dataset with its standard deviation indicated is given in Figure 3.7

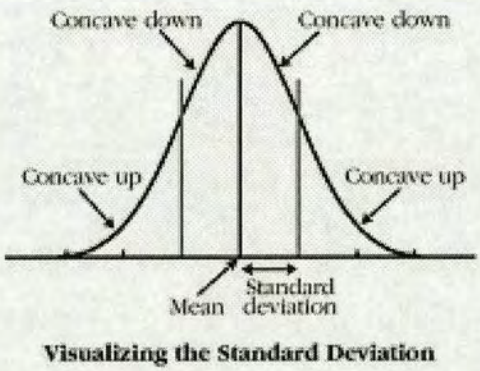

Figure 3.7: *Overview of the standard deviation of a normally distributed data-set.*

Therefore, by segmenting the same ROIs (Putamen, Thalamus) considered by the clinicians that reported the earlier in-vivo findings in this field and then calculating the mean μ, variance σ^2 and standard deviation σ of this segmented image data it will be possible to plot ranked histogram charts of these measures across the entire patient dataset thereby permitting the investigation of the existence of any correlation between earlier reported findings for in-vivo data and these results produced from post-mortem data.

3.6 Visual Inspection Segmentation and Analysis Sensitivity

Selection of the ROIs from the source images to create suitable mask images was performed throughout by identifying the ROI by visual inspection. This approach is simple and easy to implement but may be subject to small inconsistencies in the accuracy of the ROI segmentation due to basic human error that cannot realistically be avoided. This could be a cause for concern if the method of analysis used later on is sensitive to small changes in the segmentation of the ROI and therefore the degree of potential sensitivity should be investigated before using this

method further.

3.6.1 A Test for Determining Analysis Sensitivity

To address this potential concern, a simple test was devised to determine whether or not the processing techniques used later upon the segmented data were sensitive to small changes in the mask images. Two additional mask images were created for each patient case in a data-set by simply copying the original mask image and then either dilating (expanding) the mask or eroding (contracting) the mask. These two operations would provide crude simulations of an individual being slightly inaccurate in their selection of the ROI boundary thereby either including unwanted non-ROI pixels or by excluding pixels that should be included.

In fact, where an individual may gain or lose a few pixels sporadically around the ROI boundary, the dilation or erosion operations will exagerate the effect that their inaccuracy would have and demonstrate what should very much be a worst case scenario. The sensitivity of the analysis methods to the segmentation method used here can be determined by processing the dataset with the normal, eroded and dilated mask sets and then comparing the results from each case together. If the results are noticeably different then the analysis method would be demonstrating sensitivity to the segmentation technique and an alternative approach would need to be found.

Mathematical morphology examines the geometrical structure of an image by testing it with small patterns, called structuring elements which may be of varying size and shape. After the first image processing morphological techniques were introduced in 1975[40] many subsequent applications were then developed including object recognition and texture analysis. These techniques were developed further to allow the simple methods created for use with binary images to be extended for application to greyscale images [41] and such techniques are now in common use today [42].

To save time, all the morphological erosion and dilation operations carried out on the mask images used in this project were performed by PSP5 which uses, as the structuring element, a standard 3x3 flat array which is perhaps the most common used structing element for tasks of this nature.

3.6.2 Results of Testing for Analysis Sensitivity

The mask images from the first MRI dataset were copied and processed to erode and dilate the images as required. An example of an original mask along with its dilated and eroded counterparts is shown in Figure 3.8.

Figure 3.8: *Segmentation: A typical contrast mask image (left) shown with a dilated copy of the mask image (centre) and an eroded copy of the mask image. (right)*

By processing and generating statistical measures for MRI dataset 1 using the three related mask sets it was possible to chart the rank ordered histogram in each case of the difference between the mean pixel intensity of the Putamen and the mean pixel intensity of the Internal Capsule contrast region. These charts, which are listed as Figures 3.9, 3.10 and 3.11 should show little difference in the rank order between the three cases if the analysis methods are to be insensitive to small changes in the mask images.

Examining the three figures appears to show a small amount of "local neighbourhood" position swapping occuring which is both expected and acceptable as a consequence of the changes occuring to the mask image data. However, the general ordering of rank is preserved across all three cases (normal, dilated and eroded) which suggests that the analysis methods used here are not sensitive to small changes occuring to the mask image data and therefore justifies the continued use of these methods in this work.

3.7 Summary

In this chapter the processes involved in the acquisition of the MRI datasets has been described and the subsequent conversion of the native scanner data to first a proprietary format and thereafter to a series of collections of 12-bit ASCII format Portable Pixmap images that would allow

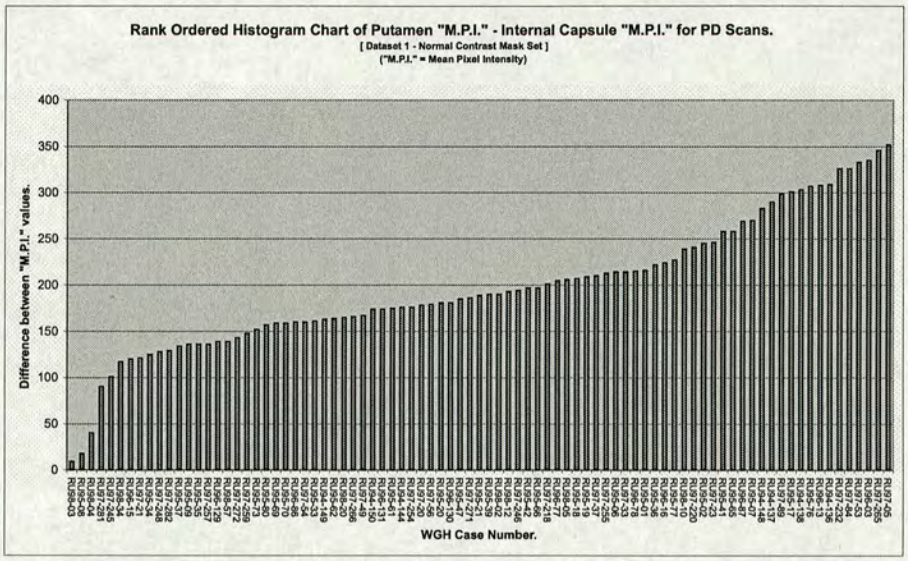

Figure 3.9: *Rank ordered histogram of Putamen "M.P.I." - Internal Capsule "M.P.I." for the normal contrast mask set.*

easy manipulation and processing was explained. The selection of Regions Of Interest (ROIs) for study and the method of image segmentation to isolate these ROIs within an image was detailed and was followed by an outline of the possible image analysis techniques that might be applied to the segmented data. Further details were provided on the actual intensity analysis methods selected and finally these methods were used in a test experiment designed to determine whether or not the analysis method was sensitive to small variations in the segmentation of the ROIs within the images. The results of this test showed that the analysis method appeared not to be sensitive.

In the following chapter the results of applying the segmentation and analysis techniques described here to the main MRI datasets will be presented and discussed.

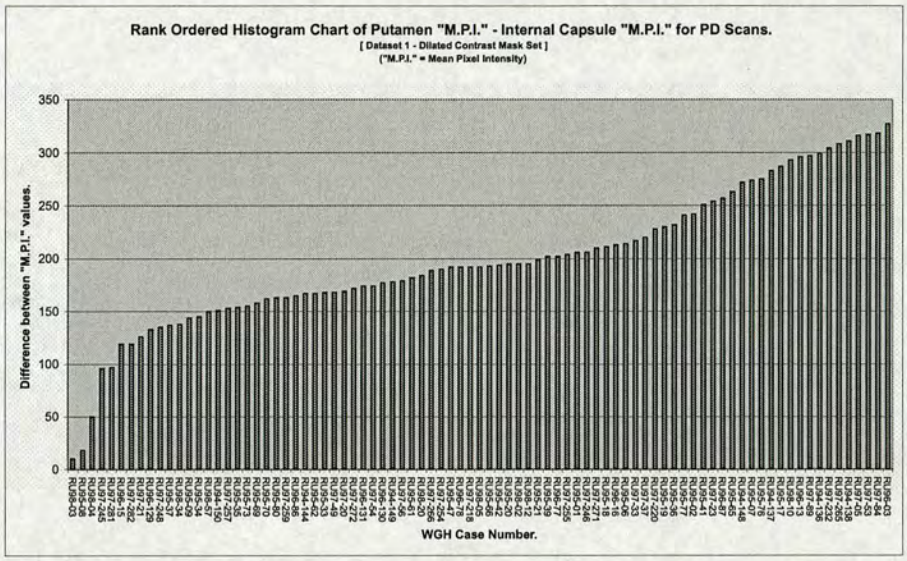

Figure 3.10: *Rank ordered histogram of Putamen "M.P.I." - Internal Capsule "M.P.I." for the dilated contrast mask set.*

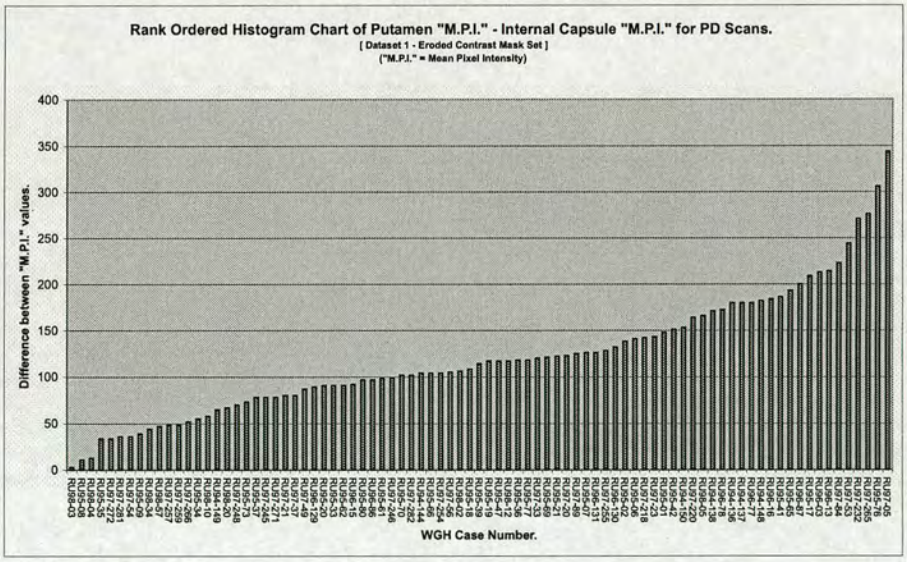

Figure 3.11: *Rank ordered histogram of Putamen "M.P.I." - Internal Capsule "M.P.I." for the eroded contrast mask set.*

Chapter 4
Analysis of Post Mortem MRI

4.1 Overview

This chapter describes the main tests that were performed on the post-mortem MRI scan datasets which were the focus of this work. Before these tests are presented, a description of one aspect of the approach taken to the tests to guard against the bias of fore-knowledge affecting the outcome of the final results is provided. This is followed by a brief description of the method of data analysis that was selected to perform on the results of the individual tests to determine whether or not, when knowledge of the data is finally revealed, there is any demonstration of statistically significant clustering within the results with regard to both Creutzfeld-Jakob disease (CJD) and variant Creutzfeld-Jakob disease (vCJD).

4.2 Blind Testing

In any experiment where a researcher knows in advance the outcome or status of any component within their own experiment upon which the success or failure of their experiment rests, it is important to recognise that this "fore-knowledge" may have a biasing effect upon their own experimental results.

A researcher's decision process may be affected by such fore-knowledge and it has therefore become common practice, especially within the medical community, to perform tests in what is known as a "Blinded" manner wherever possible.

Blinded testing is testing where the researcher does not know certain key details about the experiment they are performing and does not receive that key-information until the very end of the process when analysis of experimental data is required.

For example: in a medical experiment to test whether or not a new medical compound (say,

compound X) is effective at treating a given medical condition a researcher may prescribe that compound to a test group of patients all suffering from the condition. If the researcher gives compound X to some of the patients and gives only a simple placebo (an ineffective neutral compound) to the rest of the test group then the researcher can determine better whether the improvements or otherwise made by the patients is related to the administration of the special compound X or to other factors. This type of test would be called a Blind Test.

However, the researcher still knew which compounds were being administered to which patients in the above example and this knowledge may itself bias the results of such a study. Therefore, it is also possible to repeat the test with both the researcher and the patients being ignorant of whether a placebo or a dose of compound X is being administered. This type of test is known as a Double Blind Test and it protects the validity of the results from the potentially biasing effects of fore-knowledge held by either the researcher or by the individual patients.

Throughout the course of this research the key to the post-mortem MRI datasets being investigated that reveals an individual patient's final confirmed diagnosis (CJD, vCJD or Not CJD) was withheld so that all tests performed upon the data would not be affected by the potential bias of such fore-knowledge.

Once the tests were completed and the results data was then ready to be analysed, the key was provided to allow each individual case to be classified. It was then possible for the results data to be further analysed to determine whether or not the results demonstrated statistically significant clustering of the cases that had been confirmed with a diagnosis of CJD or vCJD.

In effect therefore, this work was conducted throughout as a Blind Test because the key to the data was withheld. In addition, all technical personnel that had prior interaction with the MRI scan data (MRI technicians, etc.) were also not provided with the key to the data.

4.2.1 Sample Identified Cases: By Final Diagnosis

In order to facilitate some level of understanding of the data, the key-holder of the data identified four cases from data-set 1 (approx. 80+ cases in total) to allow those cases to be identified in the intermediate results and therefore to allow some estimation of confidence in the techniques being used to be gained. The cases identified along with their confirmed diagnosis are listed in

Table 4.1.

WGH Case Number	Confirmed Diagnosis
RU98/34	CJD (Sporadic)
RU97/255	vCJD
RU97/220	Alzheimer's disease
RU98/12	"Other" (not CJD)

Table 4.1: Blind Testing: *Table listing four cases from MRI dataset 1 that were identified by the data's key-holder as example cases for the confirmed diagnoses listed.*

4.2.2 Sample Identified Cases: By Expert Observer

In addition to the cases identified by the data's key-holder, a further seven cases were identified by an expert observer of the equivalent hard-copy of the electronic MRI data being used in this study. The observer is an experienced Neuro-radiologist and was similarly "blinded" to the actual confirmed case diagnoses. Therefore, the example cases were selected using the criteria that they either appeared unusually "bright" in the typical Regions Of Interest (ROIs) considered when evaluating hard-copy data for a potential CJD victim or that they appeared "not-bright."

The seven cases, four "not-bright" and three "bright", are listed in Table 4.2.

WGH Case Number	Confirmed Diagnosis
RU96/131	"Bright"
RU96/78	"Bright"
RU97/23	"Bright"
RU97/05	"Not-Bright"
RU96/130	"Not-Bright"
RU96/129	"Not-Bright"
RU97/246	"Not-Bright"

Table 4.2: Blind Testing: *Table listing seven cases from MRI dataset 1 that were identified by an expert observer as either appearing "bright" or "not-bright" with respect to the Regions Of Interest considered for a potential CJD victim.*

An example histogram chart of one of the many tests run and described in more detail later in the chapter with the eleven identified cases highlighted is shown in Figure 4.1.

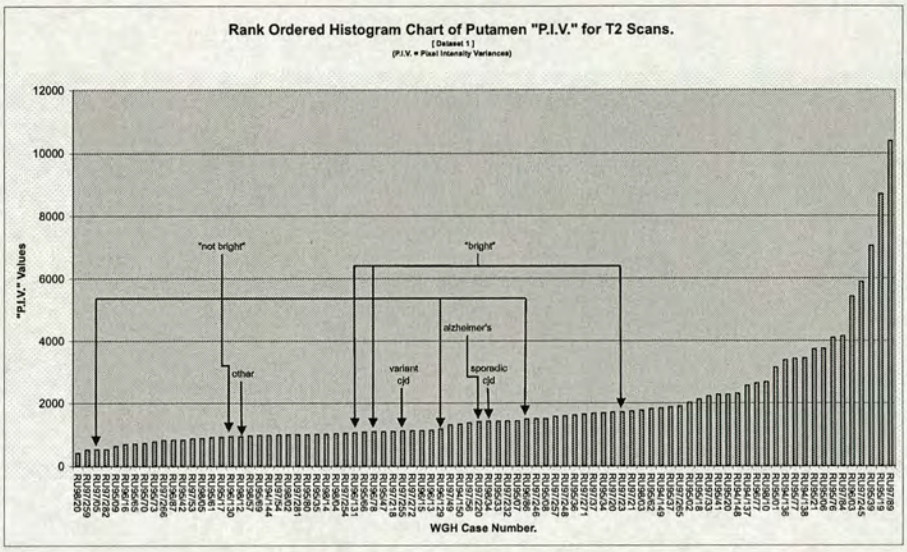

Figure 4.1: Blind Testing: *Rank ordered histogram chart of the Putamen region "P.I.V" values for the T2 weighted MRI scan-data from datasets 1 with the example cases identfied by the data-key holder and the expert observer highlighted.*

4.3 Statistical Data Analysis

As the previous section discussed, all of the tests that were performed and that are described further on in this chapter were performed in a "blinded" manner, meaning that knowledge of the individual diagnosis of any given patient case was not known at the time when the tests were conducted.

However, upon completion of all tests the key to the data was to be provided allowing each individual patient case to be labelled with its own confirmed diagnosis so that the data could then be analysed for signs of clustering that could indicate certain tendencies which may later prove to be useful.

As was described in Chapter 3 and was further illustrated in the previous section on Blind Testing, the default method of data presentation once a dataset has been processed is a ranked order histogram chart which plots values of the calculated property of the test being performed (Region of Interest (ROI) mean, ROI mean minus Internal Capsule mean, ROI variance, ROI variance minus Internal Capsule variance.) against the individual patient case number as recorded by the Western General Hospital (WGH) of Edinburgh.

With such data, one of the most effective methods for testing for statistically significant clustering of the data is to apply a test called the Chi-Squared Test.

4.3.1 The Chi-Squared Test

The Chi-Square (χ^2) Test is a test that provides a measure of the "goodness of fit" of a given hypothesis to a population of data[43]. This is a useful test when the distribution of the data within the population is unknown and when the sample sizes of data taken from the population are potentially small.

For example, for the tests that will be considered here, where the population is distrubuted along an x -axis that represents individual patient cases, the entire population can be sub-divided into a number of intervals which represent sample groups taken from the same general population. A requirement of the χ^2 Test is that each individual interval must contain at least 5 values for the test to produce valid results.

The probability of any value within a sample assuming a specific classification (a confirmed case of CJD for example) may be computed as a function of the total number of values in the population and the total number of cases matching that classification in the population. This is shown in Equation 4.1.

$$p_i = \frac{N_c}{N_p} \tag{4.1}$$

Where:
p_i is the probability that a value in the interval assume a given classification.
N_c is the total number of classified cases in the population.
N_p is the total number of values in the population.

It is then possible to calculate the Expectation Value for a given sample interval of a population which gives an indication of how many values matching the specific classification being tested are likely to appear within this sample interval. This is shown in Equation 4.2.

$$e_i = np_i \tag{4.2}$$

Where:

e_i is the Expectation value of i for this sample interval.

p_i is the probability that a value in the interval assume a given classification.

n is the number of classified values appearing in this sample interval.

From this it is then possible to calculate the χ^2 statistic for this population by considering and evaluating the following equation (4.3):

$$\chi^2 = \sum_{i=1}^{K} \frac{(b_i - e_i)^2}{e_i} \tag{4.3}$$

Where:

χ^2 is the Chi-Squared statistic.

K is the number of sample intervals in the population.

b_i is an individual value within a sample interval.

e_i is the Expectation value of i for this sample interval.

Once the χ^2 statistic has been calculated, it's significance or otherwise, is determined by comparing it to the critical value of χ^2 for a population with n degrees of freedom, calculated as $K - 1$ where K is the number of sample intervals, and a pre-selected level of significance; typically 95% or 99%. Tables of critical values for χ^2 and various degrees of freedom are available in the back of many widely available mathematical text books and a selection of χ^2 distributions for different degrees of freedom is illustrated in Figure 4.2.

If the computed value of χ^2 is greater than the chosen critical value then the population is considered to demonstrate statistically significant clustering of the values within it to the level determined by the critical value (95%, 99% etc.).

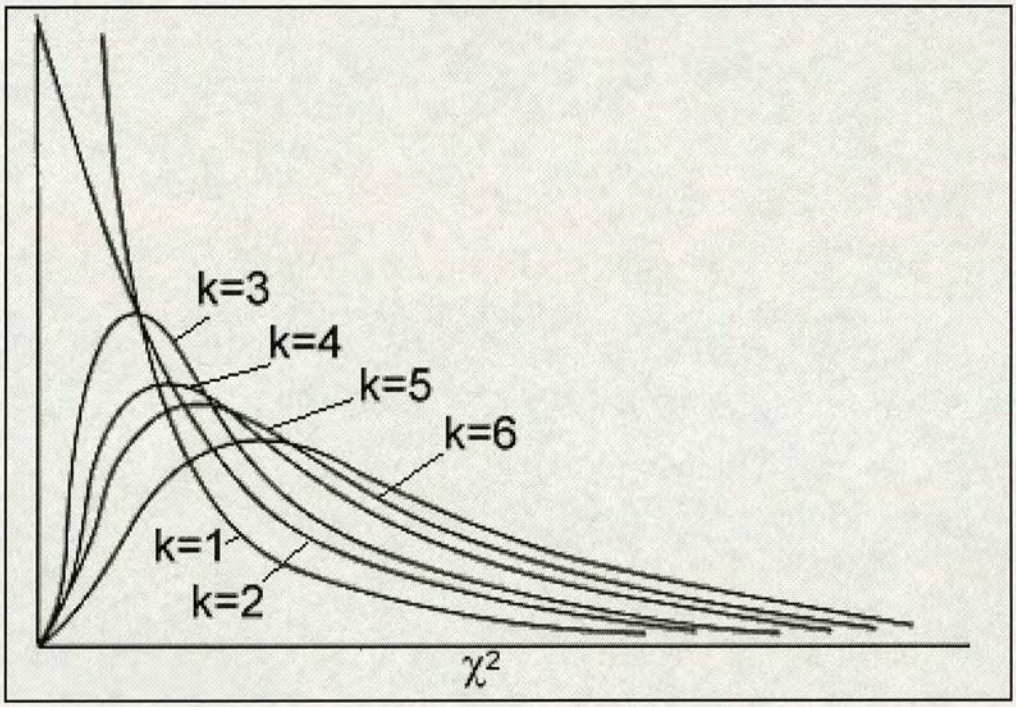

Figure 4.2: χ^2 **Distributions:** *Simple chart showing several* χ^2 *distributions for different degrees of freedom (k) demonstrating the broadening and flattening effect that increasing the value of k has on the* χ^2 *distribution.*

All of the tests that are described in this work considered a dataset as the population and split the population into four intervals. This therefore renders the critical values of χ^2 at 95% and 99% as 7.82 (3s.f. [1]) and 11.3 (3s.f.) respectively.

For the tests that are described in the remainder of this chapter, the χ^2 measure will be used as the default method of analysing the results of the tests and determining the presence or lack thereof of any statistically significant clustering of the data with respect to Creutzfeld-Jakob disease (CJD) and Variant CJD respectively.

[1] s.f. - Abreviated term for Significant Figures.

4.4 Putamen Tests

4.4.1 Introduction

This section details the tests that were performed across two combined datasets; dataset 1 plus dataset 2 (1+2) and dataset 3 plus dataset 4 (3+4). For these tests the Region Of Interest (ROI) considered was the Putamen which is located in the Basal Ganglia area of the brain and was described earlier in Chapter 2.

In total, 16 Putamen tests were conducted; 8 tests on dataset 1+2 and 8 tests on dataset 3+4. Considering the 8 tests conducted per dataset, the breakdown of these tests is as follows.

- 2 tests considering the mean value of the pixels within the ROI; the first ignoring the mean value of the adjacent contrast ROI (the Internal capsule) and the second considering the mean value of the contrast ROI.
- 2 tests considering the variance value of the pixels within the ROI; the first ignoring the variance value of the adjacent contrast ROI (the Internal capsule) and the second considering variance value of the contrast ROI.

These four tests were repeated twice per dataset; once for the Proton Density weighted MRI scans and once for the T2 weighted MRI scans.

4.4.2 Results of Putamen Tests

The rank ordered histogram charts of the results of the 16 tests conducted on the two combined datasets when considering the Putamen to be the ROI appear here.

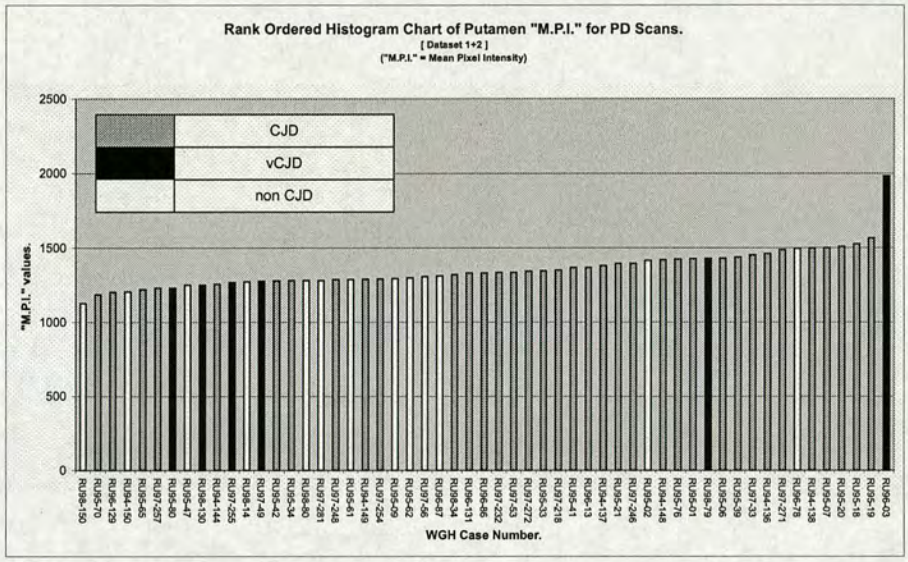

Figure 4.3: Putamen Tests: *Rank ordered histogram of the Putamen region "M.P.I." values for the PD weighted MRI scan-data from datasets 1 & 2 combined.*

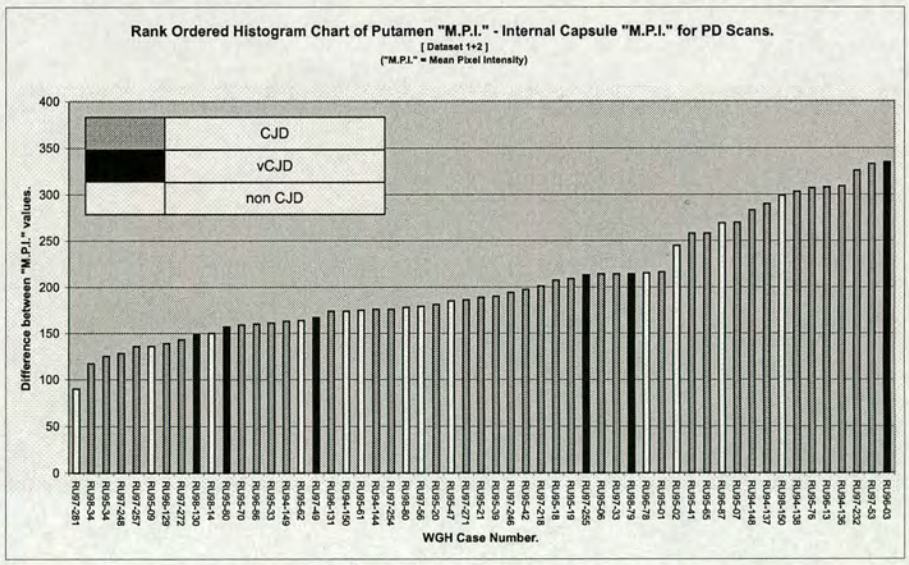

Figure 4.4: Putamen Tests: *Rank ordered histogram of the difference between the Putamen region "M.P.I." and the Internal Capsule "M.P.I." values for the PD weighted MRI scan-data from datasets 1 & 2 combined.*

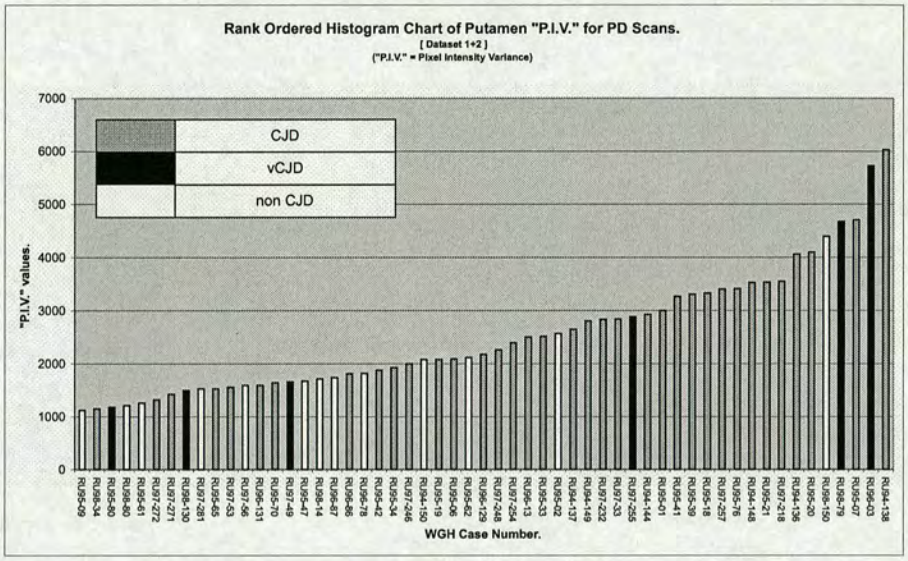

Figure 4.5: Putamen Tests: *Rank ordered histogram of the Putamen region "M.P.I." values for the PD weighted MRI scan-data from datasets 1 & 2 combined.*

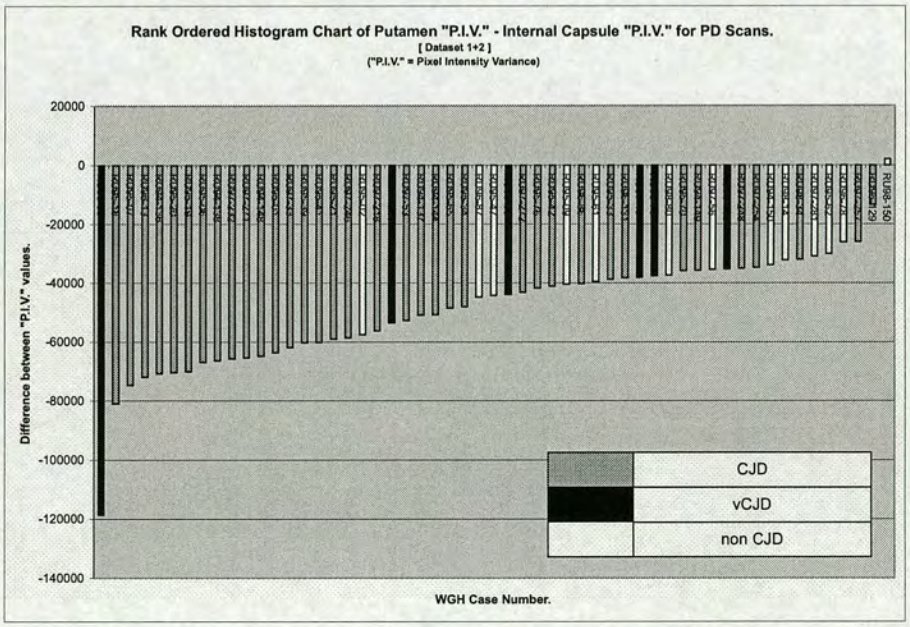

Figure 4.6: Putamen Tests: *Rank ordered histogram of the difference between the Putamen region "M.P.I." and the Internal Capsule "M.P.I." values for the PD weighted MRI scan-data from datasets 1 & 2 combined.*

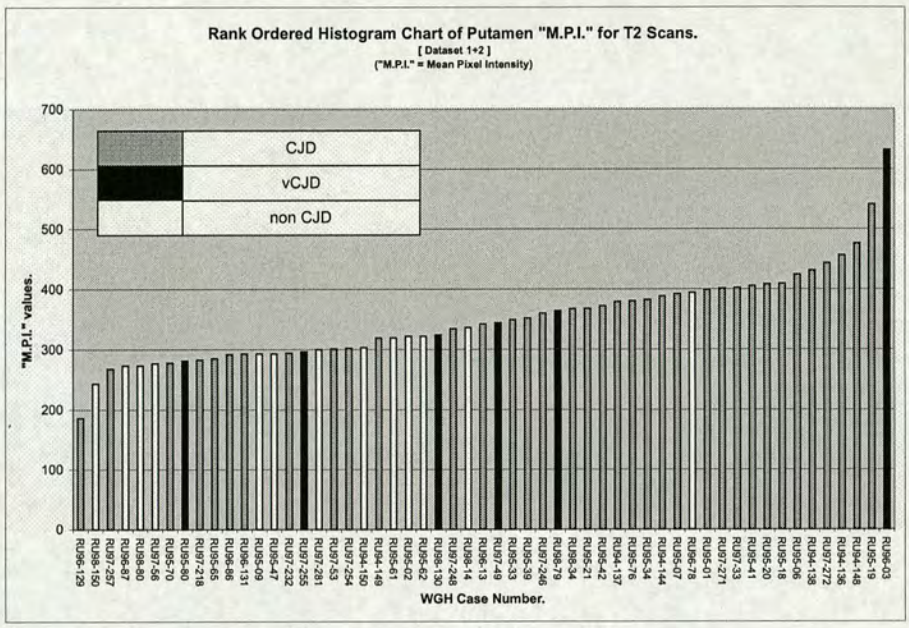

Figure 4.7: Putamen Tests: *Rank ordered histogram of the Putamen region "M.P.I." values for the T2 weighted MRI scan-data from datasets 1 & 2 combined.*

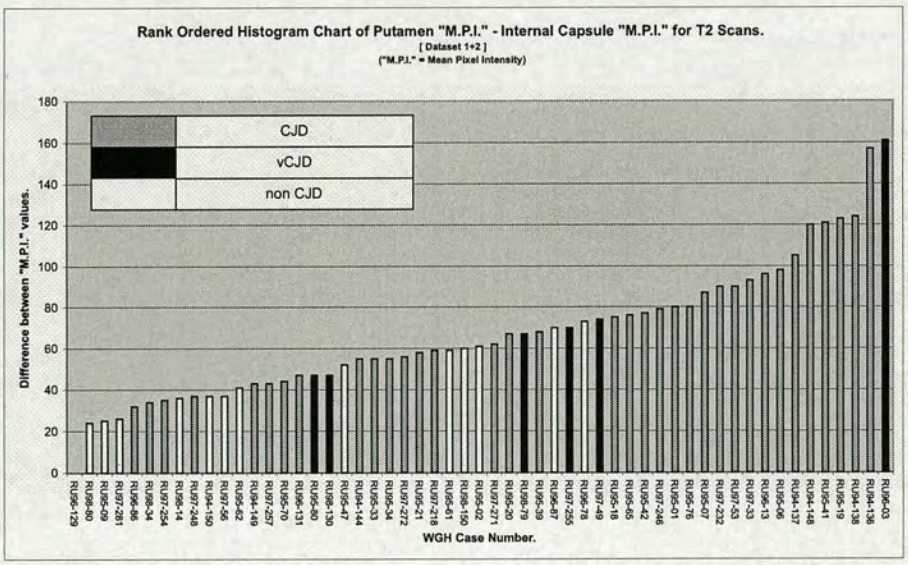

Figure 4.8: Putamen Tests: *Rank ordered histogram of the difference between the Putamen region "M.P.I." and the Internal Capsule "M.P.I." values for the T2 weighted MRI scan-data from datasets 1 & 2 combined.*

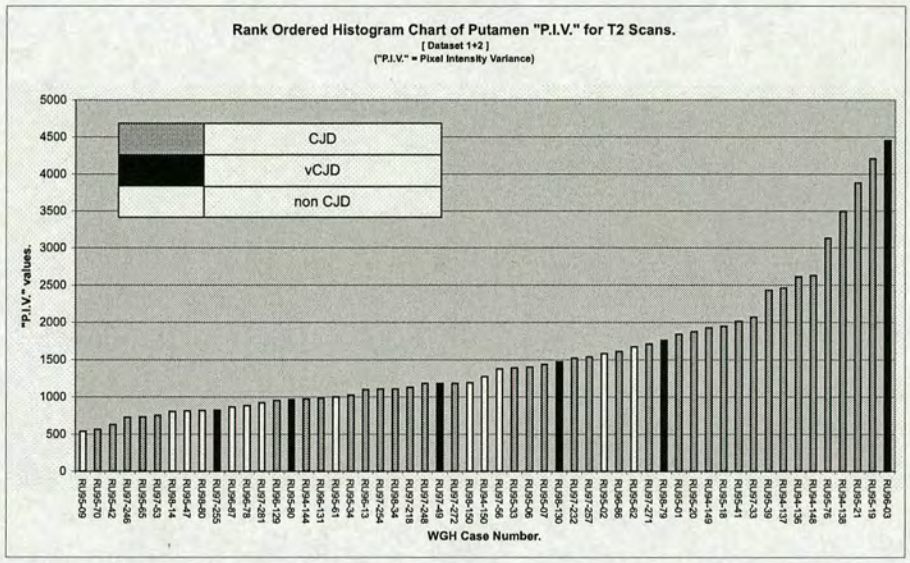

Figure 4.9: Putamen Tests: *Rank ordered histogram of the Putamen region "M.P.I." values for the T2 weighted MRI scan-data from datasets 1 & 2 combined.*

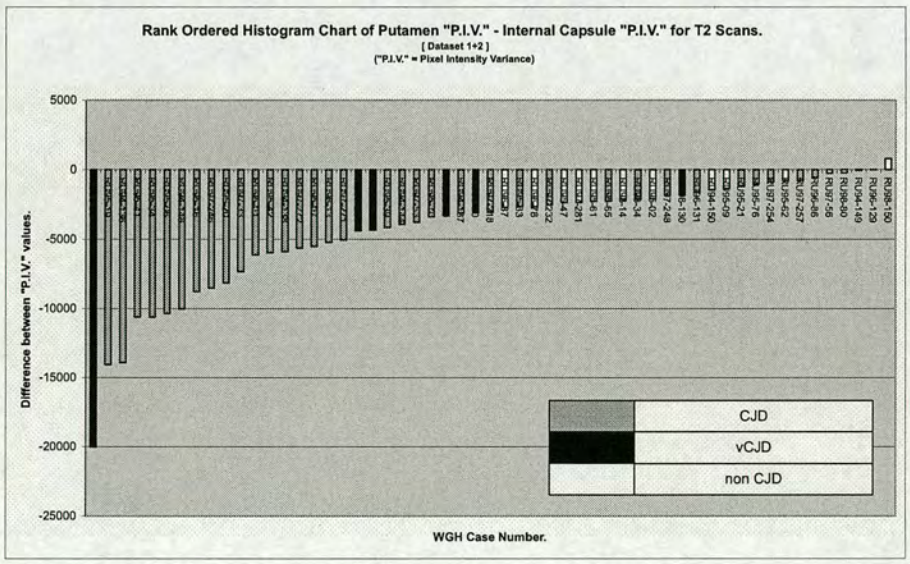

Figure 4.10: Putamen Tests: *Rank ordered histogram of the difference between the Putamen region "M.P.I." and the Internal Capsule "M.P.I." values for the T2 weighted MRI scan-data from datasets 1 & 2 combined.*

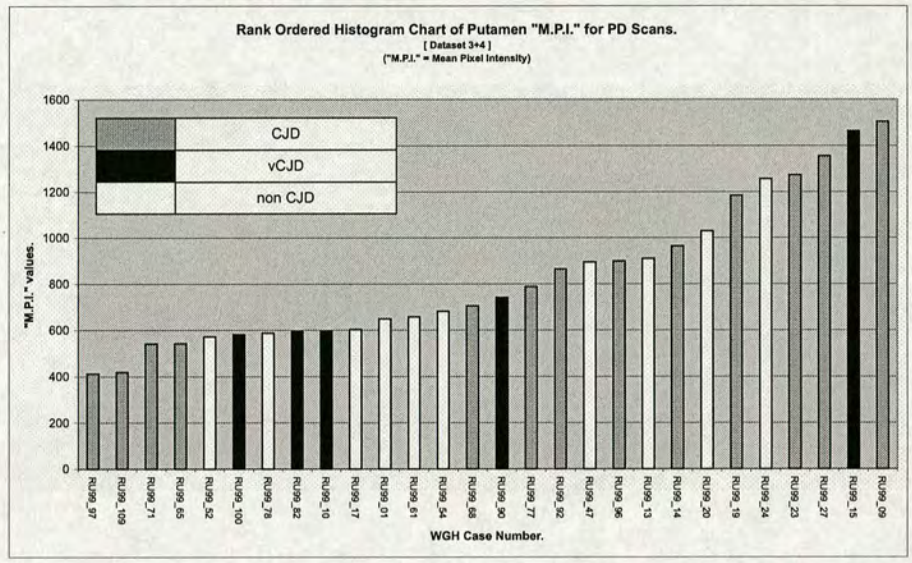

Figure 4.11: Putamen Tests: *Rank ordered histogram of the Putamen region "M.P.I." values for the PD weighted MRI scan-data from datasets 3 & 4 combined.*

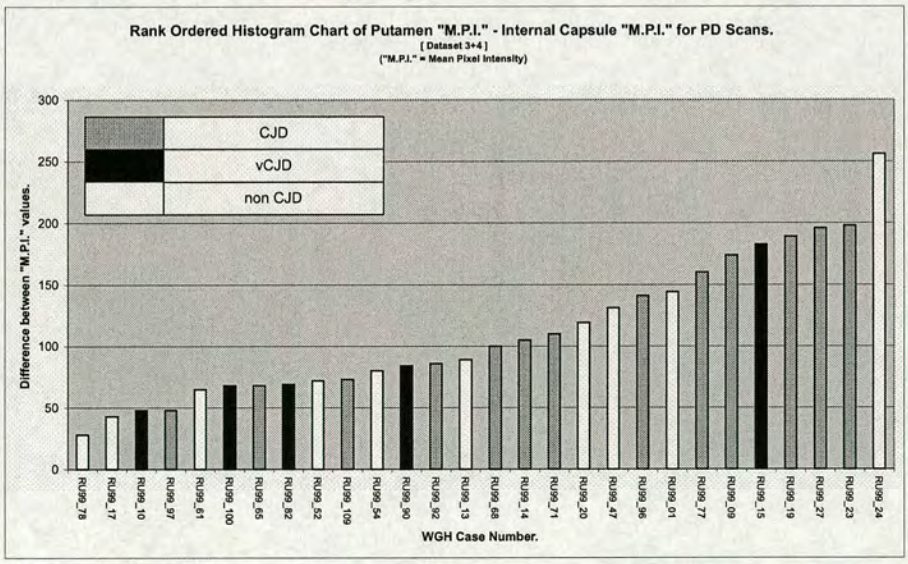

Figure 4.12: Putamen Tests: *Rank ordered histogram of the difference between the Putamen region "M.P.I." and the Internal Capsule "M.P.I." values for the PD weighted MRI scan-data from datasets 3 & 4 combined.*

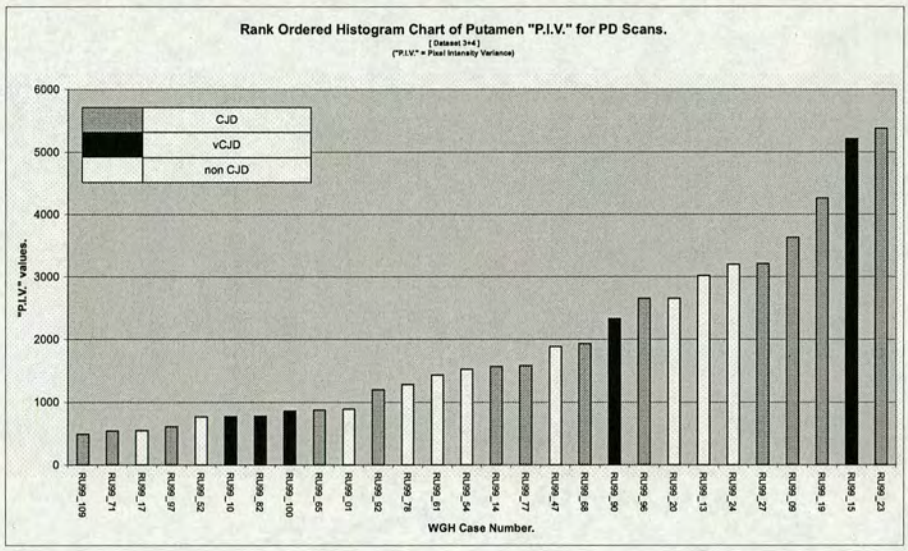

Figure 4.13: Putamen Tests: *Rank ordered histogram of the Putamen region "M.P.I." values for the PD weighted MRI scan-data from datasets 3 & 4 combined.*

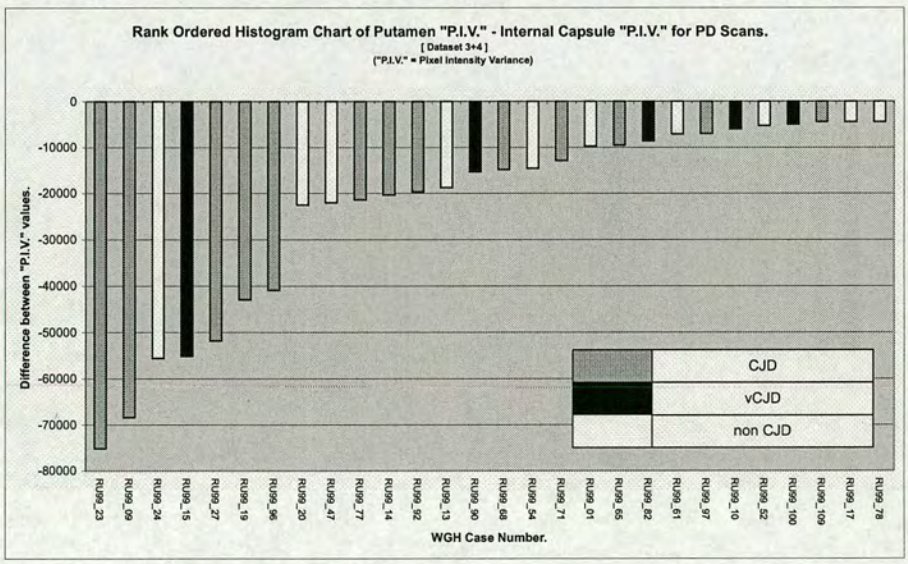

Figure 4.14: Putamen Tests: *Rank ordered histogram of the difference between the Putamen region "M.P.I." and the Internal Capsule "M.P.I." values for the PD weighted MRI scan-data from datasets 3 & 4 combined.*

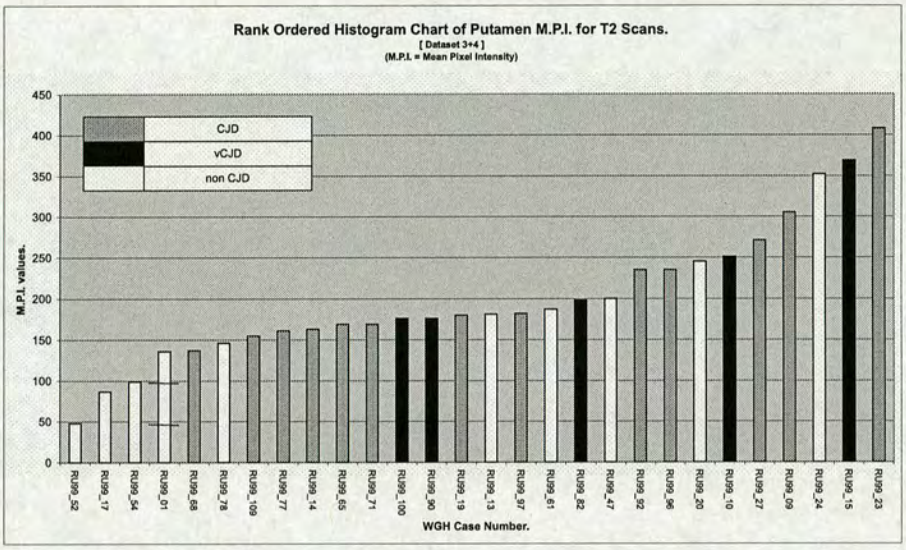

Figure 4.15: Putamen Tests: *Rank ordered histogram of the Putamen region "M.P.I." values for the T2 weighted MRI scan-data from datasets 3 & 4 combined.*

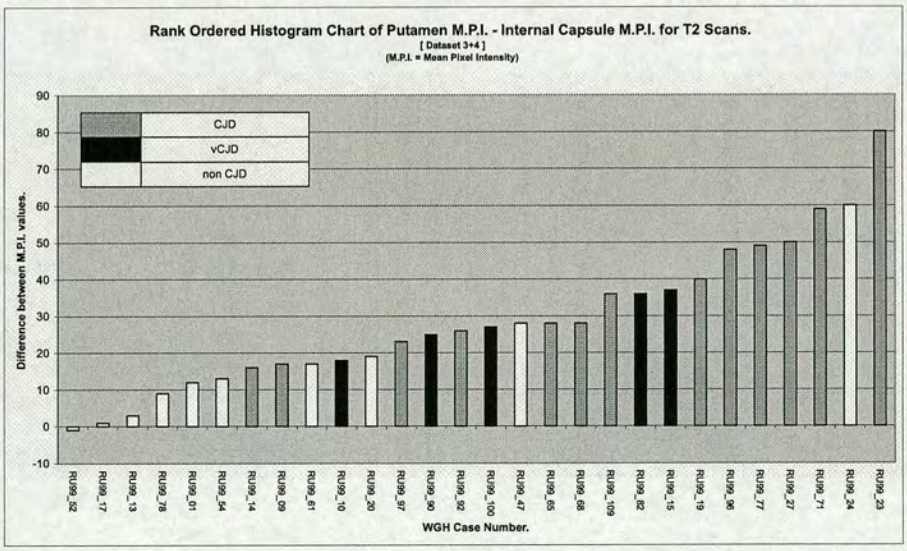

Figure 4.16: Putamen Tests: *Rank ordered histogram of the difference between the Putamen region "M.P.I." and the Internal Capsule "M.P.I." values for the T2 weighted MRI scan-data from datasets 3 & 4 combined.*

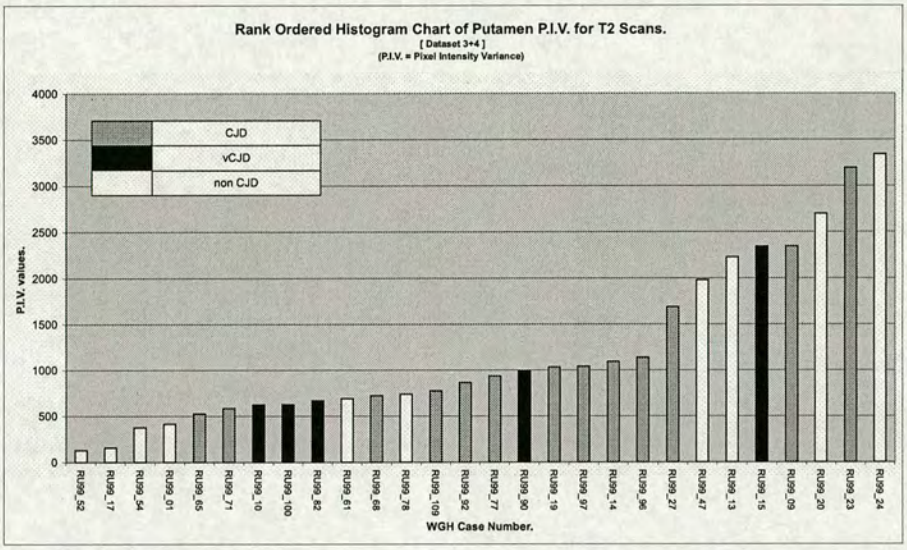

Figure 4.17: Putamen Tests: *Rank ordered histogram of the Putamen region "M.P.I." values for the T2 weighted MRI scan-data from datasets 3 & 4 combined.*

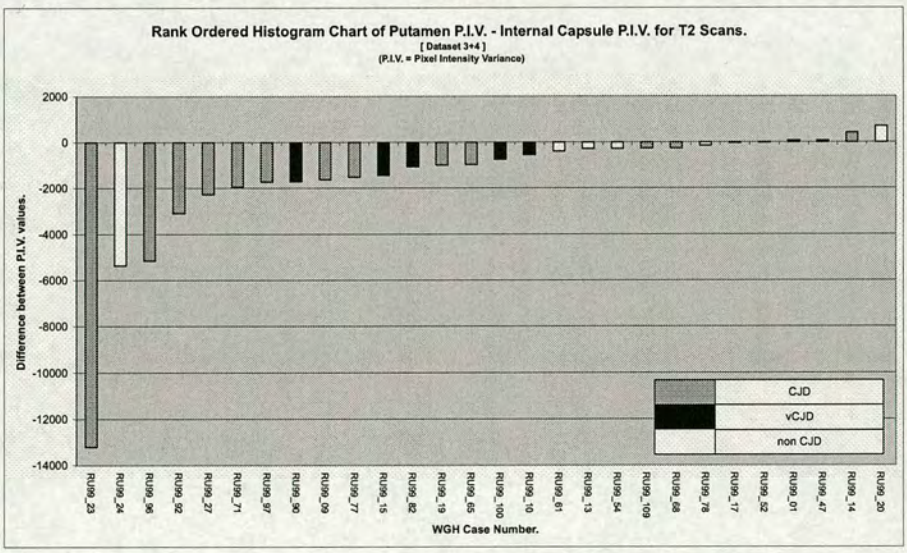

Figure 4.18: Putamen Tests: *Rank ordered histogram of the difference between the Putamen region "M.P.I." and the Internal Capsule "M.P.I." values for the T2 weighted MRI scan-data from datasets 3 & 4 combined.*

4.4.3 Analysis of Results of Putamen Tests

The χ^2 measure of statistical significance was calculated for each of the Putamen tests and a determination was made of the significance or otherwise of the clustering of CJD and vCJD cases within the dataset.

These measures are listed for each test in tables 4.3 and 4.4.

Figure	Modality	Property	Test	χ^2 (3s.f)	Clustering Sig.
4.3	PD	Putamen M.P.I.	CJD	11.4	99%
4.3	PD	Putamen M.P.I.	vCJD	8.50	95%
4.4	PD	Putamen M.P.I. - I.C. M.P.I.	CJD	5.70	Not Significant
4.4	PD	Putamen M.P.I. - I.C. M.P.I.	vCJD	1.03	Not Significant
4.5	PD	Putamen P.I.V.	CJD	6.34	Not Significant
4.5	PD	Putamen P.I.V.	vCJD	0.586	Not Significant
4.6	PD	Putamen P.I.V. - I.C. P.I.V.	CJD	12.4	99%
4.6	PD	Putamen P.I.V. - I.C. P.I.V.	vCJD	2.61	Not Significant
4.7	T2	Putamen M.P.I.	CJD	9.75	95%
4.7	T2	Putamen M.P.I.	vCJD	1.03	Not Significant
4.8	T2	Putamen M.P.I. - I.C. M.P.I.	CJD	12.4	99%
4.8	T2	Putamen M.P.I. - I.C. M.P.I.	vCJD	4.20	Not Significant
4.9	T2	Putamen P.I.V.	CJD	14.9	99%
4.9	T2	Putamen P.I.V.	vCJD	0.590	Not Significant
4.10	T2	Putamen P.I.V. - I.C. P.I.V.	CJD	16.3	99%
4.10	T2	Putamen P.I.V. - I.C. P.I.V.	vCJD	2.61	Not Significant

Table 4.3: Putamen Tests: *Table of results after applying the χ^2 data analysis test to the histograms produced by processing the combined MRI dataset 1 & 2 with the normal mask-set. A key to the column values is provided in Table 4.9*

4.4.4 Discussion of Results of Putamen Tests

From the results of the Putamen tests it appears that the Putamen demonstrates consistant significant clustering with respect to CJD throughout the majority of the tests conducted. In many cases, that clustering was measured at the 99% limit of significance.

However, only one test showed significant clustering of vCJD cases within the population of the dataset and this therefore does not support the hypothesis that the Putamen would be a generally good ROI for indicating vCJD.

For the majority of the tests, consideration of the contrast ROI (the Internal Capsule) improved

Figure	Modality	Property	Test	χ^2 (3s.f)	Clustering Sig.
4.11	PD	Putamen M.P.I.	CJD	1.87	Not Significant
4.11	PD	Putamen M.P.I.	vCJD	0.730	Not Significant
4.12	PD	Putamen M.P.I. - I.C. M.P.I.	CJD	1.87	Not Significant
4.12	PD	Putamen M.P.I. - I.C. M.P.I.	vCJD	2.68	Not Significant
4.13	PD	Putamen P.I.V.	CJD	1.87	Not Significant
4.13	PD	Putamen P.I.V.	vCJD	0.730	Not Significant
4.14	PD	Putamen P.I.V. - I.C. P.I.V.	CJD	1.87	Not Significant
4.14	PD	Putamen P.I.V. - I.C. P.I.V.	vCJD	0.730	Not Significant
4.15	T2	Putamen M.P.I.	CJD	8.09	95%
4.15	T2	Putamen M.P.I.	vCJD	2.68	Not Significant
4.16	T2	Putamen M.P.I. - I.C. M.P.I.	CJD	10.6	95%
4.16	T2	Putamen M.P.I. - I.C. M.P.I.	vCJD	6.57	Not Significant
4.17	T2	Putamen P.I.V.	CJD	6.84	Not Significant
4.17	T2	Putamen P.I.V.	vCJD	0.73	Not Significant
4.18	T2	Putamen P.I.V. - I.C. P.I.V.	CJD	13.1	99%
4.18	T2	Putamen P.I.V. - I.C. P.I.V.	vCJD	6.57	Not Significant

Table 4.4: Putamen Tests: *Table of results after applying the χ^2 data analysis test to the histograms produced by processing the combined MRI dataset 3 & 4 with the normal mask-set. A key to the column values is provided in Table 4.9*

the quality of the clustering and therefore the statistical measure of it. This would imply that this technique, recommended by the real-world practice of radiologists examining hard-copy MRI data is also applicable here.

Dataset 3+4 demonstrates fewer occurances of significant data clustering across the tests. This may be because the data was sourced from a different scanner to dataset 1+2. More likely however is that the markedly smaller size of the dataset, being approximately one third of the size of dataset 1+2, makes minor trends in the data more difficult to spot.

4.5 Thalamus Tests

4.5.1 Introduction

This section details the tests that were performed across two combined datasets; dataset 1 plus dataset 2 (1+2) and dataset 3 plus dataset 4 (3+4). For these tests the Region Of Interest (ROI) considered was the Thalamus which is located in the Basal Ganglia area of the brain and was described earlier in Chapter 2.

In total, 16 Thalamus tests were conducted; 8 tests on dataset 1+2 and 8 tests on dataset 3+4. Considering the 8 tests conducted per dataset, the breakdown of these tests is as follows.

- 2 tests considering the mean value of the pixels within the ROI; the first ignoring the mean value of the adjacent contrast ROI (the Internal capsule) and the second considering the mean value of the contrast ROI.
- 2 tests considering the variance value of the pixels within the ROI; the first ignoring the variance value of the adjacent contrast ROI (the Internal capsule) and the second considering variance value of the contrast ROI.

These four tests were repeated twice per dataset; once for the Proton Density weighted MRI scans and once for the T2 weighted MRI scans.

4.5.2 Results of Thalamus Tests

The rank ordered histogram charts of the results of the 16 tests conducted on the two combined datasets when considering the Thalamus to be the ROI appear here.

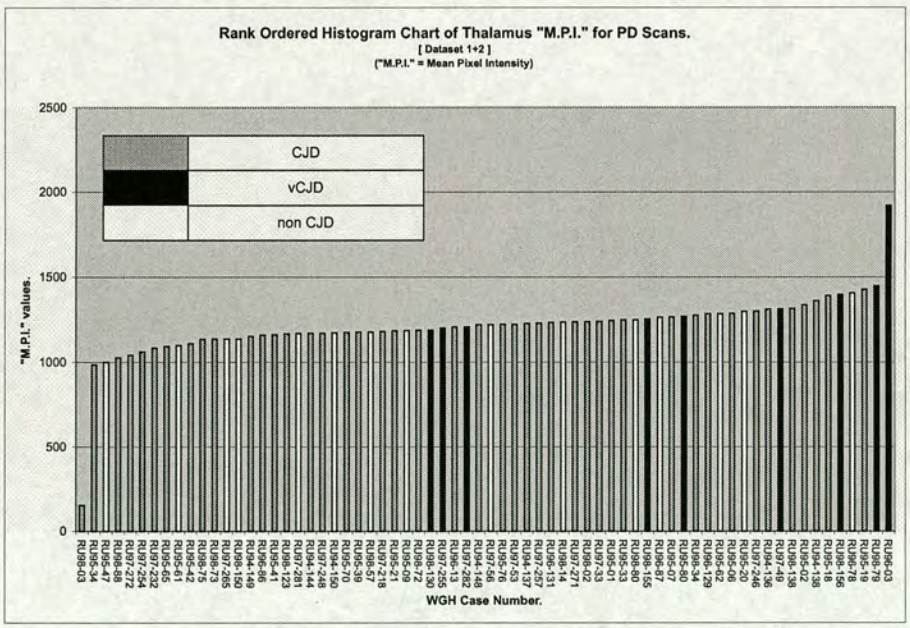

Figure 4.19: Thalamus Tests: *Rank ordered histogram of the Thalamus region "M.P.I." values for the PD weighted MRI scan-data from datasets 1 & 2 combined.*

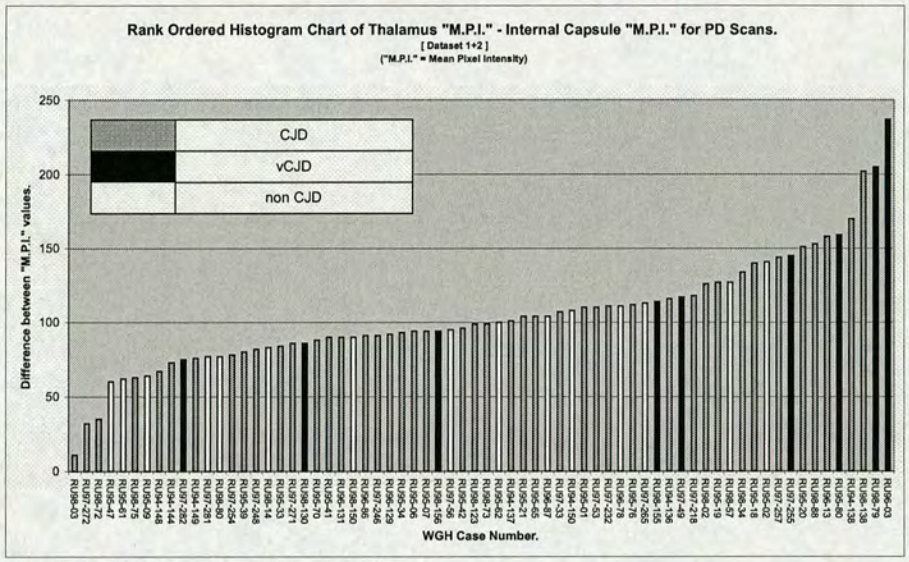

Figure 4.20: Thalamus Tests: *Rank ordered histogram of the difference between the Thalamus region "M.P.I." and the Internal Capsule "M.P.I." values for the PD weighted MRI scan-data from datasets 1 & 2 combined.*

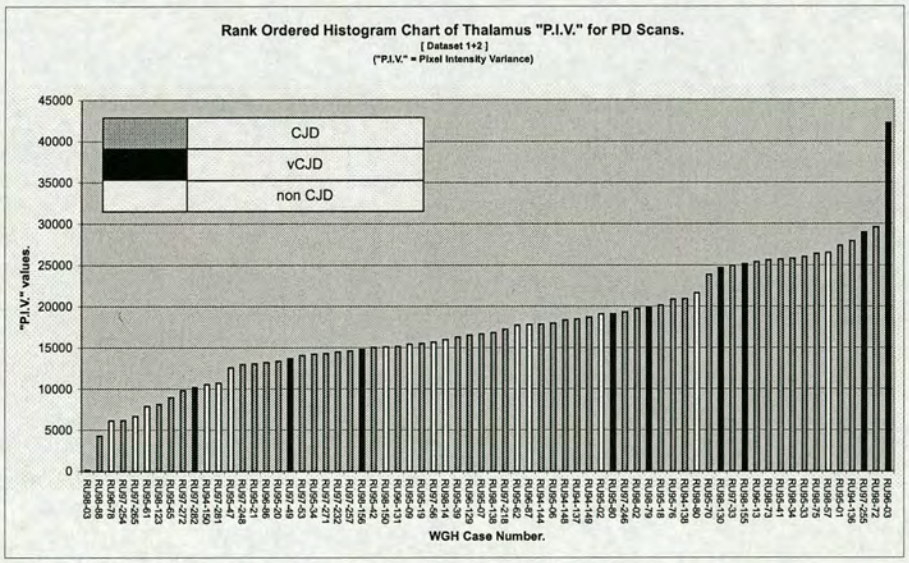

Figure 4.21: Thalamus Tests: *Rank ordered histogram of the Thalamus region "M.P.I." values for the PD weighted MRI scan-data from datasets 1 & 2 combined.*

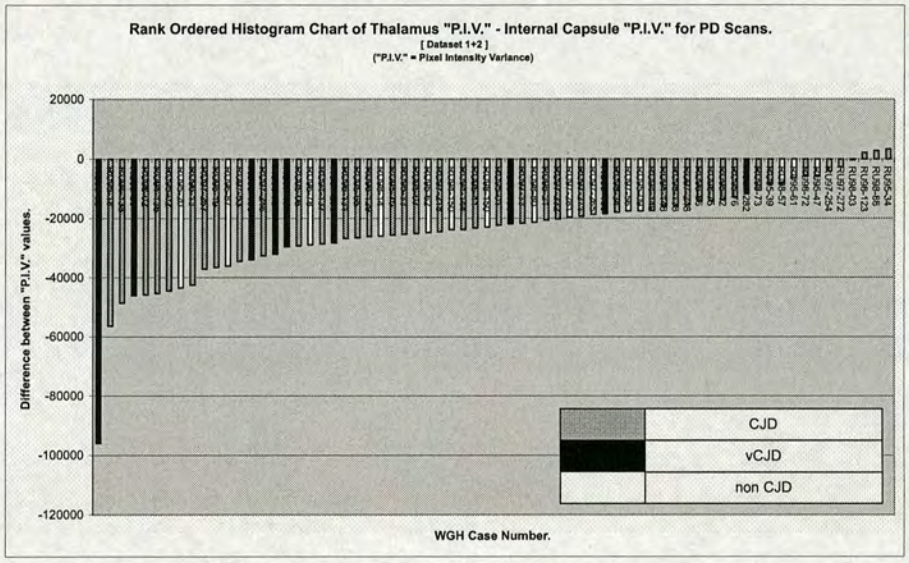

Figure 4.22: Thalamus Tests: *Rank ordered histogram of the difference between the Thalamus region "M.P.I." and the Internal Capsule "M.P.I." values for the PD weighted MRI scan-data from datasets 1 & 2 combined.*

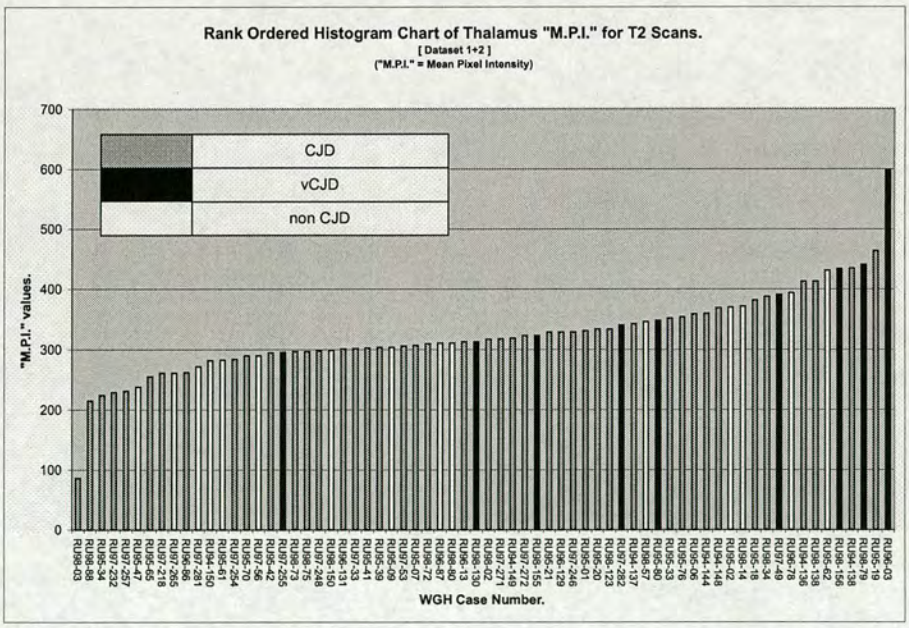

Figure 4.23: Thalamus Tests: *Rank ordered histogram of the Thalamus region "M.P.I." values for the T2 weighted MRI scan-data from datasets 1 & 2 combined.*

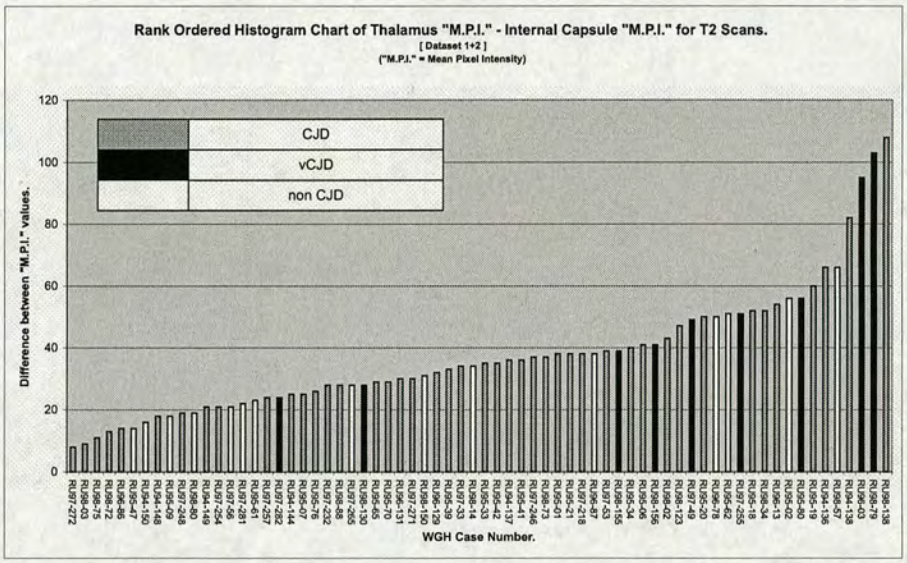

Figure 4.24: Thalamus Tests: *Rank ordered histogram of the difference between the Thalamus region "M.P.I." and the Internal Capsule "M.P.I." values for the T2 weighted MRI scan-data from datasets 1 & 2 combined.*

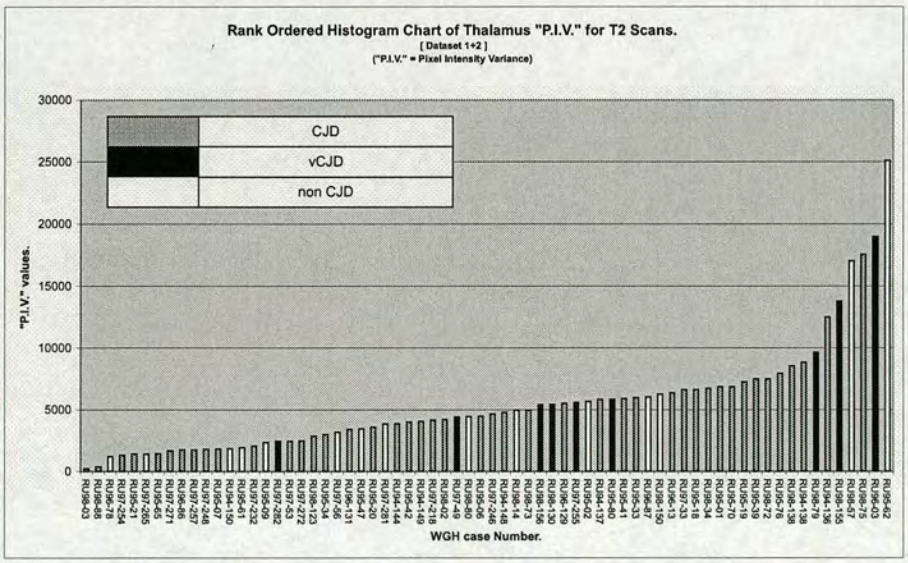

Figure 4.25: Thalamus Tests: *Rank ordered histogram of the Thalamus region "M.P.I." values for the T2 weighted MRI scan-data from datasets 1 & 2 combined.*

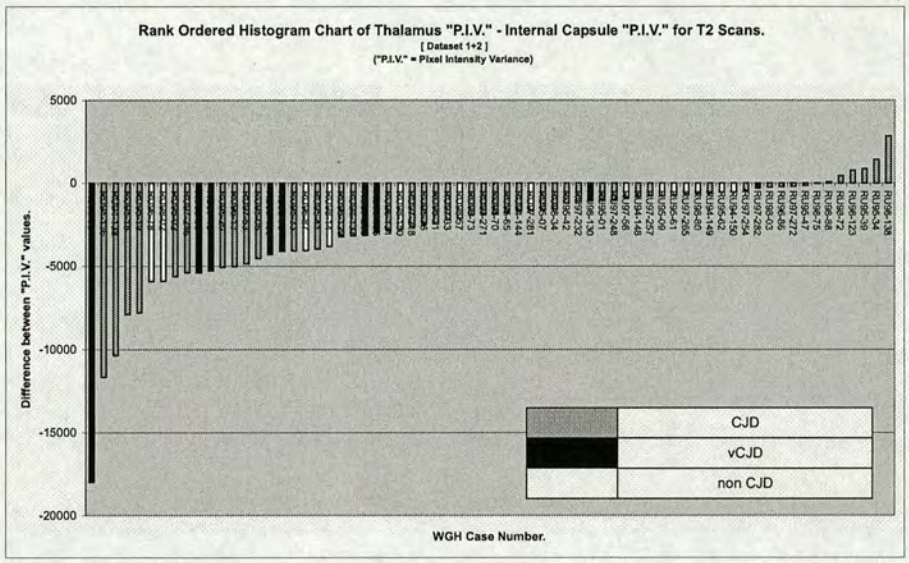

Figure 4.26: Thalamus Tests: *Rank ordered histogram of the difference between the Thalamus region "M.P.I." and the Internal Capsule "M.P.I." values for the T2 weighted MRI scan-data from datasets 1 & 2 combined.*

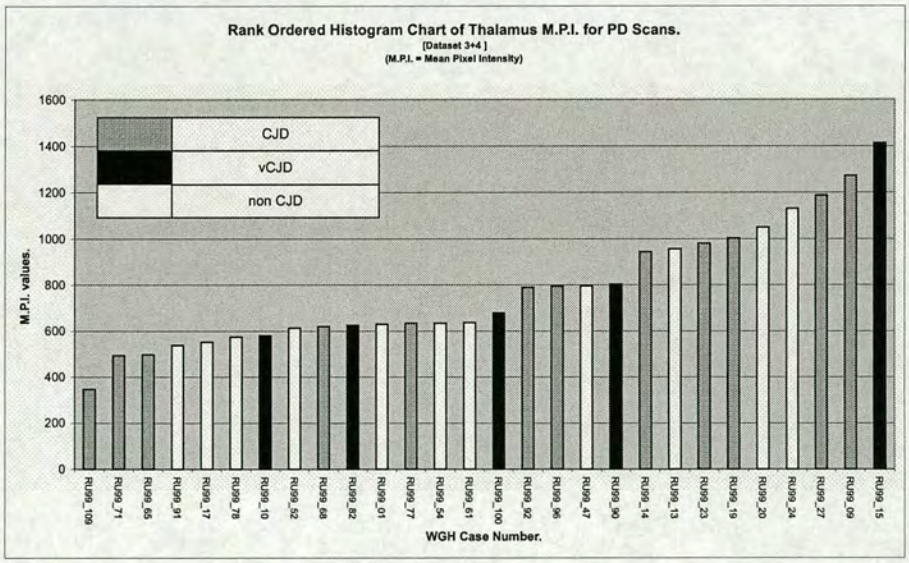

Figure 4.27: Thalamus Tests: *Rank ordered histogram of the Thalamus region "M.P.I." values for the PD weighted MRI scan-data from datasets 3 & 4 combined.*

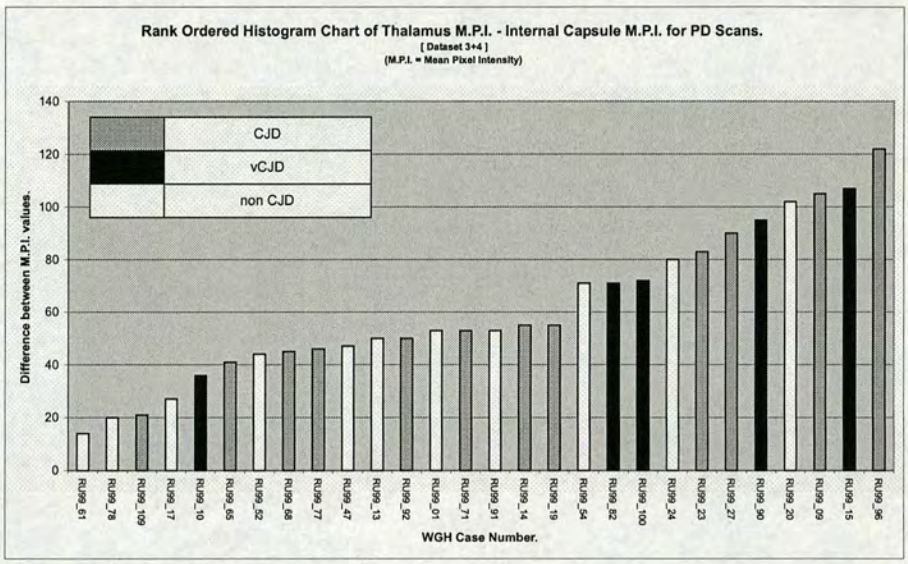

Figure 4.28: Thalamus Tests: *Rank ordered histogram of the difference between the Thalamus region "M.P.I." and the Internal Capsule "M.P.I." values for the PD weighted MRI scan-data from datasets 3 & 4 combined.*

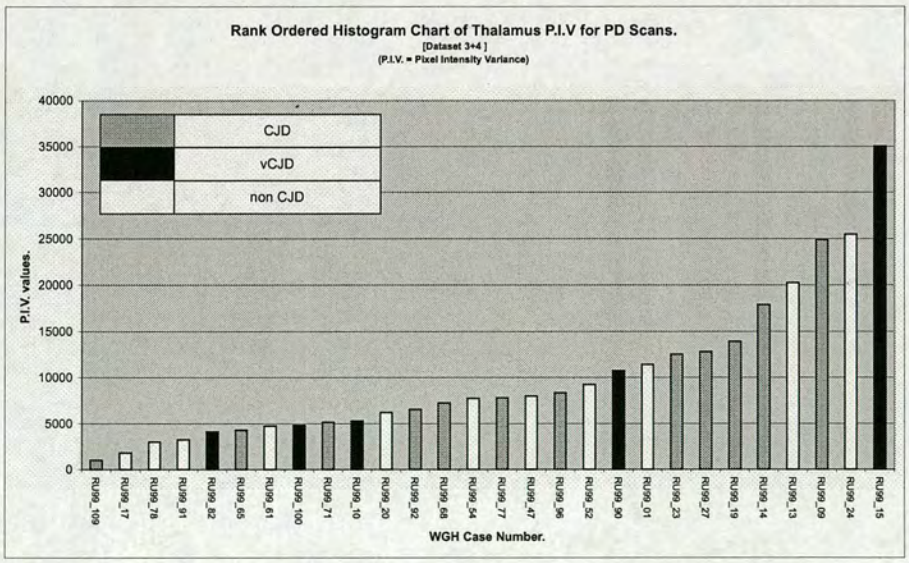

Figure 4.29: Thalamus Tests: *Rank ordered histogram of the Thalamus region "M.P.I." values for the PD weighted MRI scan-data from datasets 3 & 4 combined.*

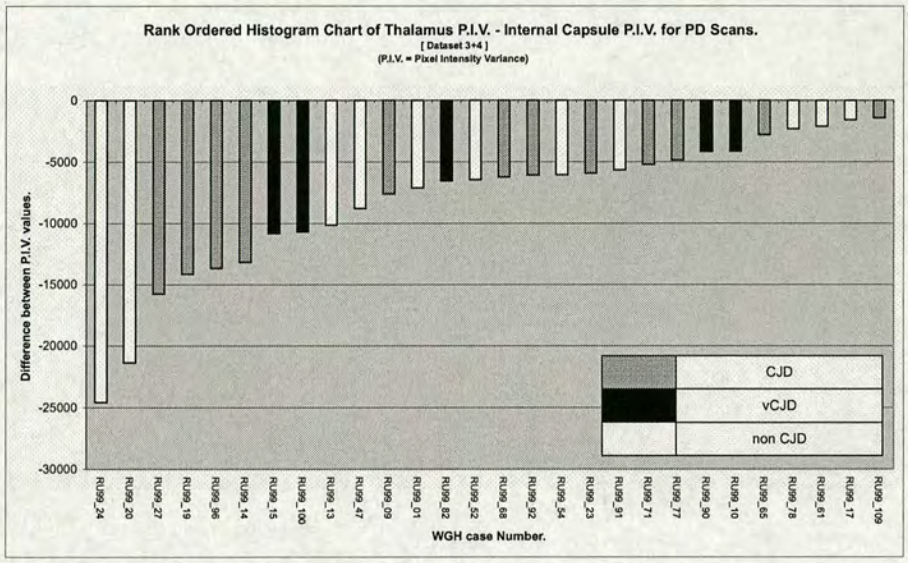

Figure 4.30: Thalamus Tests: *Rank ordered histogram of the difference between the Thalamus region "M.P.I." and the Internal Capsule "M.P.I." values for the PD weighted MRI scan-data from datasets 3 & 4 combined.*

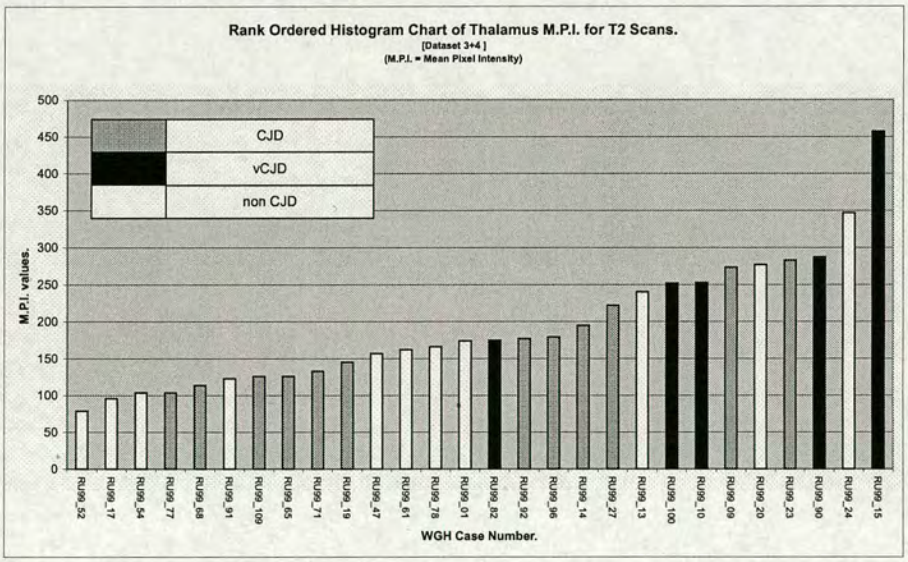

Figure 4.31: Thalamus Tests: *Rank ordered histogram of the Thalamus region "M.P.I." values for the T2 weighted MRI scan-data from datasets 3 & 4 combined.*

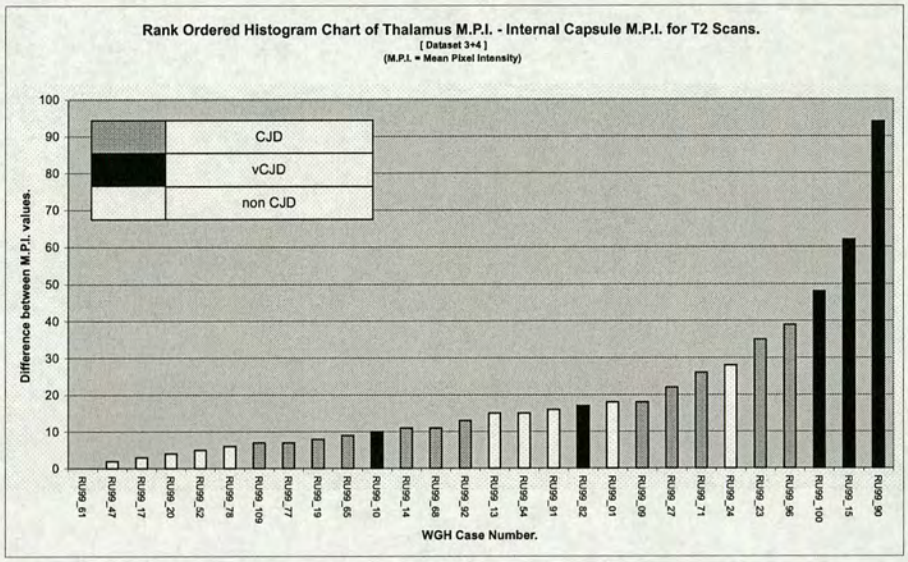

Figure 4.32: Thalamus Tests: *Rank ordered histogram of the difference between the Thalamus region "M.P.I." and the Internal Capsule "M.P.I." values for the T2 weighted MRI scan-data from datasets 3 & 4 combined.*

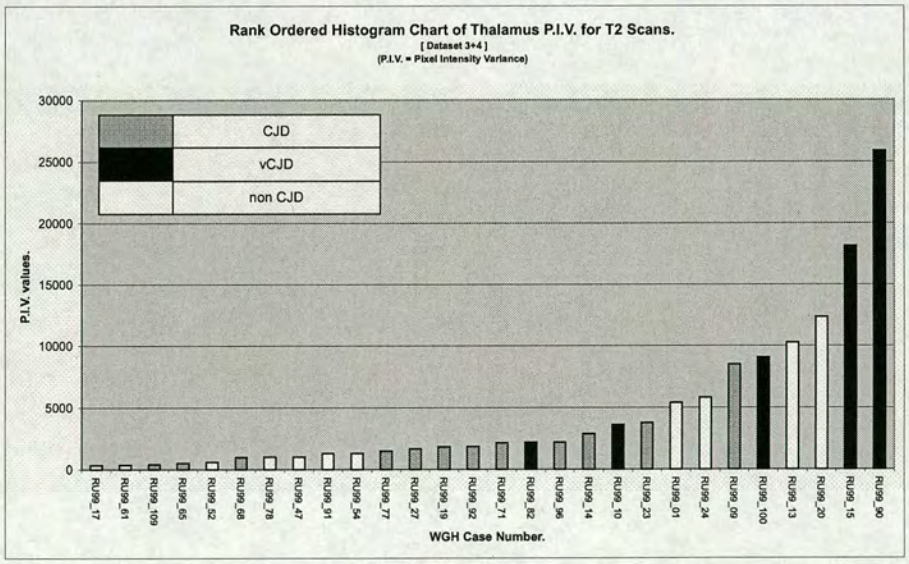

Figure 4.33: Thalamus Tests: *Rank ordered histogram of the Thalamus region "M.P.I." values for the T2 weighted MRI scan-data from datasets 3 & 4 combined.*

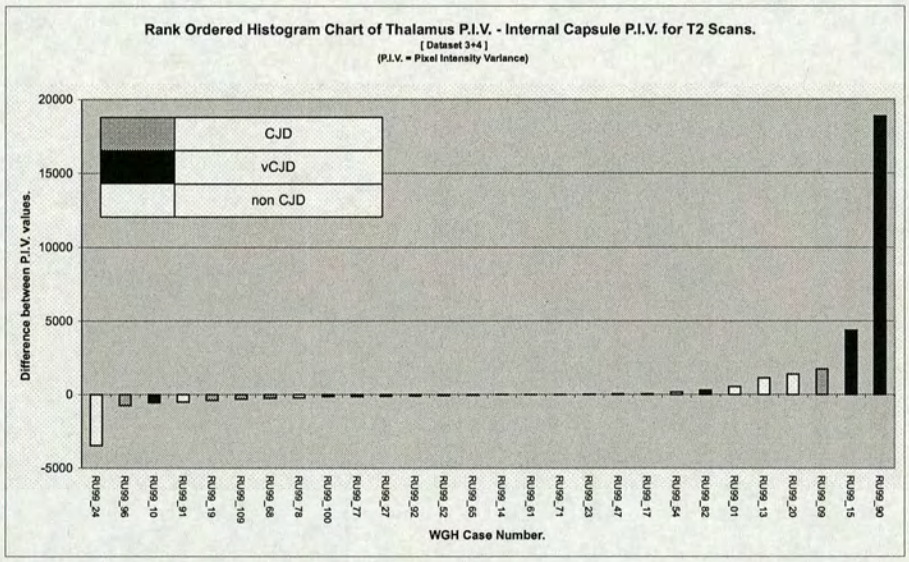

Figure 4.34: Thalamus Tests: *Rank ordered histogram of the difference between the Thalamus region "M.P.I." and the Internal Capsule "M.P.I." values for the T2 weighted MRI scan-data from datasets 3 & 4 combined.*

4.5.3 Analysis of Results of Thalamus Tests

The χ^2 measure of statistical significance was calculated for each of the Thalamus tests and a determination was made of the significance or otherwise of the clustering of CJD and vCJD cases within the dataset.

These measures are listed for each test in tables 4.5 and 4.6.

Figure	Modality	Property	Test	χ^2 (3s.f)	Clustering Sig.
4.19	PD	Thalamus M.P.I.	CJD	0.257	Not Significant
4.19	PD	Thalamus M.P.I.	vCJD	4.48	Not Significant
4.20	PD	Thalamus M.P.I. - I.C. M.P.I.	CJD	4.36	Not Significant
4.20	PD	Thalamus M.P.I. - I.C. M.P.I.	vCJD	2.43	Not Significant
4.21	PD	Thalamus P.I.V.	CJD	2.99	Not Significant
4.21	PD	Thalamus P.I.V.	vCJD	2.43	Not Significant
4.22	PD	Thalamus P.I.V. - I.C. P.I.V.	CJD	2.31	Not Significant
4.22	PD	Thalamus P.I.V. - I.C. P.I.V.	vCJD	5.51	Not Significant
4.23	T2	Thalamus M.P.I.	CJD	4.36	Not Significant
4.23	T2	Thalamus M.P.I.	vCJD	4.48	Not Significant
4.24	T2	Thalamus M.P.I. - I.C. M.P.I.	CJD	6.42	Not Significant
4.24	T2	Thalamus M.P.I. - I.C. M.P.I.	vCJD	6.53	Not Significant
4.25	T2	Thalamus P.I.V.	CJD	1.63	Not Significant
4.25	T2	Thalamus P.I.V.	vCJD	3.48	Not Significant
4.26	T2	Thalamus P.I.V. - I.C. P.I.V.	CJD	1.63	Not Significant
4.26	T2	Thalamus P.I.V. - I.C. P.I.V.	vCJD	5.51	Not Significant

Table 4.5: Thalamus Tests: *Table of results after applying the χ^2 data analysis test to the histograms produced by processing the combined MRI dataset 1 & 2 with the normal mask-set. A key to the column values is provided in Table 4.9*

4.5.4 Discussion of Results of Thalamus Tests

Perhaps surprisingly, dataset 1+2 shows no significant clustering of the data with respect to either CJD or vCJD cases at all. This may imply that the post-mortem data being tested here has a different characterstic to in-vivo data for which a-typical Thalamus findings have often been reported in the literature.

Dataset 3+4 only demonstrated significant data clustering with respect to CJD, albeit with a significance limit of 99%, in a single test. None of the tests revealed significant data clustering with respect to vCJD.

Figure	Modality	Property	Test	χ^2 (3s.f)	Clustering Sig.
4.27	PD	Thalamus M.P.I.	CJD	1.65	Not Significant
4.27	PD	Thalamus M.P.I.	vCJD	0.730	Not Significant
4.28	PD	Thalamus M.P.I. - I.C. M.P.I.	CJD	2.84	Not Significant
4.28	PD	Thalamus M.P.I. - I.C. M.P.I.	vCJD	2.68	Not Significant
4.29	PD	Thalamus P.I.V.	CJD	1.64	Not Significant
4.29	PD	Thalamus P.I.V.	vCJD	0.730	Not Significant
4.30	PD	Thalamus P.I.V. - I.C. P.I.V.	CJD	1.65	Not Significant
4.30	PD	Thalamus P.I.V. - I.C. P.I.V.	vCJD	2.68	Not Significant
4.31	T2	Thalamus M.P.I.	CJD	4.04	Not Significant
4.31	T2	Thalamus M.P.I.	vCJD	6.57	Not Significant
4.32	T2	Thalamus M.P.I. - I.C. M.P.I.	CJD	13.6	99%
4.32	T2	Thalamus M.P.I. - I.C. M.P.I.	vCJD	4.63	Not Significant
4.33	T2	Thalamus P.I.V.	CJD	2.84	Not Significant
4.33	T2	Thalamus P.I.V.	vCJD	6.57	Not Significant
4.34	T2	Thalamus P.I.V. - I.C. P.I.V.	CJD	1.65	Not Significant
4.34	T2	Thalamus P.I.V. - I.C. P.I.V.	vCJD	4.63	Not Significant

Table 4.6: Thalamus Tests: *Table of results after applying the χ^2 data analysis test to the histograms produced by processing the combined MRI dataset 3 & 4 with the normal mask-set. A key to the column values is provided in Table 4.9*

Figure 4.32 appears to show that case number RU99/90 demonstrates an exceptionally high value compared to the rest of the dataset. Examination of the original image revealed a much higher than normal signal level which may imply an anomaly with the datapoint. However, later removal of this case did not appear to affect the overall results produced due to the general low values associated with the majority of the other cases. In addition, this figure shows that the clustering appears to be split across non-neighbouring sample groups, which the χ^2 test correctly permits, and this may imply that separate clustering groups within the gross population of cases may occur. However, to confirm this it will be necessary to observe the same effect occur in other tests.

4.6 Posterior Thalamus Tests

4.6.1 Introduction

This section details the tests that were performed across two combined datasets; dataset 1 plus dataset 2 (1+2) and dataset 3 plus dataset 4 (3+4). For these tests the Region Of Interest (ROI) considered was the Posterior Thalamus which is located in the Basal Ganglia area of the brain and was described earlier in Chapter 2.

In total, 16 Posterior Thalamus tests were conducted; 8 tests on dataset 1+2 and 8 tests on dataset 3+4. Considering the 8 tests conducted per dataset, the breakdown of these tests is as follows.

- 2 tests considering the mean value of the pixels within the ROI; the first ignoring the mean value of the adjacent contrast ROI (the Internal capsule) and the second considering the mean value of the contrast ROI.
- 2 tests considering the variance value of the pixels within the ROI; the first ignoring the variance value of the adjacent contrast ROI (the Internal capsule) and the second considering variance value of the contrast ROI.

These four tests were repeated twice per dataset; once for the Proton Density weighted MRI scans and once for the T2 weighted MRI scans.

4.6.2 Results of Posterior Thalamus Tests

The rank ordered histogram charts of the results of the 16 tests conducted on the two combined datasets when considering the Posterior Thalamus to be the ROI appear here.

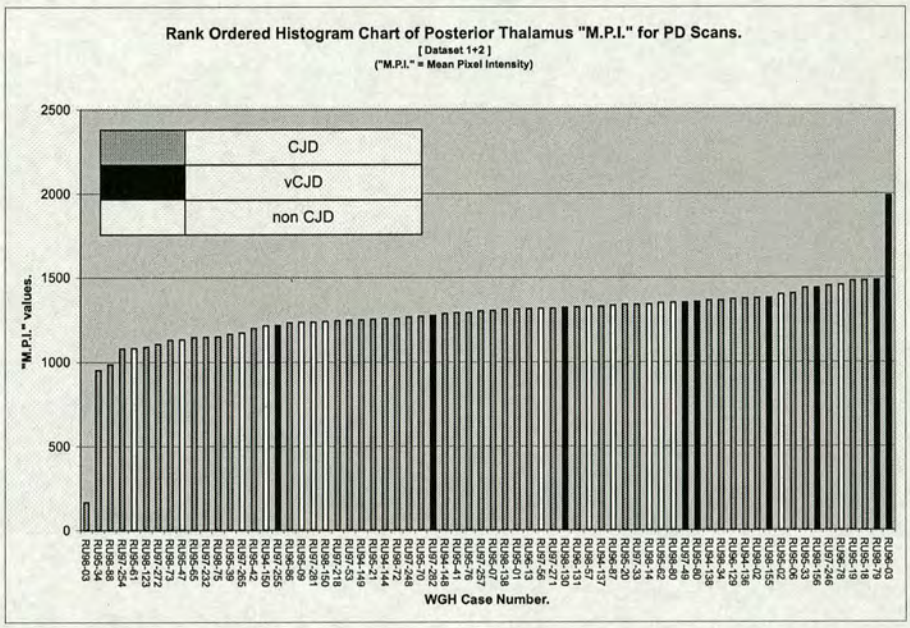

Figure 4.35: Posterior Thalamus Tests: *Rank ordered histogram of the Posterior Thalamus region "M.P.I." values for the PD weighted MRI scan-data from datasets 1 & 2 combined.*

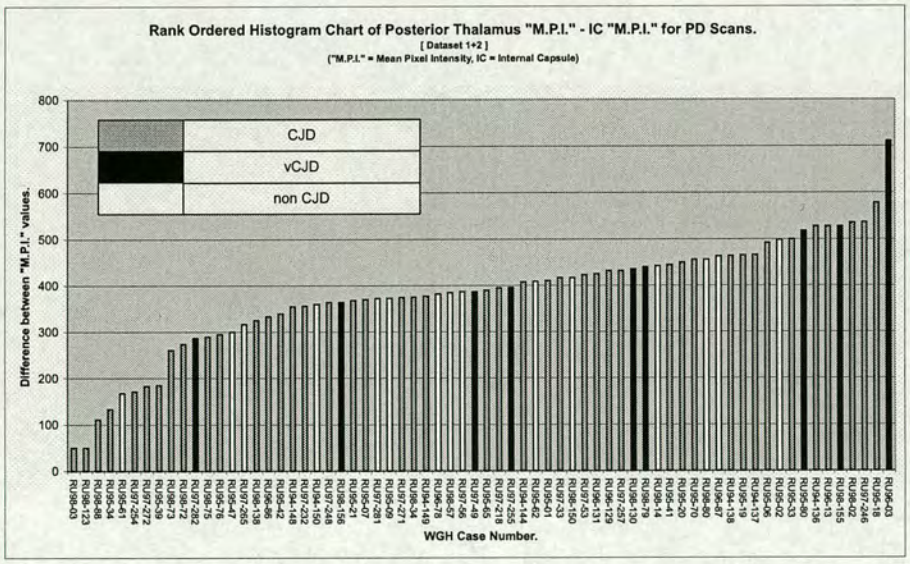

Figure 4.36: Posterior Thalamus Tests: *Rank ordered histogram of the difference between the Posterior Thalamus region "M.P.I." and the Internal Capsule "M.P.I." values for the PD weighted MRI scan-data from datasets 1 & 2 combined.*

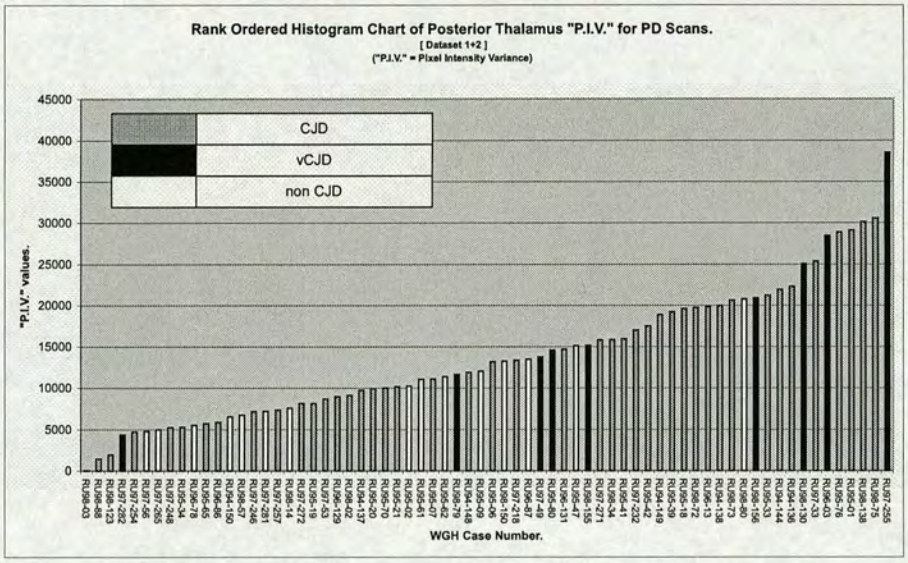

Figure 4.37: Posterior Thalamus Tests: *Rank ordered histogram of the Posterior Thalamus region "M.P.I." values for the PD weighted MRI scan-data from datasets 1 & 2 combined.*

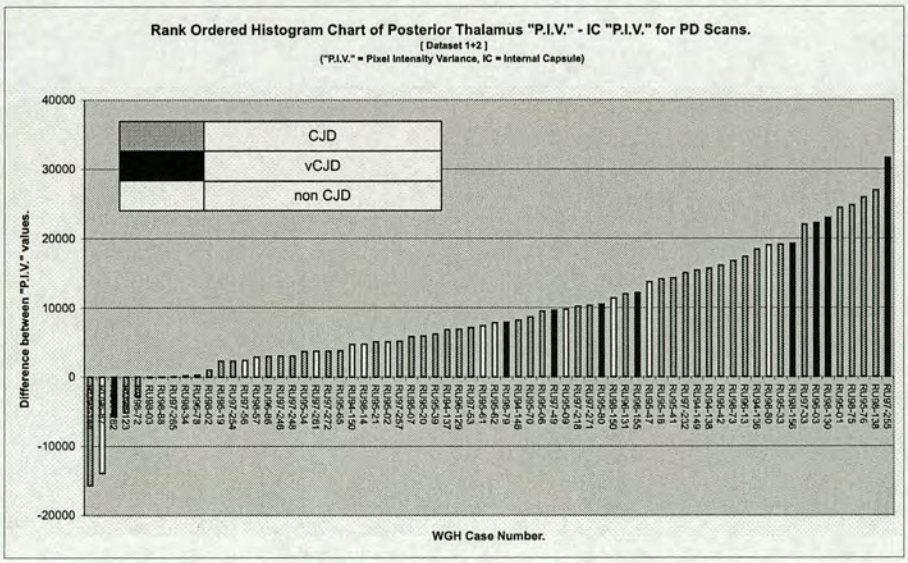

Figure 4.38: Posterior Thalamus Tests: *Rank ordered histogram of the difference between the Posterior Thalamus region "M.P.I." and the Internal Capsule "M.P.I." values for the PD weighted MRI scan-data from datasets 1 & 2 combined.*

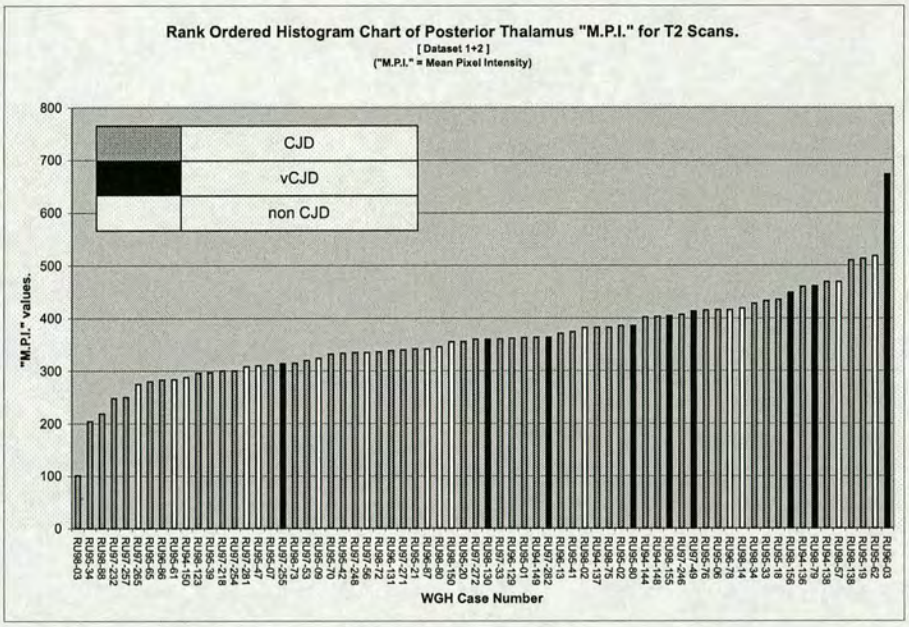

Figure 4.39: Posterior Thalamus Tests: *Rank ordered histogram of the Posterior Thalamus region "M.P.I." values for the T2 weighted MRI scan-data from datasets 1 & 2 combined.*

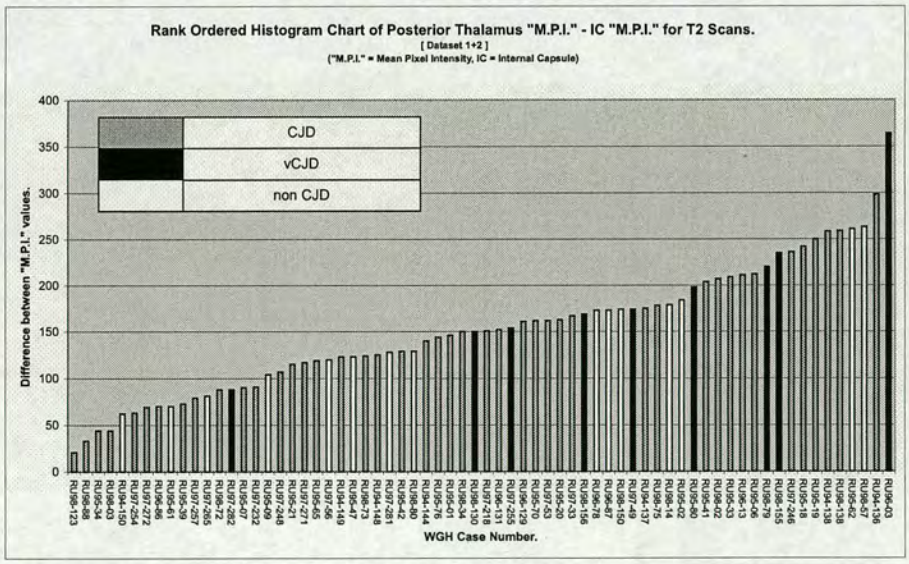

Figure 4.40: Posterior Thalamus Tests: *Rank ordered histogram of the difference between the Posterior Thalamus region "M.P.I." and the Internal Capsule "M.P.I." values for the T2 weighted MRI scan-data from datasets 1 & 2 combined.*

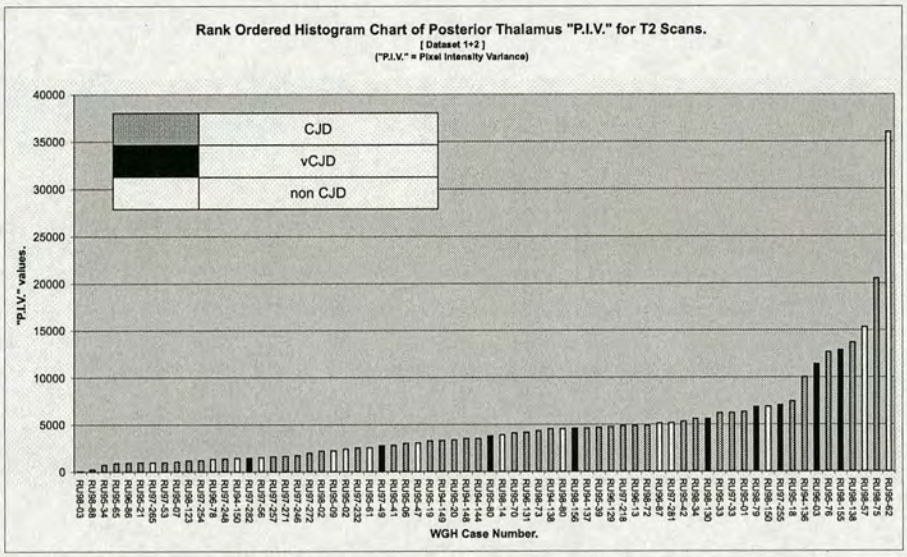

Figure 4.41: Posterior Thalamus Tests: *Rank ordered histogram of the Posterior Thalamus region "M.P.I." values for the T2 weighted MRI scan-data from datasets 1 & 2 combined.*

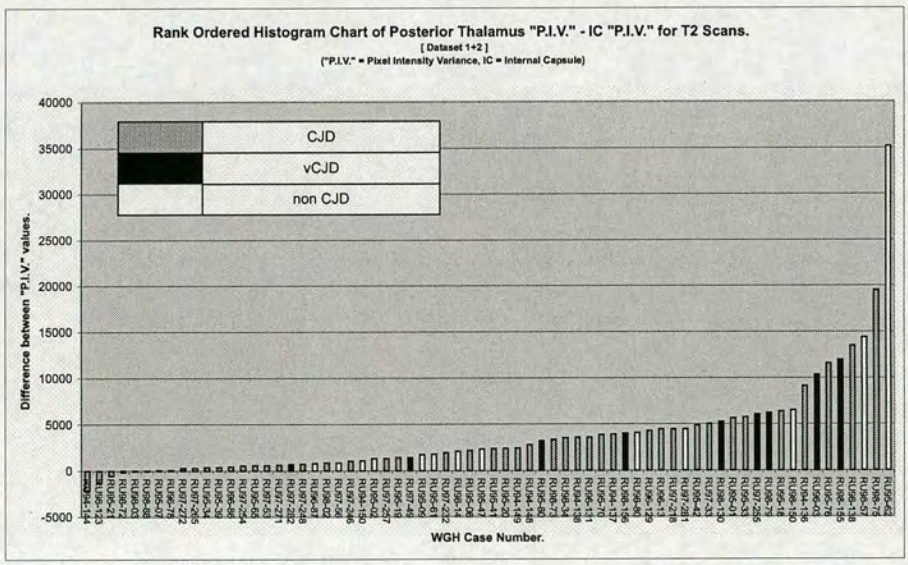

Figure 4.42: Posterior Thalamus Tests: *Rank ordered histogram of the difference between the Posterior Thalamus region "M.P.I." and the Internal Capsule "M.P.I." values for the T2 weighted MRI scan-data from datasets 1 & 2 combined.*

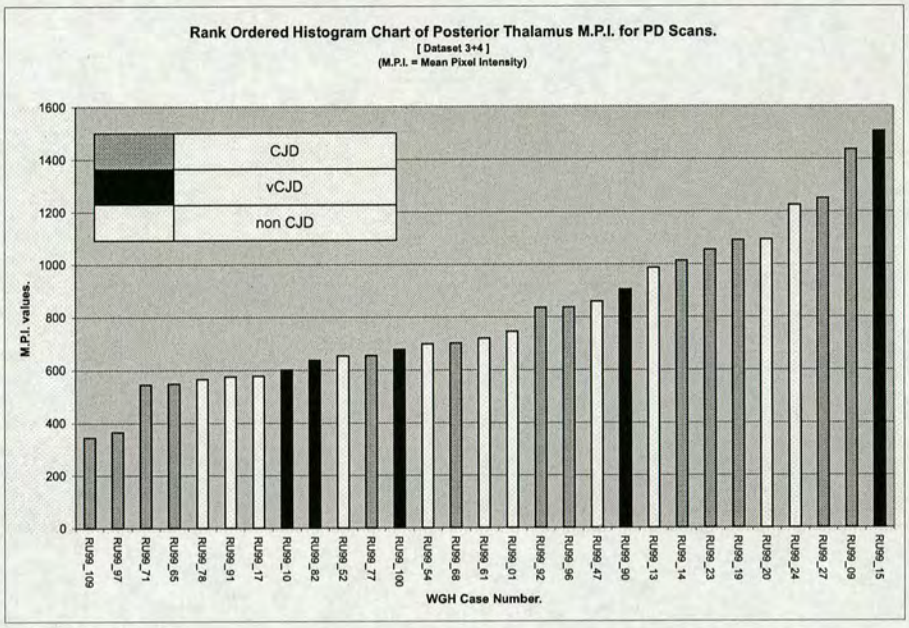

Figure 4.43: Posterior Thalamus Tests: *Rank ordered histogram of the Posterior Thalamus region "M.P.I." values for the PD weighted MRI scan-data from datasets 3 & 4 combined.*

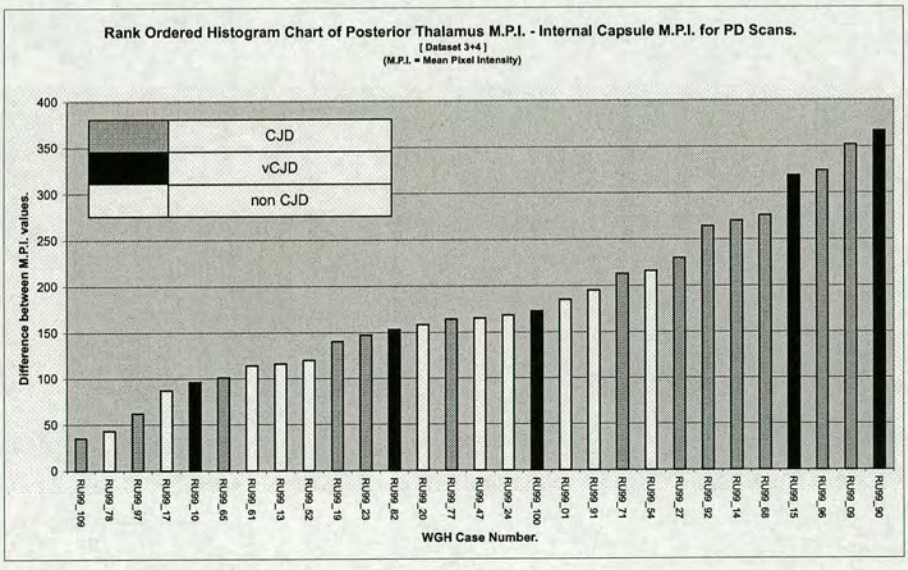

Figure 4.44: Posterior Thalamus Tests: *Rank ordered histogram of the difference between the Posterior Thalamus region "M.P.I." and the Internal Capsule "M.P.I." values for the PD weighted MRI scan-data from datasets 3 & 4 combined.*

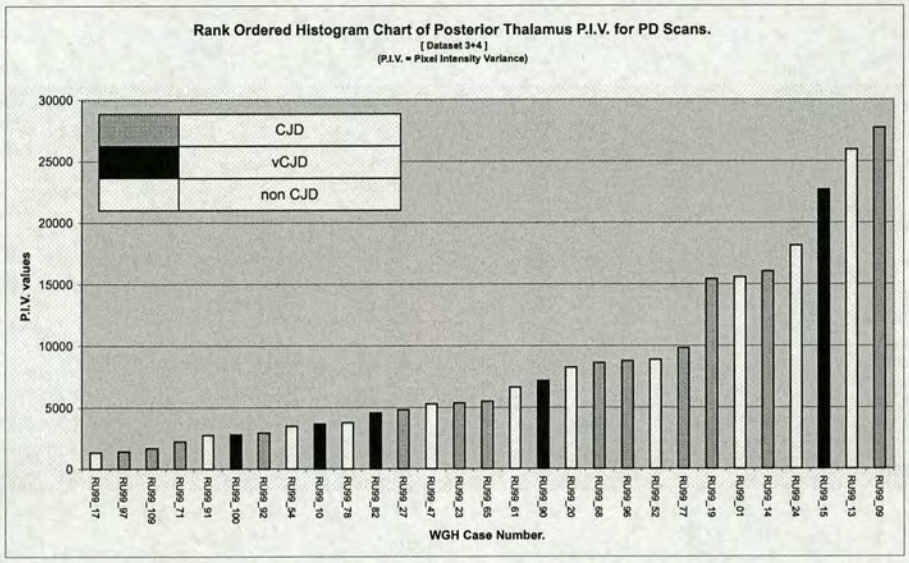

Figure 4.45: Posterior Thalamus Tests: *Rank ordered histogram of the Posterior Thalamus region "M.P.I." values for the PD weighted MRI scan-data from datasets 3 & 4 combined.*

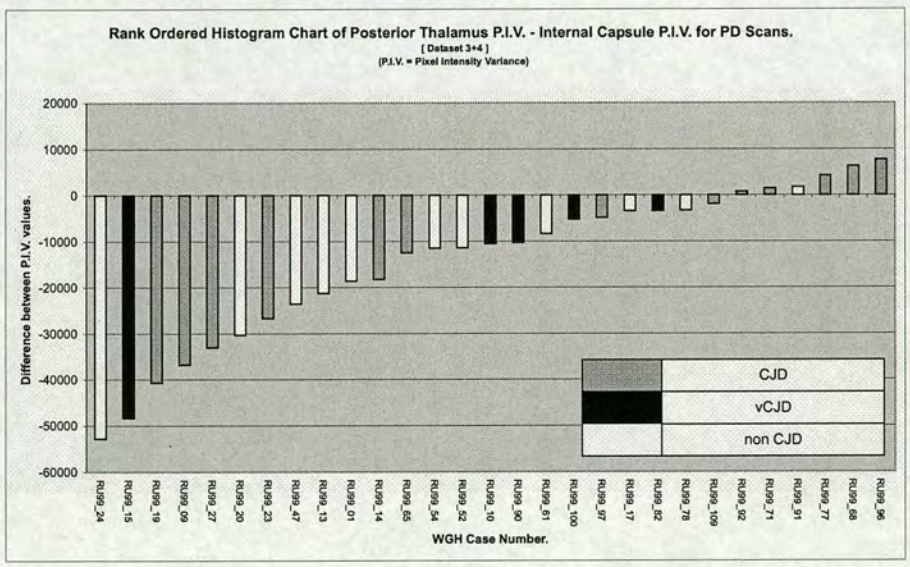

Figure 4.46: Posterior Thalamus Tests: *Rank ordered histogram of the difference between the Posterior Thalamus region "M.P.I." and the Internal Capsule "M.P.I." values for the PD weighted MRI scan-data from datasets 3 & 4 combined.*

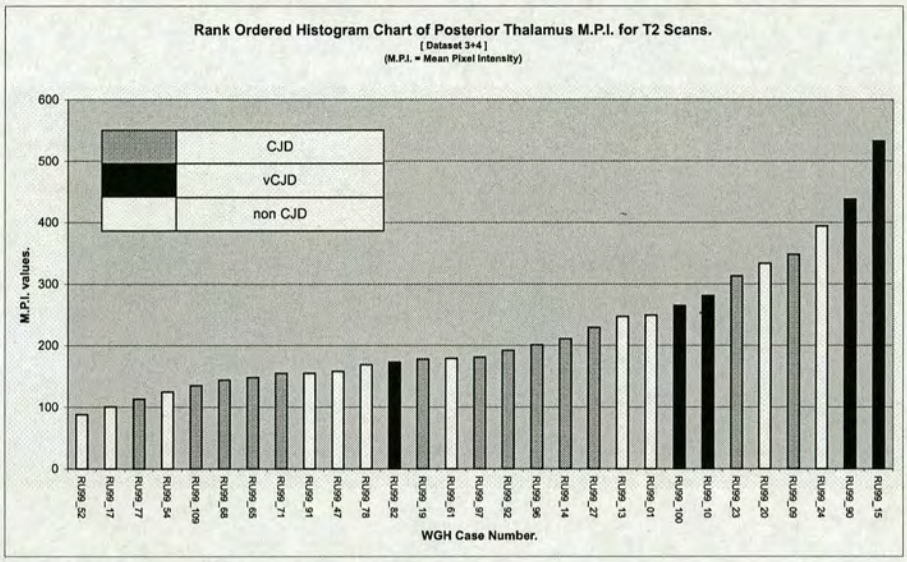

Figure 4.47: Posterior Thalamus Tests: *Rank ordered histogram of the Posterior Thalamus region "M.P.I." values for the T2 weighted MRI scan-data from datasets 3 & 4 combined.*

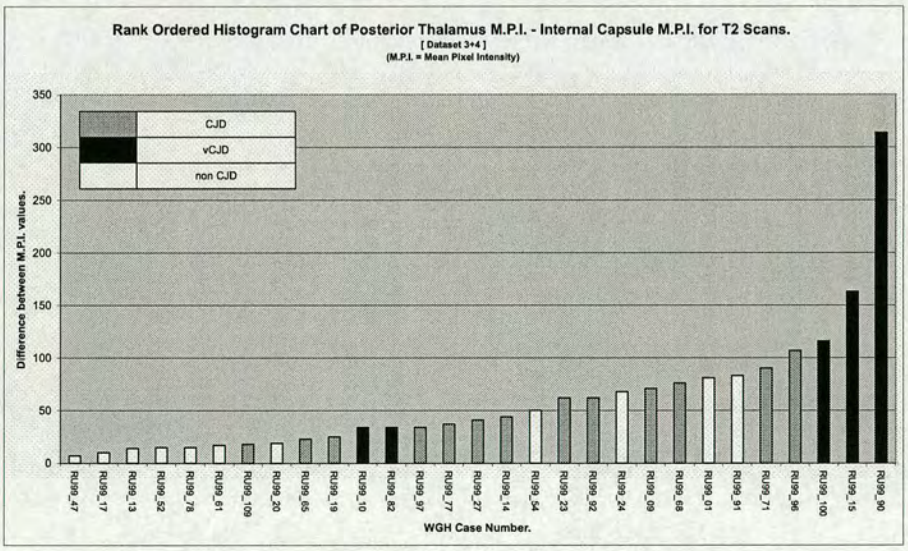

Figure 4.48: Posterior Thalamus Tests: *Rank ordered histogram of the difference between the Posterior Thalamus region "M.P.I." and the Internal Capsule "M.P.I." values for the T2 weighted MRI scan-data from datasets 3 & 4 combined.*

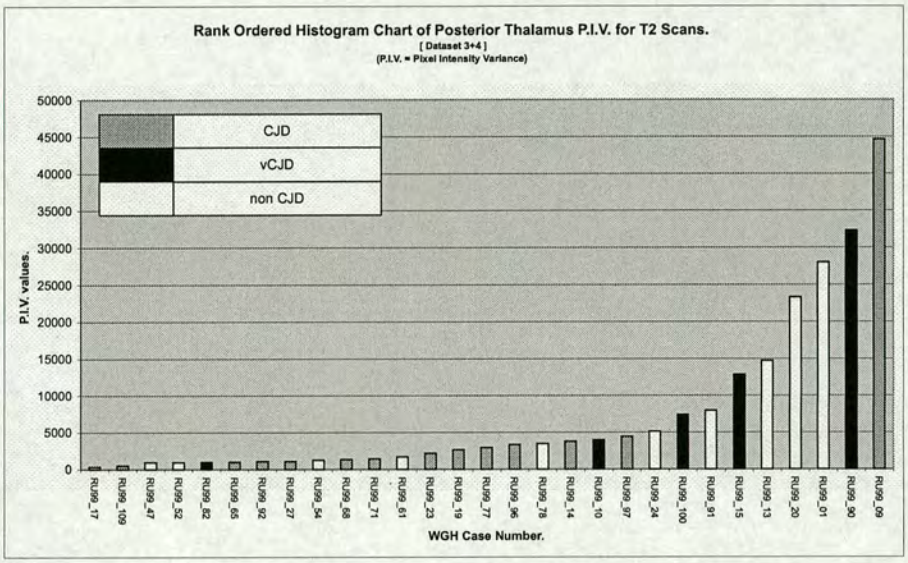

Figure 4.49: Posterior Thalamus Tests: *Rank ordered histogram of the Posterior Thalamus region "M.P.I." values for the T2 weighted MRI scan-data from datasets 3 & 4 combined.*

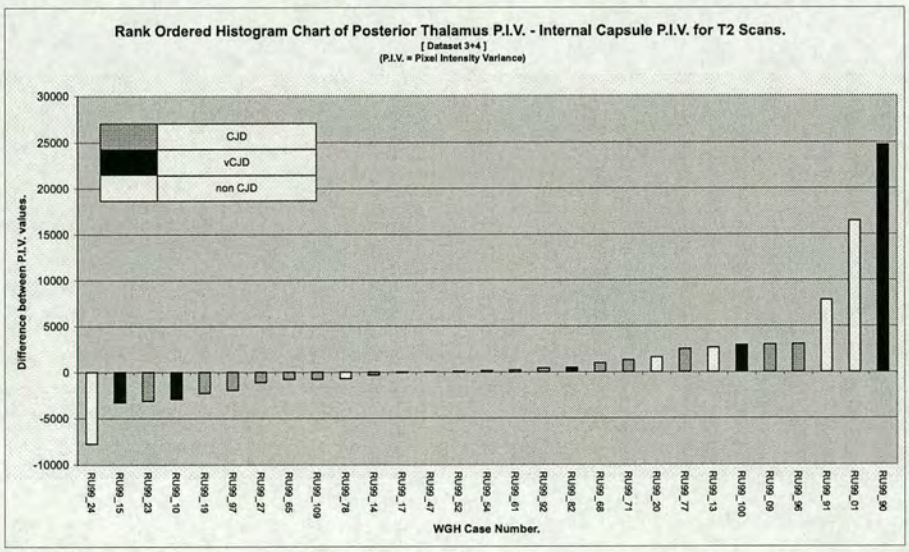

Figure 4.50: Posterior Thalamus Tests: *Rank ordered histogram of the difference between the Posterior Thalamus region "M.P.I." and the Internal Capsule "M.P.I." values for the T2 weighted MRI scan-data from datasets 3 & 4 combined.*

4.6.3 Analysis of Results of Posterior Thalamus Tests

The χ^2 measure of statistical significance was calculated for each of the Posterior Thalamus tests and a determination was made of the significance or otherwise of the clustering of CJD and vCJD cases within the dataset.

These measures are listed for each test in tables 4.7 and 4.8.

Figure	Modality	Property	Test	χ^2 (3s.f)	Clustering Sig.
4.35	PD	P.Thal. M.P.I.	CJD	3.00	Not Significant
4.35	PD	P.Thal. M.P.I.	vCJD	5.51	Not Significant
4.36	PD	P.Thal. M.P.I. - I.C. M.P.I.	CJD	2.31	Not Significant
4.36	PD	P.Thal. M.P.I. - I.C. M.P.I.	vCJD	1.40	Not Significant
4.37	PD	P.Thal. P.I.V.	CJD	5.05	Not Significant
4.37	PD	P.Thal. P.I.V.	vCJD	3.46	Not Significant
4.38	PD	P.Thal. P.I.V. - I.C. P.I.V.	CJD	3.68	Not Significant
4.38	PD	P.Thal. P.I.V. - I.C. P.I.V.	vCJD	6.53	Not Significant
4.39	T2	P.Thal. M.P.I.	CJD	3.68	Not Significant
4.39	T2	P.Thal. M.P.I.	vCJD	6.53	Not Significant
4.40	T2	P.Thal. M.P.I. - I.C. M.P.I.	CJD	1.63	Not Significant
4.40	T2	P.Thal. M.P.I. - I.C. M.P.I.	vCJD	3.46	Not Significant
4.41	T2	P.Thal. P.I.V.	CJD	0.26	Not Significant
4.41	T2	P.Thal. P.I.V.	vCJD	5.51	Not Significant
4.42	T2	P.Thal. P.I.V. - I.C. P.I.V.	CJD	8.47	95%
4.42	T2	P.Thal. P.I.V. - I.C. P.I.V.	vCJD	6.53	Not Significant

Table 4.7: Posterior Thalamus Tests: *Table of results after applying the χ^2 data analysis test to the histograms produced by processing the combined MRI dataset 1 & 2 with the normal mask-set. A key to the column values is provided in Table 4.9*

4.6.4 Discussion of Results of Posterior Thalamus Tests

For dataset 1+2, only one test demonstrated significant clustering of the data with respect to CJD. Dataset 3+4 demonstrated clustering significance in four tests; twice for CJD and twice for vCJD although interestingly the clustering occurred in different tests for each significant result. This may suggest a difference in the signature of the two disease-types on this type of MRI data.

Both the single test from dataset 1+2 and three of the four tests from dataset 3+4 that indicated significant clustering occuring were tests that considered the contrast ROI, the Internal Capsule. In each case, the same test but without consideration of the contrast ROI did not show

Figure	Modality	Property	Test	χ^2 (3s.f)	Clustering Sig.
4.43	PD	P.Thal. M.P.I.	CJD	2.00	Not Significant
4.43	PD	P.Thal. M.P.I.	vCJD	1.85	Not Significant
4.44	PD	P.Thal. M.P.I. - I.C. M.P.I.	CJD	8.37	95%
4.44	PD	P.Thal. M.P.I. - I.C. M.P.I.	vCJD	0.47	Not Significant
4.45	PD	P.Thal. P.I.V.	CJD	0.405	Not Significant
4.45	PD	P.Thal. P.I.V.	vCJD	0.841	Not Significant
4.46	PD	P.Thal. P.I.V. - I.C. P.I.V.	CJD	4.43	Not Significant
4.46	PD	P.Thal. P.I.V. - I.C. P.I.V.	vCJD	11.0	95%
4.47	T2	P.Thal. M.P.I.	CJD	2.00	Not Significant
4.47	T2	P.Thal. M.P.I.	vCJD	8.98	95%
4.48	T2	P.Thal. M.P.I. - I.C. M.P.I.	CJD	9.28	95%
4.48	T2	P.Thal. M.P.I. - I.C. M.P.I.	vCJD	5.85	Not Significant
4.49	T2	P.Thal. P.I.V.	CJD	1.09	Not Significant
4.49	T2	P.Thal. P.I.V.	vCJD	3.85	Not Significant
4.50	T2	P.Thal. P.I.V. - I.C. P.I.V.	CJD	2.83	Not Significant
4.50	T2	P.Thal. P.I.V. - I.C. P.I.V.	vCJD	2.47	Not Significant

Table 4.8: Posterior Thalamus Tests: *Table of results after applying the χ^2 data analysis test to the histograms produced by processing the combined MRI dataset 3 & 4 with the normal mask-set. A key to the column values is provided in Table 4.9*

a significant result. This supports and strengthens the finding from the results of the Putamen tests that consideration of the contrast ROI has a positive effect in most cases.

Label	Description
Clustering Sig.	Significance of Clustering.
PD	Proton Density Weighted M.R.I.
T2	T2 Weighted M.R.I.
P.Thal.	Posterior Thalamus.
I.C.	Internal Capsule.
M.P.I.	Mean Pixel Intensity
P.I.V.	Pixel Intensity Variance
ADJ.	Adjusted Dataset (Clearly erroneous points ommitted.)
CJD	Creutzfeld-Jakob disease.
vCJD	Variant Creutzfeld-Jakob disease.

Table 4.9: Key Table: *Table providing a key to the data-labels used in the results tables that appear earlier on in this chapter.*

4.7 Summary

In this chapter, three key Regions of Interest (ROIs) have been tested and analysed with a view to determining whether or not there is a significant clustering of either CJD or vCJD cases

within the respective data populations when observing this type of MRI scan data.

Of the three ROIs tested (Putamen, Thalamus and Posterior Thalamus), the Putamen appears to consistently demonstrate a significant clustering occuring within the data with respect to CJD. As such, it proved to be the most promising region for use as an indicator of the condition.

By contrast, the Thalamus does not appear to be a good ROI for consideration as an indicator of condition based upon these tests and the specifics of the post-mortem MRI data being tested.

The Posterior Thalamus ROI appears to be marginally more indicative of condition than the Thalamus although this indicator was only seen in three of the tests performed on the data.

One useful finding from the tests performed here is that the consideration of a contrast ROI, here the Internal Capsule, appears to have a marked and beneficial effect on the results of the tests. For the eight tests performed on dataset 1+2 with the Putamen as the ROI, consideration of the contrast ROI improved the final test results in five cases, made no difference in two cases and only worsened the result in one case when compared to the same tests performed whilst ignoring the contrast ROI. This finding would suggest that the adoption of this technique to future tests would probably be beneficial.

The tests performed within this chapter took ROIs based upon the findings of the published body of literature that exists for in-vivo data. The following chapter describes a test that examines an alternative ROI and reports upon the results of running that test. Additionally, a further test designed to examine whether there is a significant difference between the right and left brain with respect to these tests is described and reported.

Chapter 5
Further Analysis of Post Mortem MRI

5.1 Overview

This chapter describes two additional tests that were conducted on the post-mortem MRI datasets which were the focus of this work.

The first test is similar to those described and reported on in the previous chapter but here considers a new Region of Interest (ROI) which has been selected for alternative reasons to those which suggested the selection of the original ROIs already considered.

The second test, although conducted in a similar manner to earlier tests, seeks to determine whether the brain exhibits a symmetric effect in these tests or whether the right and left hemispheres of the brain provide differing results when considered independently.

Both tests are presented in the same manner as those of Chapter 4 to preserve familiarity with the format of reporting used here.

5.2 White Matter Changes Tests

5.2.1 Introduction

It was already discussed in Chapter 2 that Creutzfeld-Jakob disease (CJD) is difficult to diagnose in the clinical enviromnment, and although clinical practice is constantly improving, thereby allowing ever more accurate diagnoses to be made, the similarity of symptoms between CJD and other acute degenerative neurological disorders can still inhibit the process of reaching an accurate and correct diagnosis.

To this end, following discussions with a neuro-pathologist experienced with CJD and other

neuro-degenerative disorders, an alternative ROI was identified that might permit better seperation between CJD and non-CJD cases such as Alzheimer's disease. The ROI selected is an area of white matter in the cerebral cortex which is called the Centrum Semiovale.

The Centrum Semiovale is the collective name for all the white matter in the cerebral hemisphere; its name has the meaning "half oval centre" and it is located higher in the brain than the Basal Ganglia regions that have been examined in the previous chapter.

By creating a set of mask images for the Centrum Semiovale to allow this new ROI to be segmented, a similar set of tests may be conducted.

In total, 8 Centrum Semiovale tests were conducted; 4 tests on dataset 1+2 and 4 tests on dataset 3+4. Considering the 4 tests conducted per dataset, the breakdown of these tests is as follows.

- 2 tests considering the mean value of the pixels within the ROI; the first for the PD modality MRI data and the second for the T2 modality MRI data.
- 2 tests considering the variance value of the pixels within the ROI; the first for the PD modality MRI data and the second for the T2 modality MRI data.

5.2.2 Results of White Matter Changes Tests

The rank ordered histogram charts of the results of the 8 tests conducted on the two combined datasets when considering the Centrum Semiovale to be the ROI appear here.

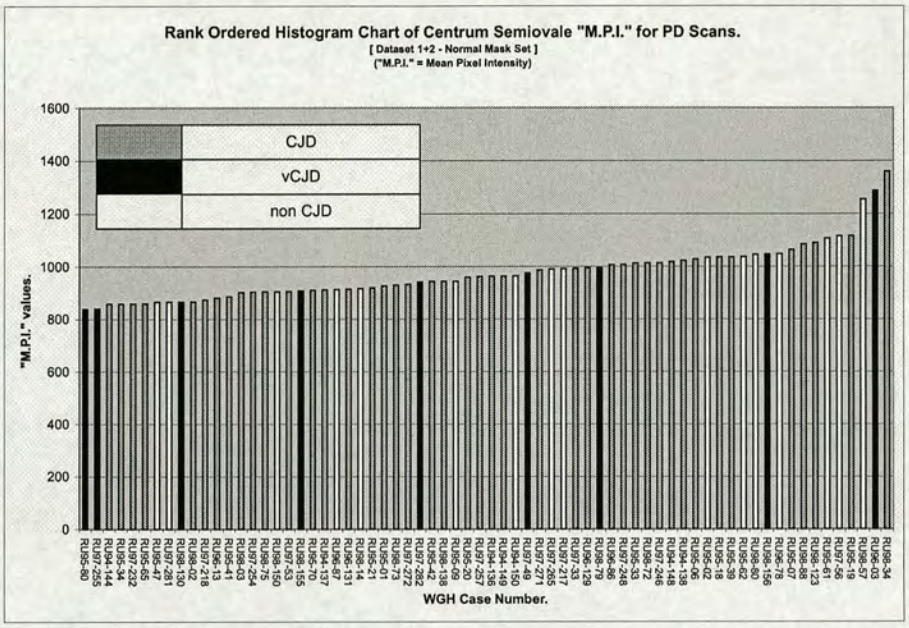

Figure 5.1: White Matter Changes Tests: *Rank ordered histogram of Centrum Semiovale "M.P.I." for the PD weighted MRI scan-data.*

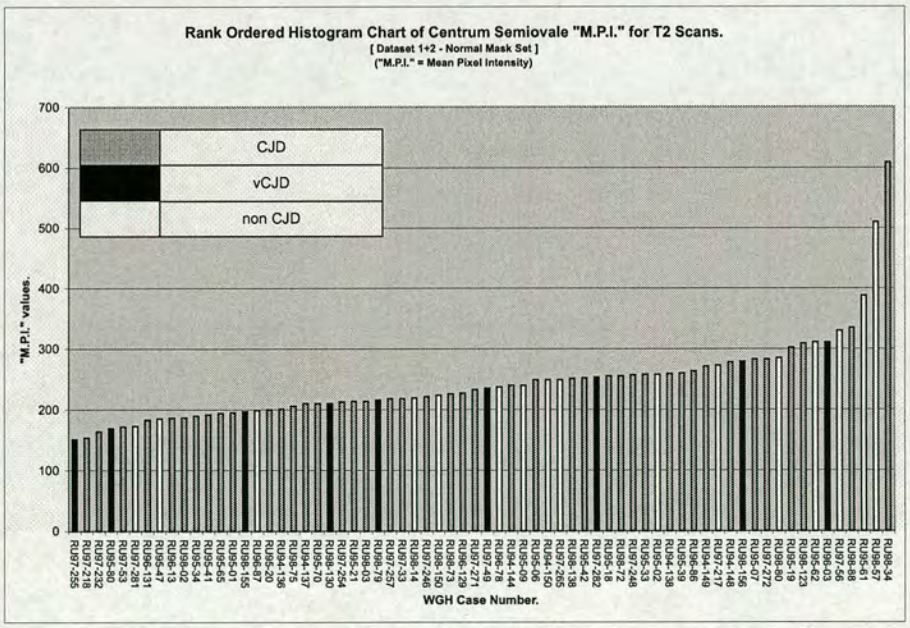

Figure 5.2: White Matter Changes Tests: *Rank ordered histogram of Centrum Semiovale "M.P.I." for the T2 weighted MRI scan-data.*

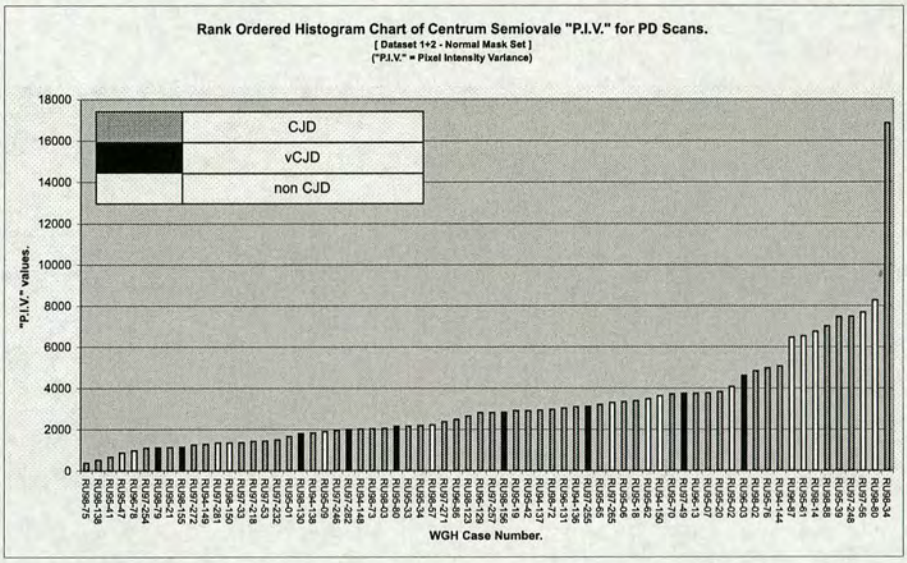

Figure 5.3: White Matter Changes Tests: *Rank ordered histogram of Centrum Semiovale "P.I.V." for the PD weighted MRI scan-data.*

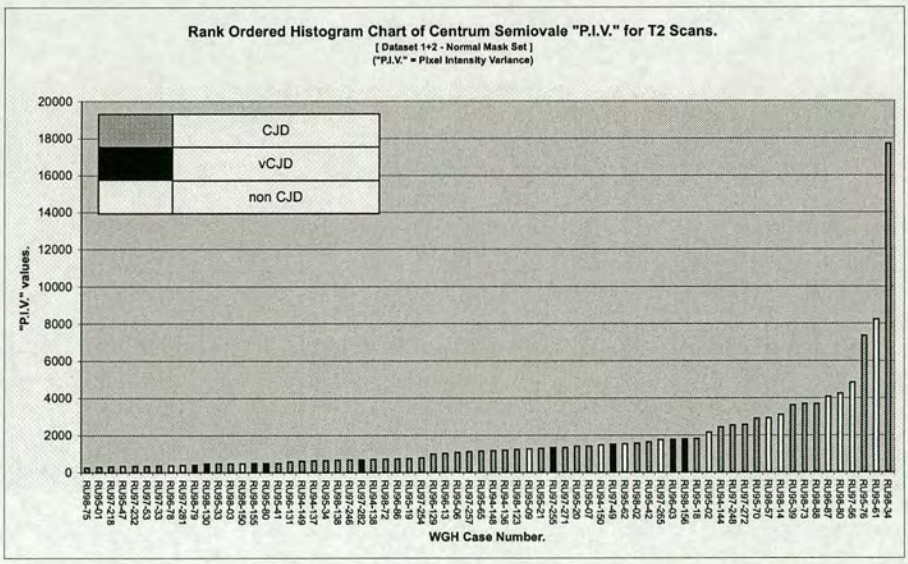

Figure 5.4: White Matter Changes Tests: *Rank ordered histogram of Centrum Semiovale "P.I.V." for the T2 weighted MRI scan-data.*

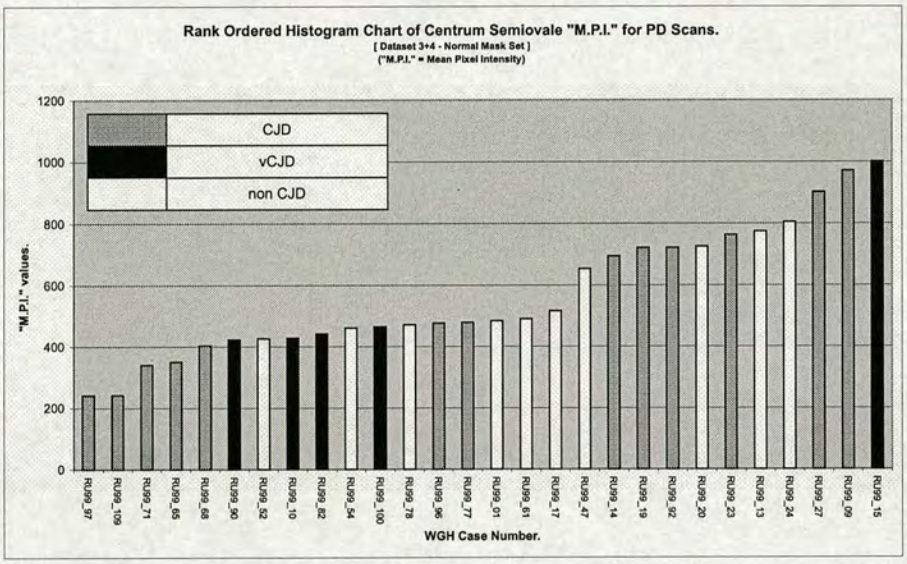

Figure 5.5: White Matter Changes Tests: *Rank ordered histogram of Centrum Semiovale "M.P.I." for the PD weighted MRI scan-data.*

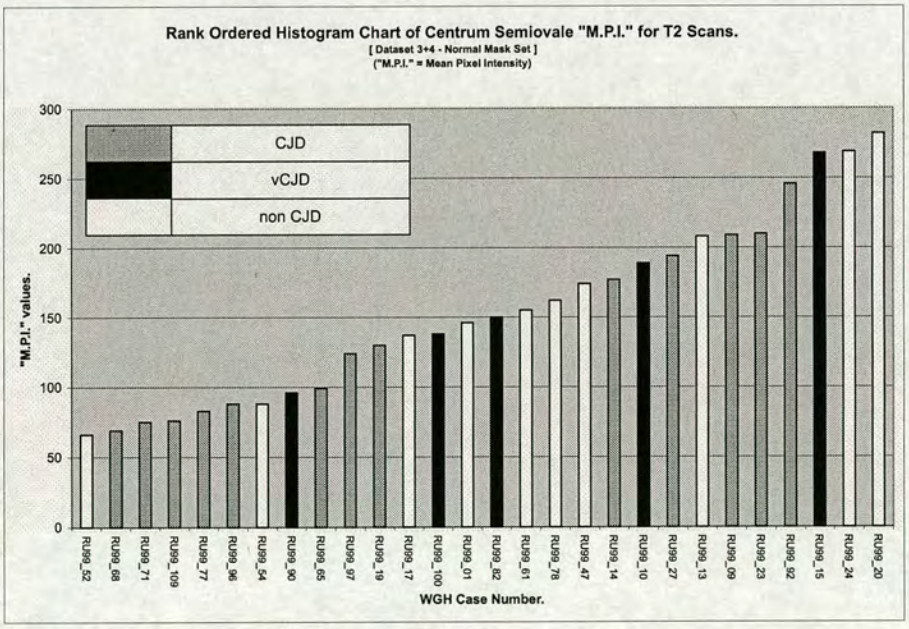

Figure 5.6: White Matter Changes Tests: *Rank ordered histogram of Centrum Semiovale "M.P.I." for the T2 weighted MRI scan-data.*

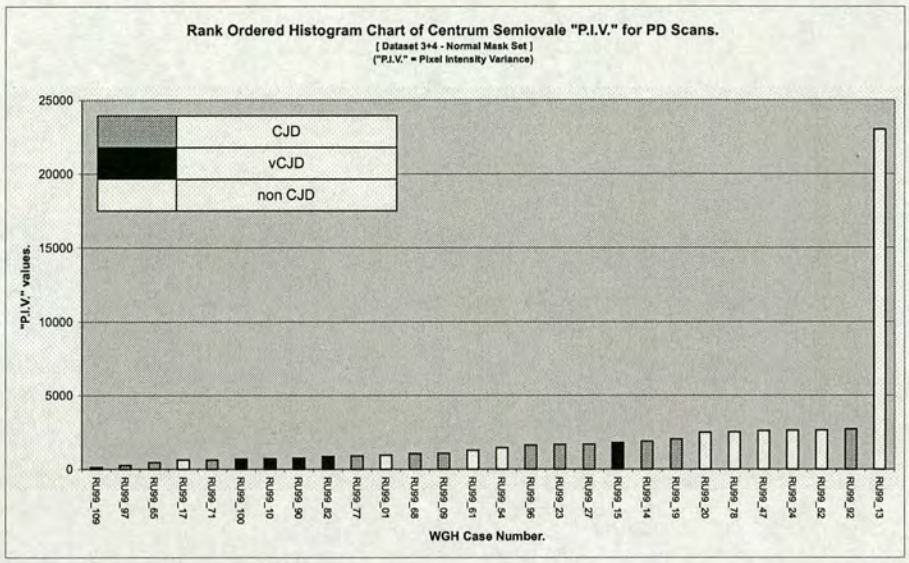

Figure 5.7: White Matter Changes Tests: *Rank ordered histogram of Centrum Semiovale "P.I.V." for the PD weighted MRI scan-data.*

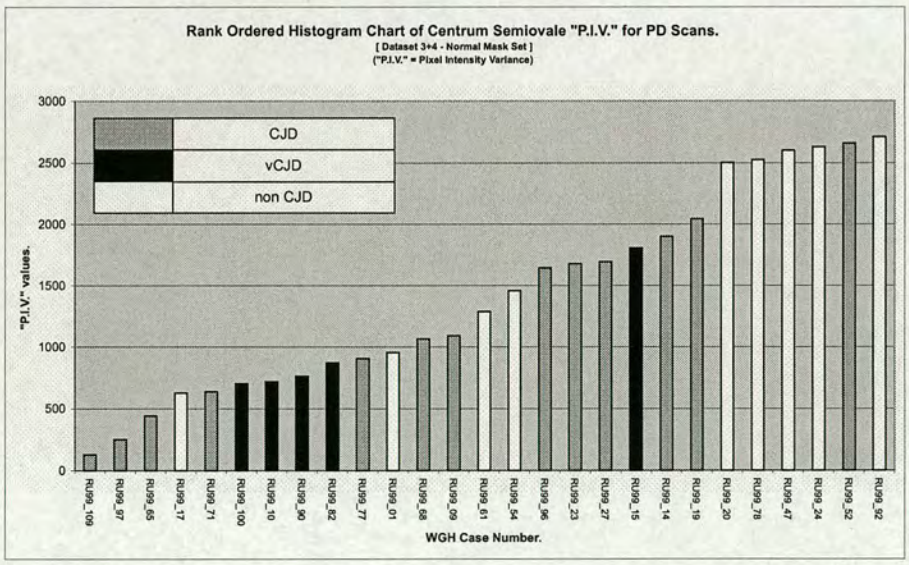

Figure 5.8: White Matter Changes Tests: *Rank ordered histogram of Centrum Semiovale "P.I.V." for the PD weighted MRI scan-data with anomalous data removed.*

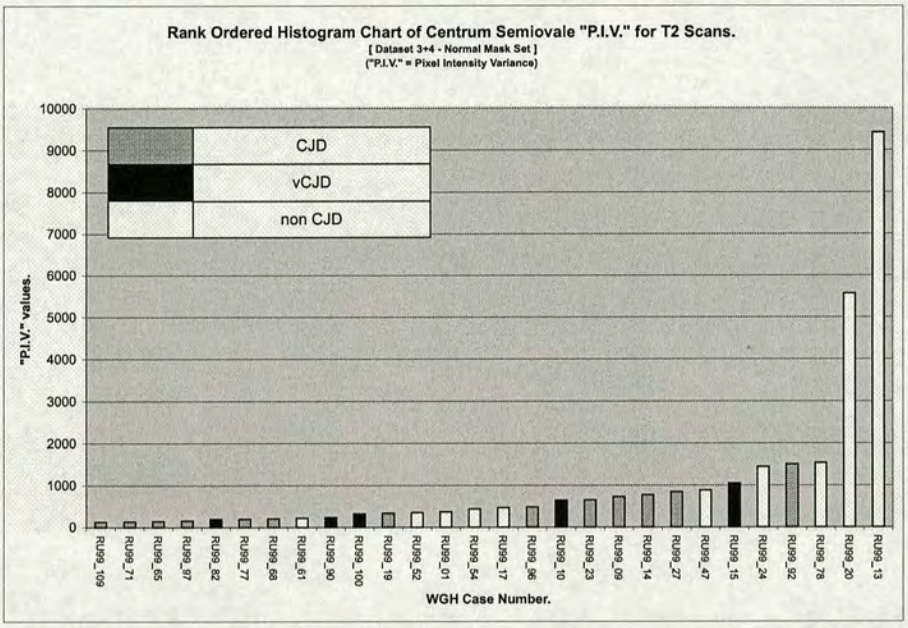

Figure 5.9: White Matter Changes Tests: *Rank ordered histogram of Centrum Semiovale "P.I.V." for the T2 weighted MRI scan-data.*

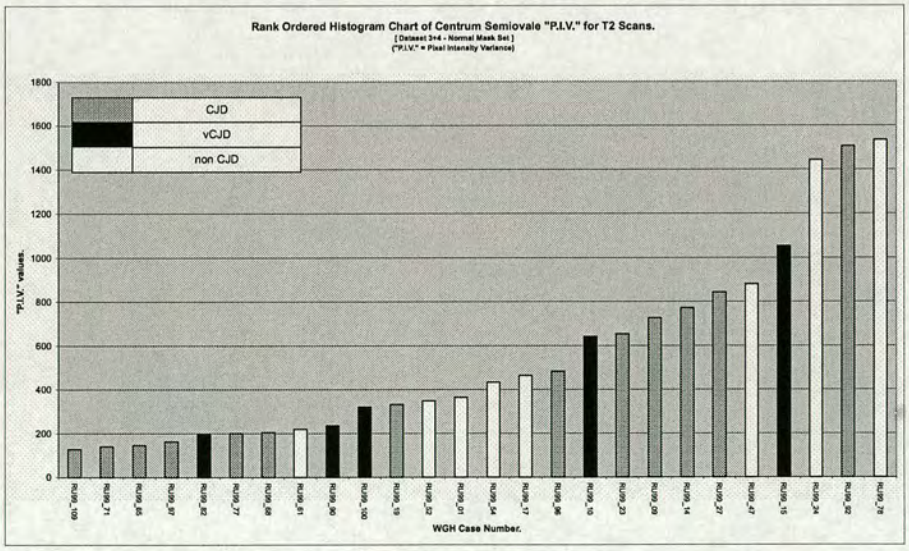

Figure 5.10: White Matter Changes Tests: *Rank ordered histogram of Centrum Semiovale "P.I.V." for the T2 weighted MRI scan-data with anomalous data removed.*

5.2.3 Analysis of Results of White Matter Changes Tests

The χ^2 measure of statistical significance was calculated for each of the White Matter Changes tests and a determination was made of the significance or otherwise of the clustering of CJD and vCJD cases within the dataset.

These measures are listed for each test in tables 5.1 and 5.2.

Figure	Modality	Property	Test	χ^2 (3s.f)	Clustering Sig.
5.1	PD	Cent.S'vale. M.P.I.	CJD	3.37	Not Significant
5.1	PD	Cent.S'vale. M.P.I.	vCJD	0.426	Not Significant
5.3	PD	Cent.S'vale. P.I.V.	CJD	2.99	Not Significant
5.3	PD	Cent.S'vale. P.I.V.	vCJD	1.41	Not Significant
5.2	T2	Cent.S'vale. M.P.I.	CJD	3.27	Not Significant
5.2	T2	Cent.S'vale. M.P.I.	vCJD	0.384	Not Significant
5.4	T2	Cent.S'vale. P.I.V.	CJD	8.47	95%
5.4	T2	Cent.S'vale. P.I.V.	vCJD	6.53	Not Significant

Table 5.1: White Matter Changes Tests: *Table of results after applying the χ^2 data analysis test to the histograms produced by processing the combined MRI dataset 1 & 2 with the normal mask-set for this data. A key to the column values is provided in Table 5.6*

Figure	Modality	Property	Test	χ^2 (3s.f)	Clustering Sig.
5.5	PD	Cent.S'vale. M.P.I.	CJD	3.11	Not Significant
5.5	PD	Cent.S'vale. M.P.I.	vCJD	4.63	Not Significant
5.7	PD	Cent.S'vale. P.I.V.	CJD	10.6	95%
5.7	PD	Cent.S'vale. P.I.V.	vCJD	2.68	Not Significant
5.8	PD	Cent.S'vale. P.I.V. ADJ.	CJD	9.11	95%
5.8	PD	Cent.S'vale. P.I.V. ADJ.	vCJD	2.38	Not Significant
5.6	T2	Cent.S'vale. M.P.I.	CJD	0.622	Not Significant
5.6	T2	Cent.S'vale. M.P.I.	vCJD	2.68	Not Significant
5.9	T2	Cent.S'vale. P.I.V.	CJD	10.6	95%
5.9	T2	Cent.S'vale. P.I.V.	vCJD	0.730	Not Significant
5.10	T2	Cent.S'vale. P.I.V. ADJ.	CJD	8.30	95%
5.10	T2	Cent.S'vale. P.I.V. ADJ.	vCJD	0.616	Not Significant

Table 5.2: White Matter Changes Tests: *Table of results after applying the χ^2 data analysis test to the histograms produced by processing the combined MRI dataset 3 & 4 with the normal mask-set for this data. A key to the column values is provided in Table 5.6*

5.2.4 Discussion of Results of White Matter Changes Tests

Two of the tests on dataset 3+4 appeared to be affected by a small number (1 or 2) of cases with extremely anomalous values which skewed distribution of data on the resultant charts. For

these two cases (both the P.I.V. tests) the same results were also plotted without including the "1 or 2" erroneous cases in each instance. This explains the presence of the two "ADJ." or adjusted charts in the results previously.

The results of running these tests on dataset 1+2 largely shows no significant clustering of the data to reveal whether or not the CJD and the Not-CJD cases are separable. One test produced a 95% significant result for clustering of CJD cases and this was with regard to the variance of the ROI.

However, for dataset 3+4, two of the original tests demonstrated statistically significant clustering with respect to CJD and the two adjusted sets of results also demonstrated similar levels of significance.

In all cases, the significant clustering has only been seen from tests considering the ROI variance values. This might suggest that the variance is a useful measure with indicator potential in future experiments on the Centrum Semiovale.

In general, these results do appear to suggest that the Centrum Semiovale may be a useful ROI for potential CJD condition indicator purposes. In some cases, it was more indicative than the more commonly considered ROIs examined in the previous chapter.

5.3 Bilateral Symmetry Tests

5.3.1 Introduction

In-vivo MRI scan data always, excepting extremely bizarre circumstances, has the whole brain organ available for imaging. However, due to various requirements and needs from different bodies in the medical community, when post-mortem scans are the issue it is more and more likely that only a portion, typically one half of the brain organ will be available for scanning.

This would naturally raise the concern that if there were a fundamental difference between the left and right brain characteristics with respect to their appearance on a post-mortem MRI or to their prior susceptibility to and modification by a condition such as CJD then by only viewing half of the brain organ important details might not be present for detection where a

whole brain organ would provide the opportunity.

To investigate this, a new test was devised to look at the left and right hemispheres of the brain independently and then to compare the results to an original case where the left and right hemispheres were considered together as part of a whole brain.

Taking the combined dataset 1 plus dataset 2 (1+2) for this test and considering the Putamen ROI, which was shown previously to be the most conistent and reliable indicator so far for CJD, two additional mask sets were created based upon the original mask set for the Putamen but in each case either the left hemisphere or the right hemisphere was removed respectively.

This would allow three series of tests to be run: The first considering the whole brain (leftside + rightside) masks, the second considering only the leftside masks and the third considering only the rightside masks.

In total, for each of the three series of masks, 24 Putamen tests were conducted; 8 tests on dataset 1+2 and 8 tests on dataset 3+4 for the three different masksets. Considering the 8 tests conducted per maskset, the breakdown of these tests is as follows.

- 2 tests considering the mean value of the pixels within the ROI; the first ignoring the mean value of the adjacent contrast ROI (the Internal capsule) and the second considering the mean value of the contrast ROI.
- 2 tests considering the variance value of the pixels within the ROI; the first ignoring the variance value of the adjacent contrast ROI (the Internal capsule) and the second considering variance value of the contrast ROI.

These four tests were repeated twice per dataset; once for the Proton Density weighted MRI scans and once for the T2 weighted MRI scans.

5.3.2 Results of Bilateral Symmetry Tests

The rank ordered histogram charts of the results of the 24 tests conducted on the two combined datasets when considering the Putamen to be the ROI appear here. The first 8 consider the whole

brain maskset, the next 8 consider the leftside maskset and the final 8 consider the rightside maskset.

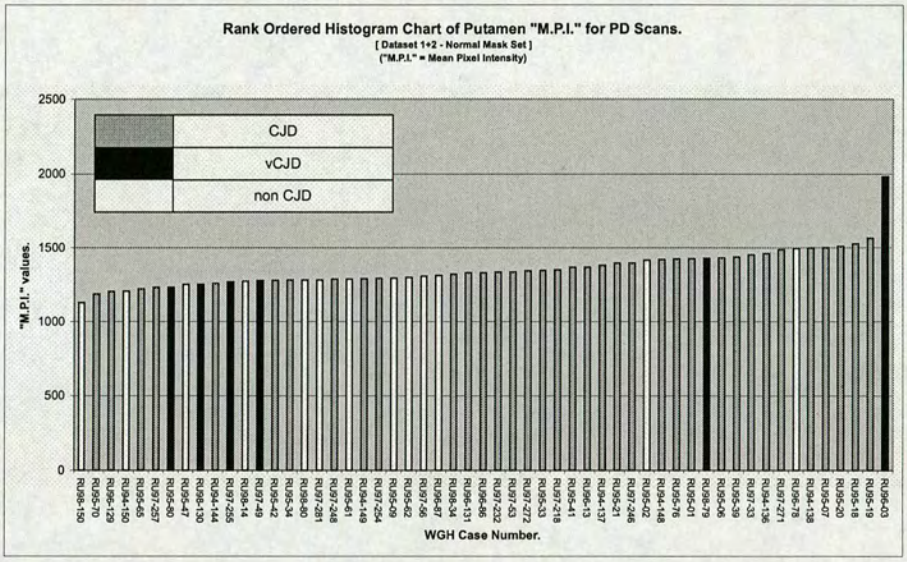

Figure 5.11: Bilateral Symmetry Tests: *Rank ordered histogram of the Putamen "M.P.I." for the PD weighted MRI scan-data from the combined data-sets 1 & 2 generated using the normal (leftside+rightside) mask image-set.*

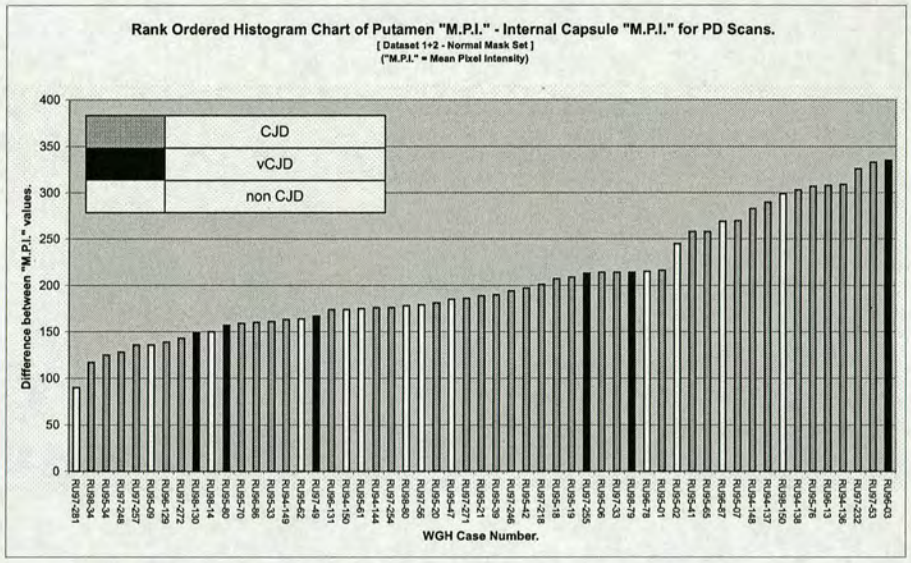

Figure 5.12: Bilateral Symmetry Tests: *Rank ordered histogram of the difference between the Putamen "M.P.I." and the Internal Capsule "M.P.I." for the PD weighted MRI scan-data from the combined data-sets 1 & 2 generated using the normal (leftside+rightside) mask image-set.*

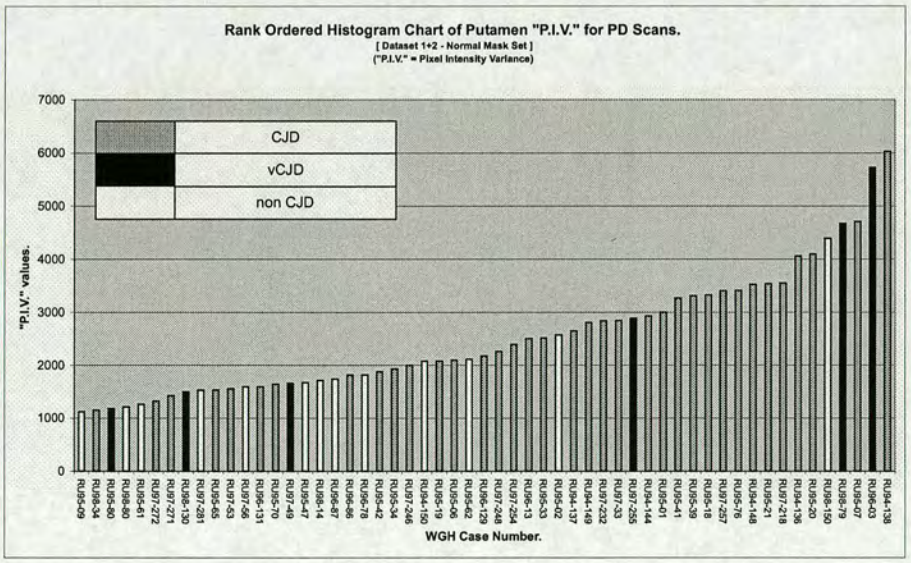

Figure 5.13: Bilateral Symmetry Tests: *Rank ordered histogram of the Putamen "P.I.V." for the PD weighted MRI scan-data from the combined data-sets 1 & 2 generated using the normal (leftside+rightside) mask image-set.*

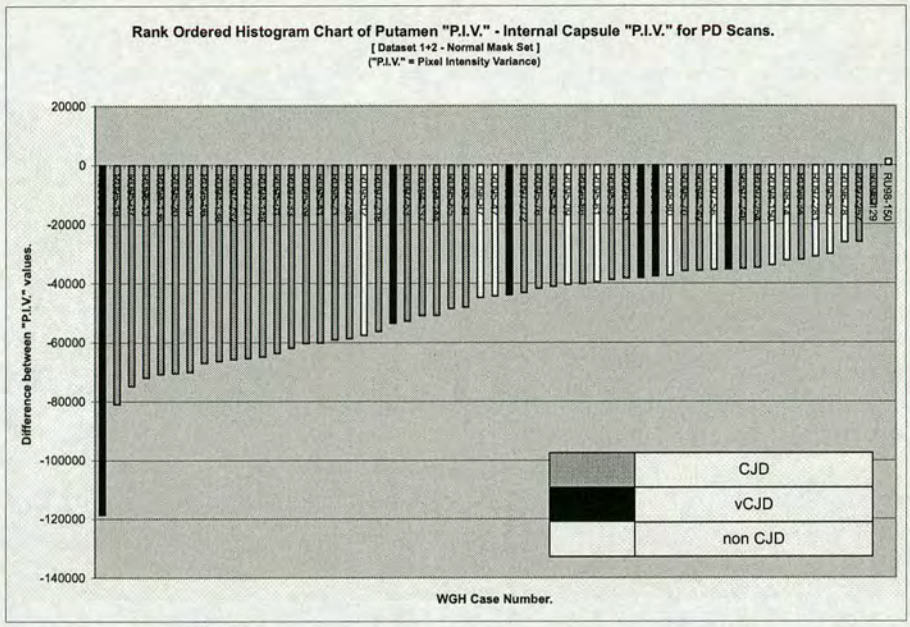

Figure 5.14: Bilateral Symmetry Tests: *Rank ordered histogram of the difference between the Putamen "P.I.V" and the Internal Capsule "P.I.V." for the PD weighted MRI scan-data from the combined data-sets 1 & 2 generated using the normal (left-side+rightside) mask image-set.*

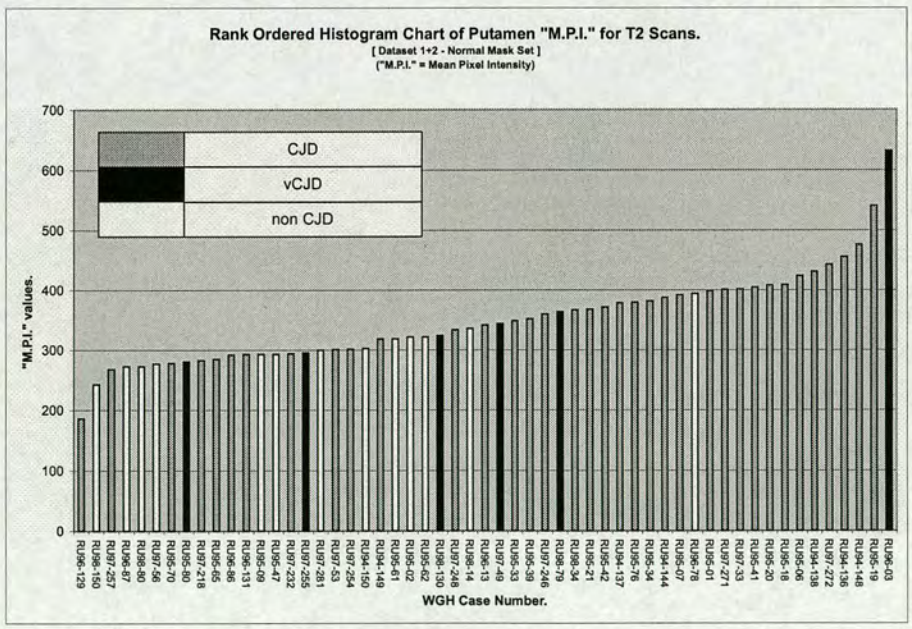

Figure 5.15: Bilateral Symmetry Tests: *Rank ordered histogram of the Putamen "M.P.I." for the T2 weighted MRI scan-data from the combined data-sets 1 & 2 generated using the normal (leftside+rightside) mask image-set.*

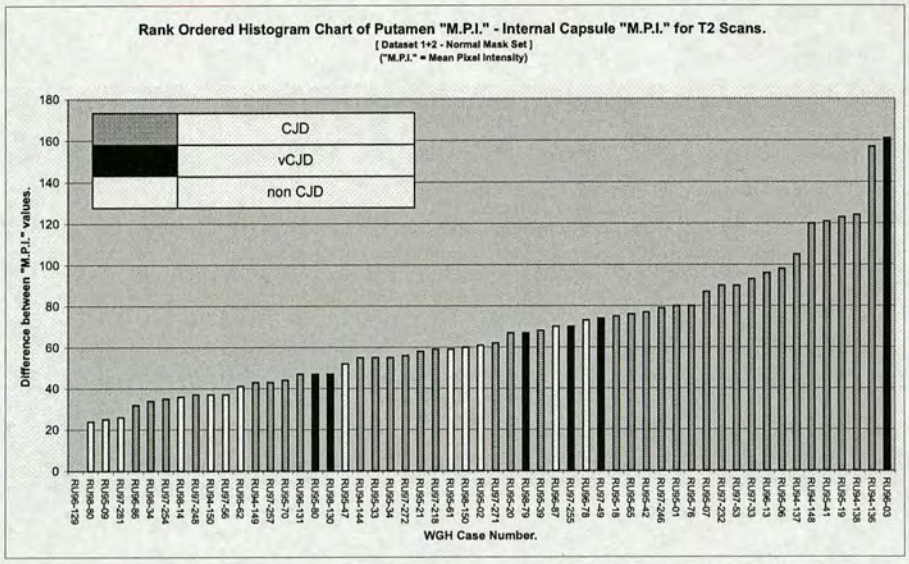

Figure 5.16: Bilateral Symmetry Tests: *Rank ordered histogram of the difference between the Putamen "M.P.I." and the Internal Capsule "M.P.I." for the T2 weighted MRI scan-data from the combined data-sets 1 & 2 generated using the normal (left-side+rightside) mask image-set.*

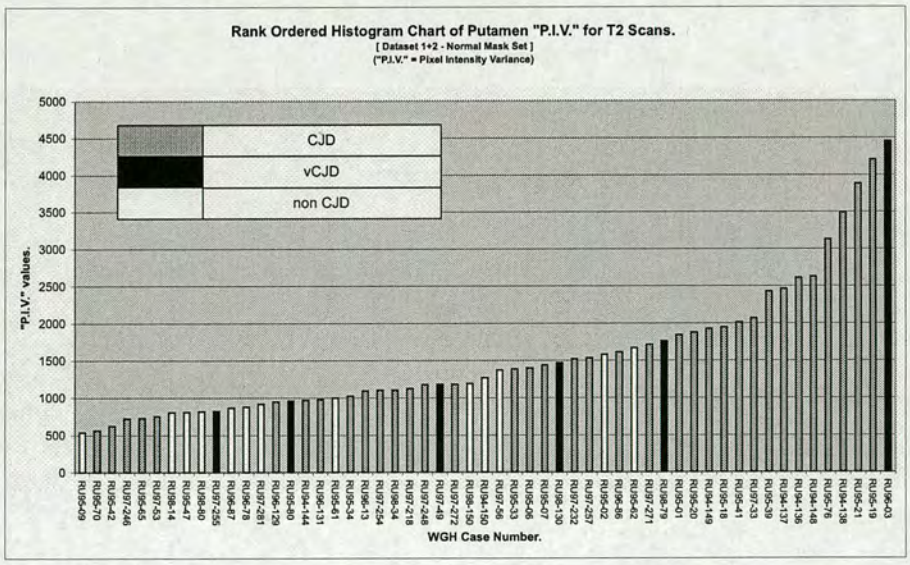

Figure 5.17: Bilateral Symmetry Tests: *Rank ordered histogram of the Putamen "P.I.V." for the T2 weighted MRI scan-data from the combined data-sets 1 & 2 generated using the normal (leftside+rightside) mask image-set.*

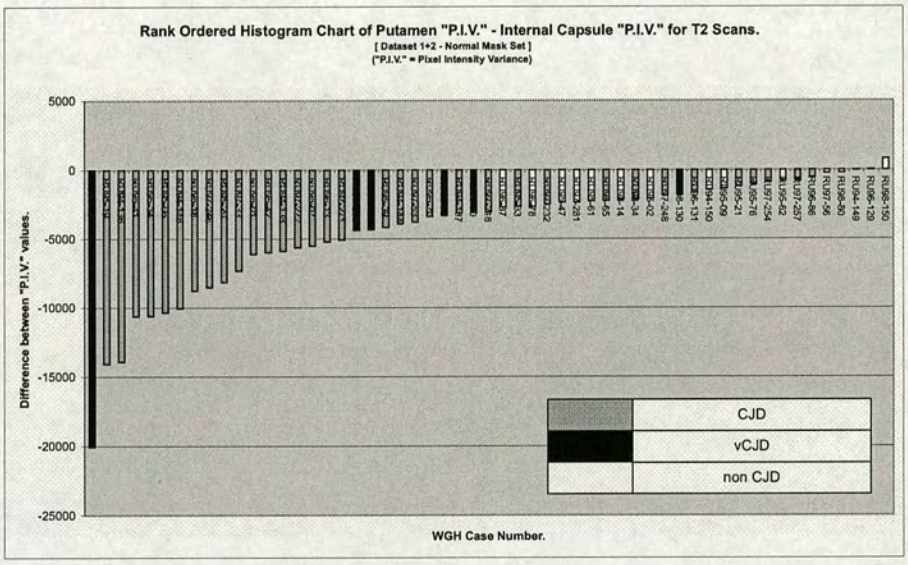

Figure 5.18: Bilateral Symmetry Tests: *Rank ordered histogram of the difference between the Putamen "P.I.V" and the Internal Capsule "P.I.V." for the T2 weighted MRI scan-data from the combined data-sets 1 & 2 generated using the normal (left-side+rightside) mask image-set.*

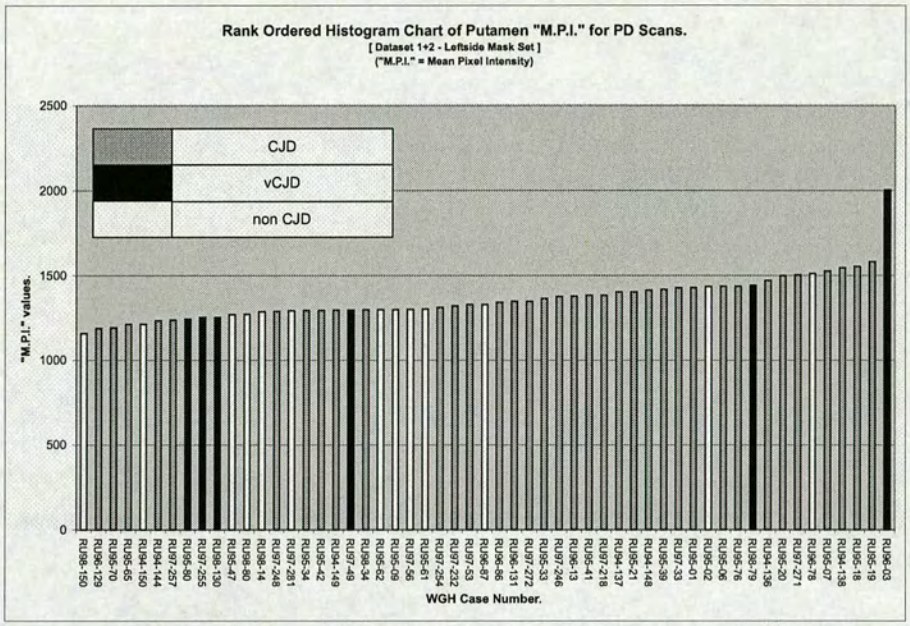

Figure 5.19: Bilateral Symmetry Tests: *Rank ordered histogram of the Putamen "M.P.I." for the PD weighted MRI scan-data from the combined data-sets 1 & 2 generated using the leftside mask image-set.*

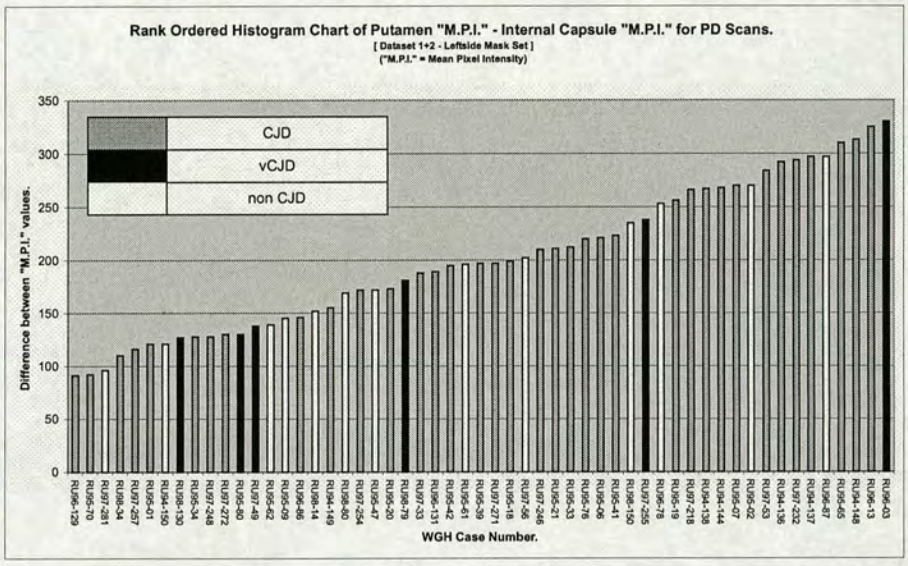

Figure 5.20: Bilateral Symmetry Tests: *Rank ordered histogram of the difference between the Putamen "M.P.I." and the Internal Capsule "M.P.I." for the PD weighted MRI scan-data from the combined data-sets 1 & 2 generated using the leftside mask image-set.*

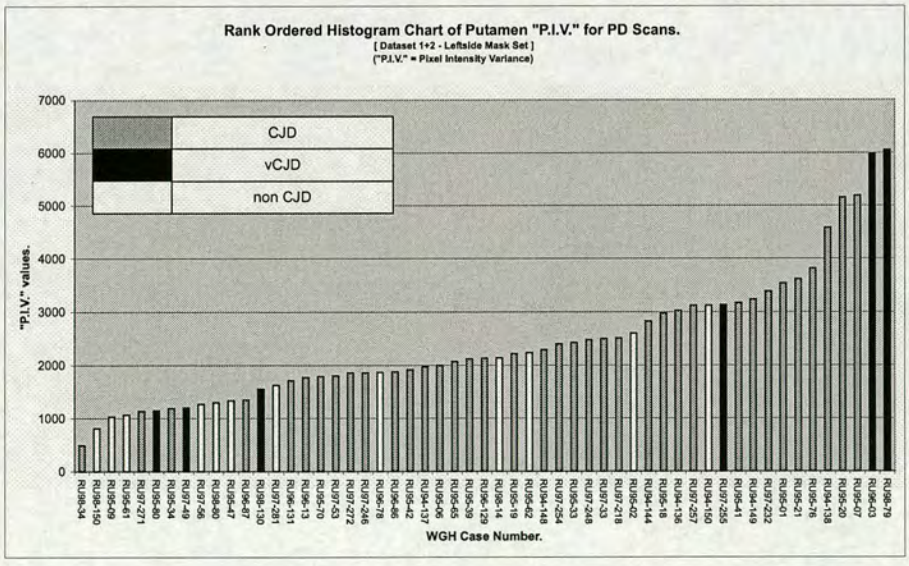

Figure 5.21: Bilateral Symmetry Tests: *Rank ordered histogram of the Putamen "P.I.V." for the PD weighted MRI scan-data from the combined data-sets 1 & 2 generated using the leftside mask image-set.*

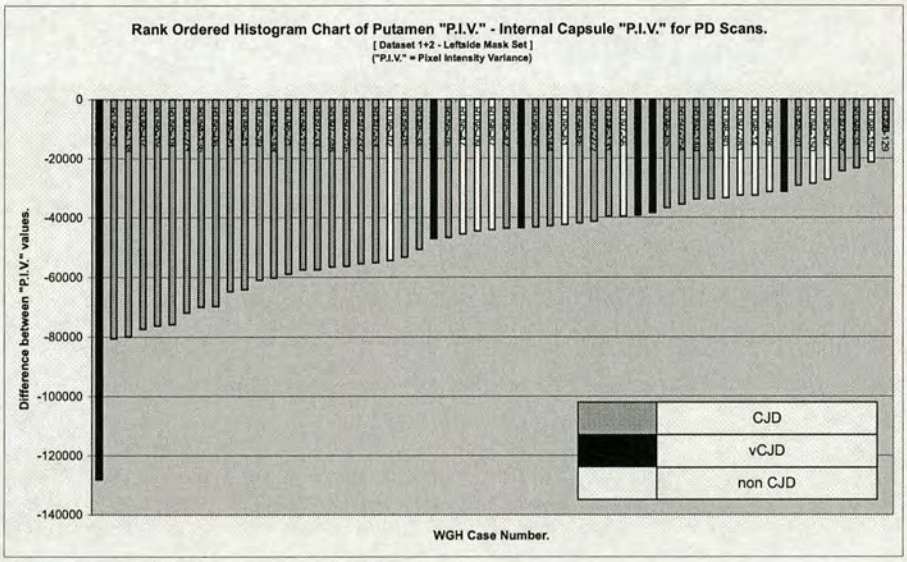

Figure 5.22: Bilateral Symmetry Tests: *Rank ordered histogram of the difference between the Putamen "P.I.V" and the Internal Capsule "P.I.V." for the PD weighted MRI scan-data from the combined data-sets 1 & 2 generated using the leftside mask image-set.*

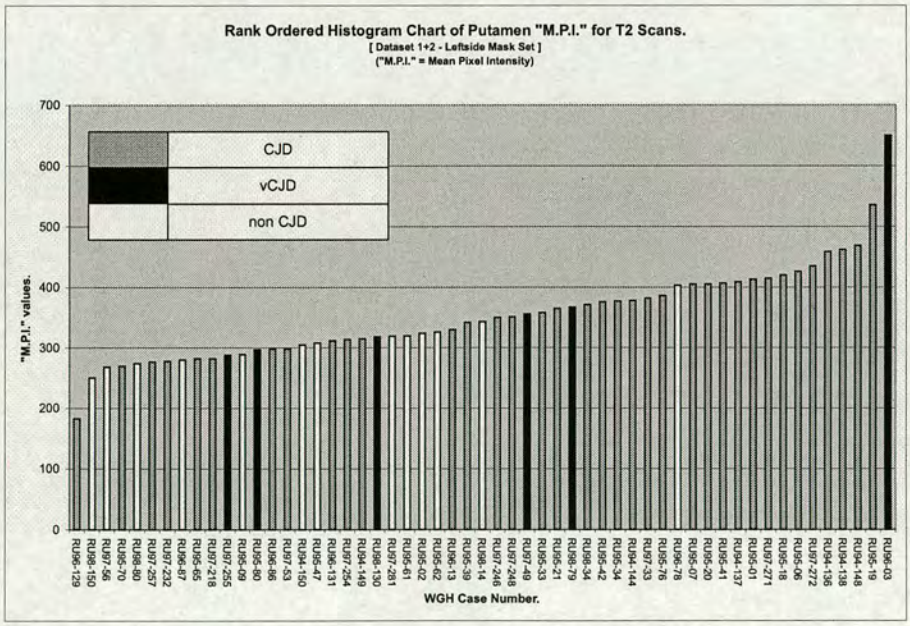

Figure 5.23: Bilateral Symmetry Tests: *Rank ordered histogram of the Putamen "M.P.I." for the T2 weighted MRI scan-data from the combined data-sets 1 & 2 generated using the leftside mask image-set.*

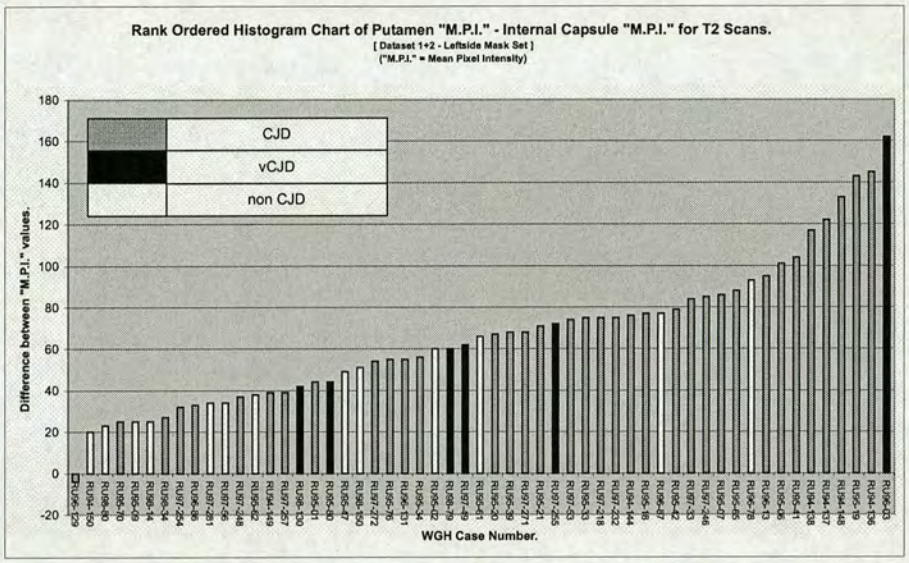

Figure 5.24: Bilateral Symmetry Tests: *Rank ordered histogram of the difference between the Putamen "M.P.I." and the Internal Capsule "M.P.I." for the T2 weighted MRI scan-data from the combined data-sets 1 & 2 generated using the leftside mask image-set.*

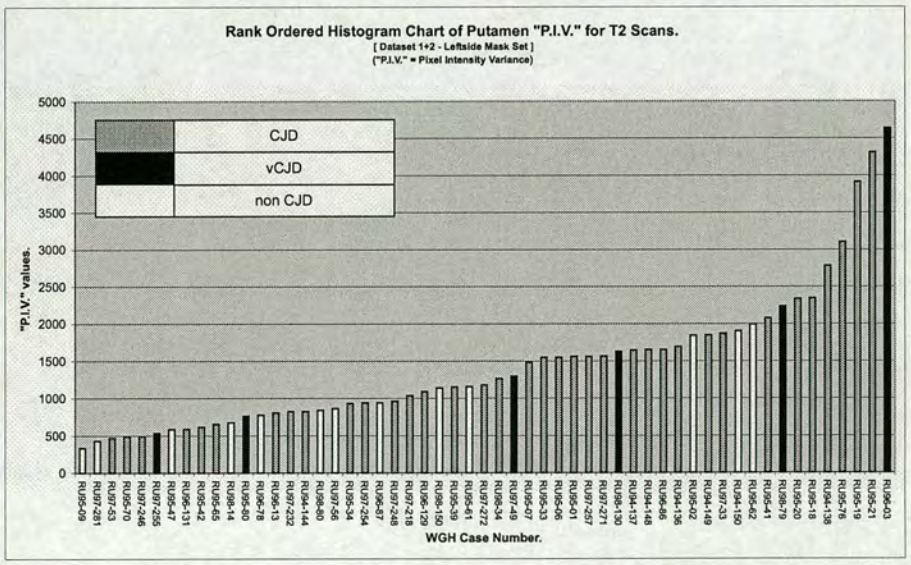

Figure 5.25: Bilateral Symmetry Tests: *Rank ordered histogram of the Putamen "P.I.V." for the T2 weighted MRI scan-data from the combined data-sets 1 & 2 generated using the leftside mask image-set.*

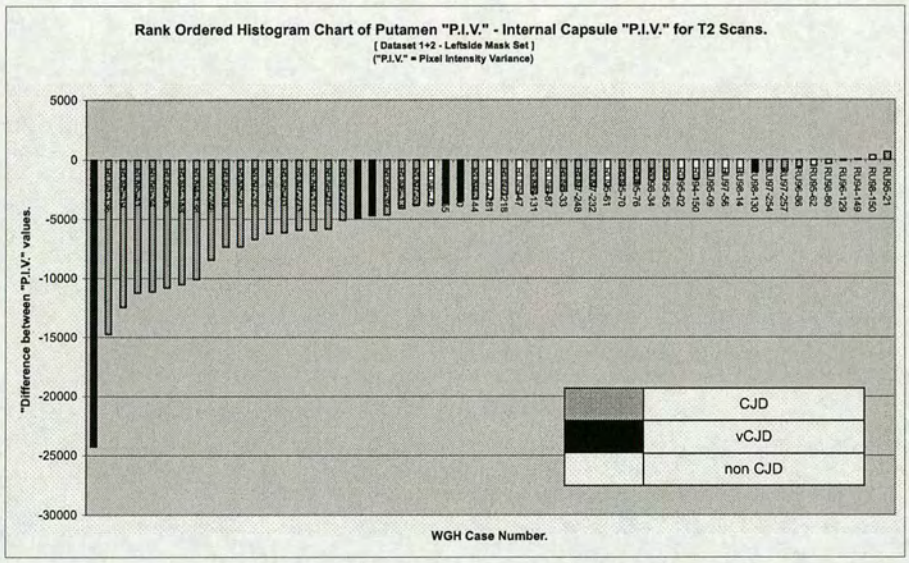

Figure 5.26: Bilateral Symmetry Tests: *Rank ordered histogram of the difference between the Putamen "P.I.V" and the Internal Capsule "P.I.V." for the T2 weighted MRI scan-data from the combined data-sets 1 & 2 generated using the leftside mask image-set.*

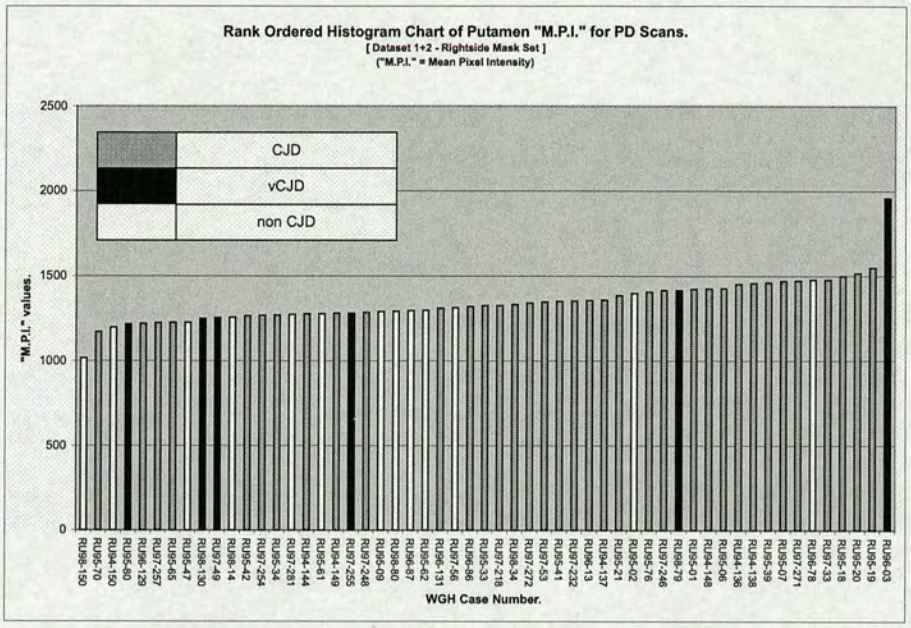

Figure 5.27: Bilateral Symmetry Tests: *Rank ordered histogram of the Putamen "M.P.I." for the PD weighted MRI scan-data from the combined data-sets 1 & 2 generated using the rightside mask image-set.*

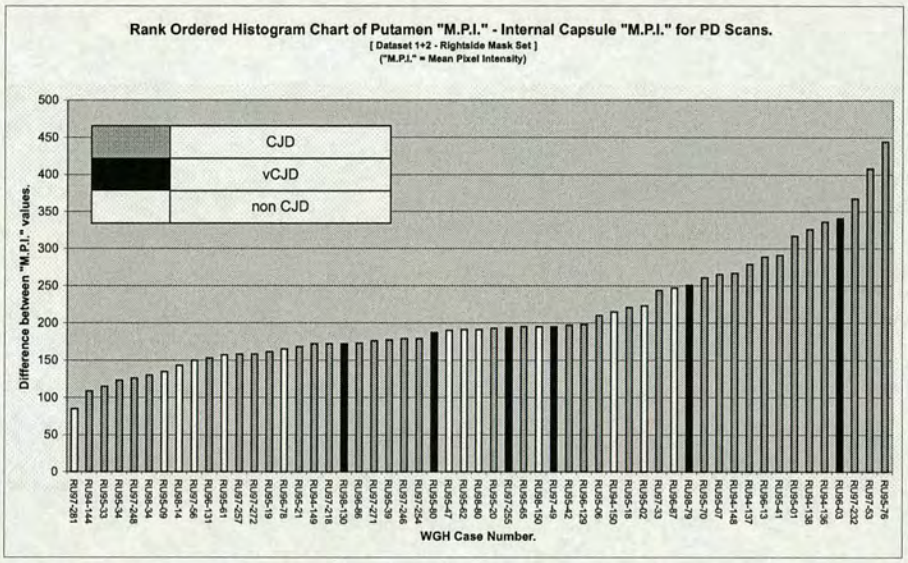

Figure 5.28: Bilateral Symmetry Tests: *Rank ordered histogram of the difference between the Putamen "M.P.I." and the Internal Capsule "M.P.I." for the PD weighted MRI scan-data from the combined data-sets 1 & 2 generated using the rightside mask image-set.*

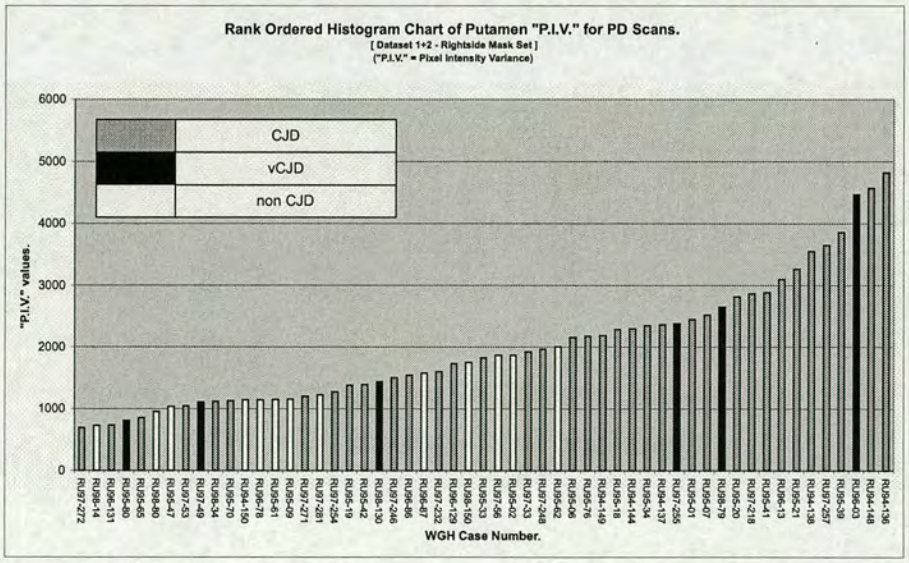

Figure 5.29: Bilateral Symmetry Tests: *Rank ordered histogram of the Putamen "P.I.V." for the PD weighted MRI scan-data from the combined data-sets 1 & 2 generated using the rightside mask image-set.*

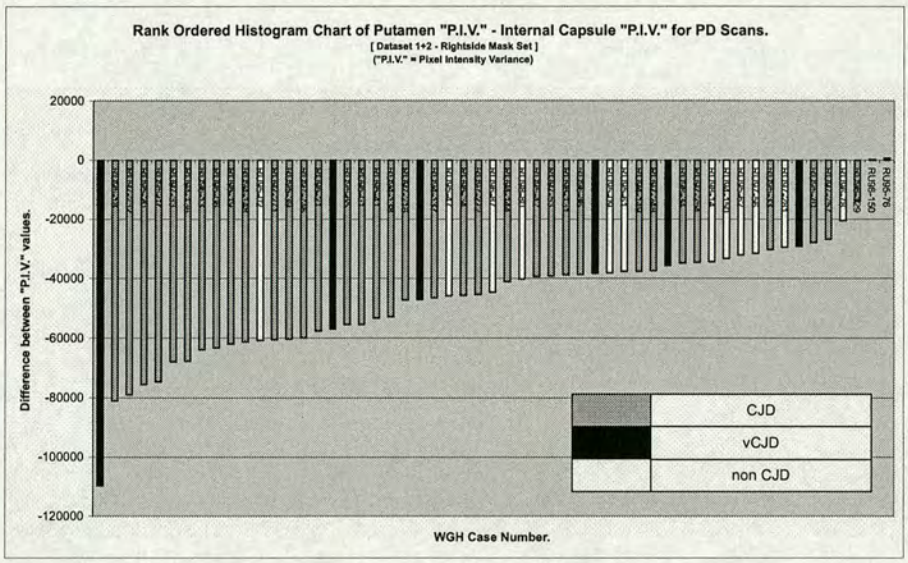

Figure 5.30: Bilateral Symmetry Tests: *Rank ordered histogram of the difference between the Putamen "P.I.V" and the Internal Capsule "P.I.V." for the PD weighted MRI scan-data from the combined data-sets 1 & 2 generated using the rightside mask image-set.*

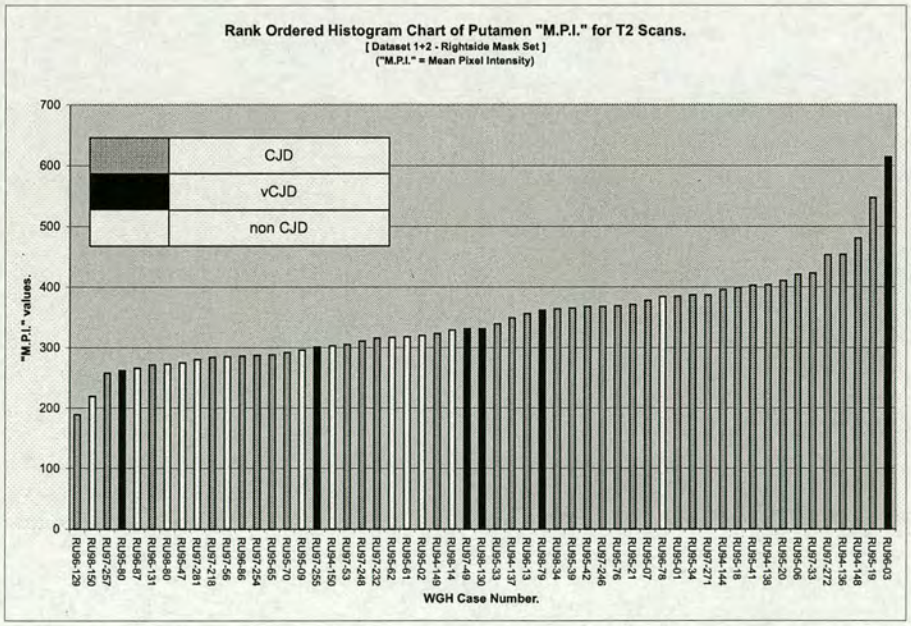

Figure 5.31: Bilateral Symmetry Tests: *Rank ordered histogram of the Putamen "M.P.I." for the T2 weighted MRI scan-data from the combined data-sets 1 & 2 generated using the rightside mask image-set.*

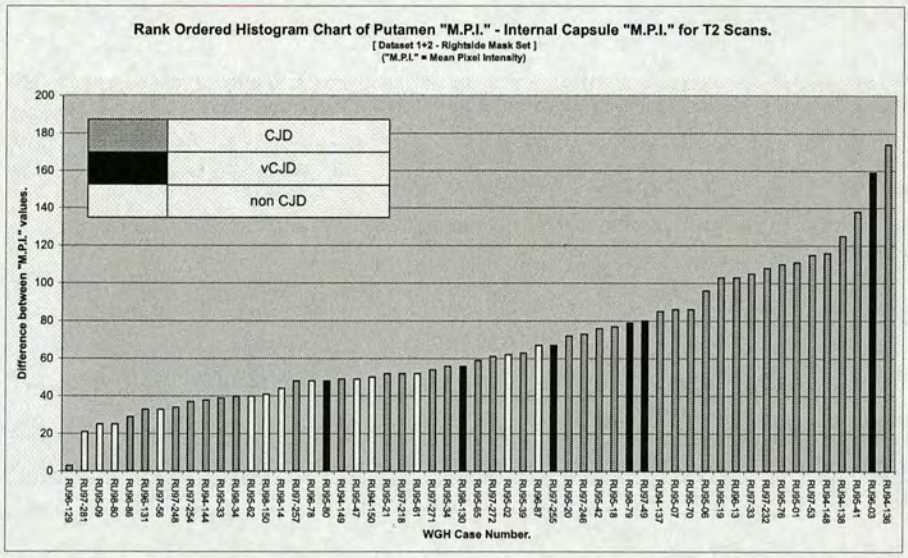

Figure 5.32: Bilateral Symmetry Tests: *Rank ordered histogram of the difference between the Putamen "M.P.I." and the Internal Capsule "M.P.I." for the T2 weighted MRI scan-data from the combined data-sets 1 & 2 generated using the rightside mask image-set.*

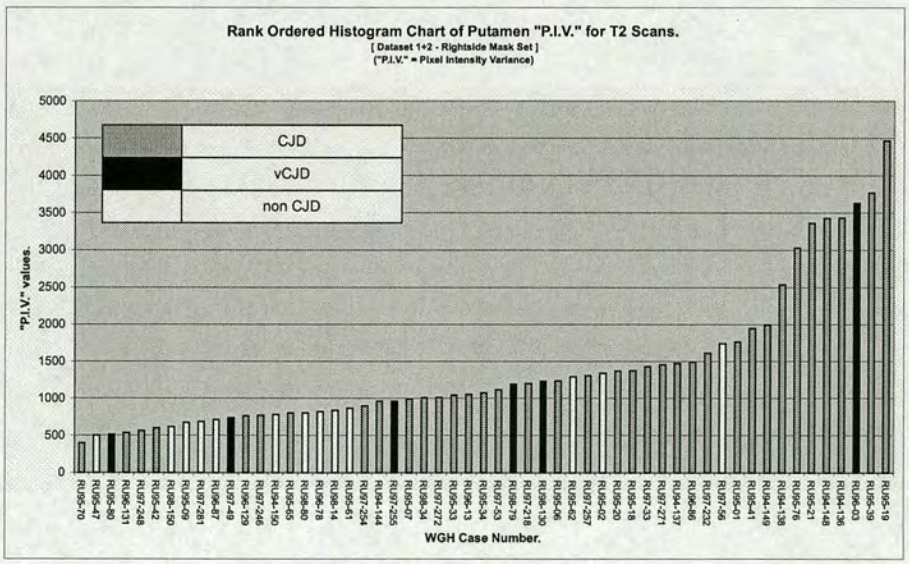

Figure 5.33: Bilateral Symmetry Tests: *Rank ordered histogram of the Putamen "P.I.V." for the T2 weighted MRI scan-data from the combined data-sets 1 & 2 generated using the rightside mask image-set.*

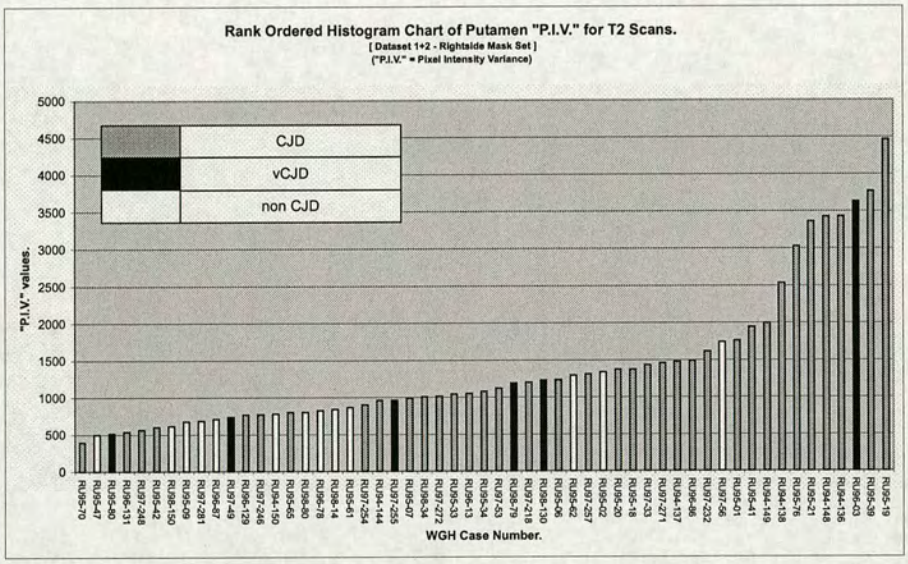

Figure 5.34: Bilateral Symmetry Tests: *Rank ordered histogram of the difference between the Putamen "P.I.V" and the Internal Capsule "P.I.V." for the T2 weighted MRI scan-data from the combined data-sets 1 & 2 generated using the rightside mask image-set.*

5.3.3 Analysis of Results of Bilateral Symmetry Tests

The χ^2 measure of statistical significance was calculated for each of the White Matter Changes tests and a determination was made of the significance or otherwise of the clustering of CJD and vCJD cases within the dataset.

These measures are listed for each test in tables 5.3, 5.4 and 5.5

Figure	Modality	Property	Test	χ^2 (3s.f)	Clustering Sig.
5.11	PD	Putamen M.P.I.	CJD	11.4	99%
5.11	PD	Putamen M.P.I.	vCJD	8.50	95%
5.12	PD	Putamen M.P.I. - I.C. M.P.I.	CJD	5.70	Not Significant
5.12	PD	Putamen M.P.I. - I.C. M.P.I.	vCJD	1.03	Not Significant
5.13	PD	Putamen P.I.V.	CJD	6.34	Not Significant
5.13	PD	Putamen P.I.V.	vCJD	0.586	Not Significant
5.14	PD	Putamen P.I.V. - I.C. P.I.V.	CJD	12.4	99%
5.14	PD	Putamen P.I.V. - I.C. P.I.V.	vCJD	2.61	Not Significant
5.15	T2	Putamen M.P.I.	CJD	9.75	95%
5.15	T2	Putamen M.P.I.	vCJD	1.03	Not Significant
5.16	T2	Putamen M.P.I. - I.C. M.P.I.	CJD	12.4	99%
5.16	T2	Putamen M.P.I. - I.C. M.P.I.	vCJD	4.20	Not Significant
5.17	T2	Putamen P.I.V.	CJD	14.9	99%
5.17	T2	Putamen P.I.V.	vCJD	0.590	Not Significant
5.18	T2	Putamen P.I.V. - I.C. P.I.V.	CJD	16.3	99%
5.18	T2	Putamen P.I.V. - I.C. P.I.V.	vCJD	2.61	Not Significant

Table 5.3: Bilateral Symmetry Tests: *Table of results after applying the χ^2 data analysis test to the histograms produced by processing the combined MRI dataset 1 & 2 with the normal (leftside+rightside) mask-set. A key to the column values is provided in Table 5.6 (This table is a repeat of Table 4.3*

5.3.4 Discussion of Results of Bilateral Symmetry Tests

Once again, as was shown in Chapter 4, considering the whole brain and using the Putamen ROI demonstrates consistent and reliable clustering of the CJD cases.

However, considering the leftside maskset and the rightside maskset results shows that when only one hemisphere is tested the clustering significances are reduced such that fewer tests produce statistically significant clustering. In only one case did a test show the statistical measure of significance increase when compared to the equivalent whole brain test. This therefore suggests that although the observation of statistically significant clustering may be more difficult

Figure	Modality	Property	Test	χ^2 (3s.f)	Clustering Sig.
5.19	PD	Putamen M.P.I.	CJD	6.10	Not Significant
5.19	PD	Putamen M.P.I.	vCJD	3.75	Not Significant
5.20	PD	Putamen M.P.I. - I.C. M.P.I.	CJD	2.29	Not Significant
5.20	PD	Putamen M.P.I. - I.C. M.P.I.	vCJD	2.61	Not Significant
5.21	PD	Putamen P.I.V.	CJD	7.11	Not Significant
5.21	PD	Putamen P.I.V.	vCJD	6.18	Not Significant
5.22	PD	Putamen P.I.V. - I.C. P.I.V.	CJD	8.47	95%
5.22	PD	Putamen P.I.V. - I.C. P.I.V.	vCJD	2.61	Not Significant
5.23	T2	Putamen M.P.I.	CJD	9.75	95%
5.23	T2	Putamen M.P.I.	vCJD	1.03	Not Significant
5.24	T2	Putamen M.P.I. - I.C. M.P.I.	CJD	9.51	95%
5.24	T2	Putamen M.P.I. - I.C. M.P.I.	vCJD	4.20	Not Significant
5.25	T2	Putamen P.I.V.	CJD	3.99	Not Significant
5.25	T2	Putamen P.I.V.	vCJD	2.17	Not Significant
5.26	T2	Putamen P.I.V. - I.C. P.I.V.	CJD	12.4	99%
5.26	T2	Putamen P.I.V. - I.C. P.I.V.	vCJD	7.36	Not Significant

Table 5.4: Bilateral Symmetry Tests: *Table of results after applying the χ^2 data analysis test to the histograms produced by processing the combined MRI dataset 1 & 2 with the leftside mask-set. A key to the column values is provided in Table 5.6*

when only one hemisphere of the brain is considered, the single hemisphere is still reporting the same overall trend and characteristic.

In addition, although certain tests were influenced more by one hemisphere than another, the demonstration of statistically significant clustering across a range of different tests suggests that the test suite itself is a more likely indicator than a single individual test when considered alone.

For the purposes of this study, a half brain scan should therefore contain similar characteristic indicators that the whole brain would have possessed and is therefore an acceptable substitute for a whole-brain scan where necessary.

5.4 Summary

In this chapter, two tests have been described and reported that were designed to look at ROIs that have not been widely investigated with regard to studies on MRI data and its relationship with CJD.

Figure	Modality	Property	Test	χ^2 (3s.f)	Clustering Sig.
5.27	PD	Putamen M.P.I.	CJD	11.5	99%
5.27	PD	Putamen M.P.I.	vCJD	3.75	95%
5.28	PD	Putamen M.P.I. - I.C. M.P.I.	CJD	6.34	Not Significant
5.28	PD	Putamen M.P.I. - I.C. M.P.I.	vCJD	2.17	Not Significant
5.29	PD	Putamen P.I.V.	CJD	7.27	Not Significant
5.29	PD	Putamen P.I.V.	vCJD	3.01	Not Significant
5.30	PD	Putamen P.I.V. - I.C. P.I.V.	CJD	7.61	Not Significant
5.30	PD	Putamen P.I.V. - I.C. P.I.V.	vCJD	0.586	Not Significant
5.31	T2	Putamen M.P.I.	CJD	14.0	99%
5.31	T2	Putamen M.P.I.	vCJD	2.61	Not Significant
5.32	T2	Putamen M.P.I. - I.C. M.P.I.	CJD	10.7	95%
5.32	T2	Putamen M.P.I. - I.C. M.P.I.	vCJD	7.36	Not Significant
5.33	T2	Putamen P.I.V.	CJD	6.33	Not Significant
5.33	T2	Putamen P.I.V.	vCJD	1.03	Not Significant
5.34	T2	Putamen P.I.V. - I.C. P.I.V.	CJD	12.4	99%
5.34	T2	Putamen P.I.V. - I.C. P.I.V.	vCJD	4.35	Not Significant

Table 5.5: Bilateral Symmetry Tests: *Table of results after applying the χ^2 data analysis test to the histograms produced by processing the combined MRI dataset 1 & 2 with the rightside mask-set. A key to the column values is provided in Table 5.6*

The first test examined an a-typical Region of Interest (ROI) called the Centrum Semiovale, located in the Cerebral cortex, and discovered that this region was both a potentially useful region for use in such tests and that it out-performed some of the more traditional ROIs which were the basis of the tests detailed in Chapter 4. Examination of this region with MRI may prove to be useful in cases where other neuro-degenerative disorders may be suspected due to a conflict in the clinical symptoms appreciated by an attending consultant.

The second test examined the potential differences that might exist between the left and right hemispheres of the brain with reference to the fact that many post-mortem brains available for MRI scanning are now only available as a half-organ due to other requirements for the organ within the medical community.

This test discovered that although minor variations between the two hemispheres can be detected within the results, the overall trends between single-hemisphere and dual-hemisphere tests concur and that although a dual-hemisphere test is preferable, a single-hemisphere test is acceptable in most cases.

The following chapter presents the conclusions of this study

Label	Description
Cent.S'vale.	Centrum Semiovale.
Clustering Sig.	Significance of Clustering.
PD	Proton Density Weighted M.R.I.
T2	T2 Weighted M.R.I.
I.C.	Internal Capsule.
M.P.I.	Mean Pixel Intensity
P.I.V.	Pixel Intensity Variance
ADJ.	Adjusted Dataset (Clearly erroneous points ommitted.)
CJD	Creutzfeld-Jakob disease.
vCJD	Variant Creutzfeld-Jakob disease.

Table 5.6: Key Table: *Table providing a key to the data-labels used in the results tables that appear earlier on in this chapter.*

Chapter 6
Conclusions

6.1 Introduction

The study presented here sought to investigate the potential use of post-mortem MRI scan data in the task of identifying and classifying medical patients whose clinical presentation suggested CJD. A body of published work already exists for in-vivo data but the findings reported in the field are hampered by lack of sufficient data, problems with interpreting in-vivo data which often suffers from artifacts related to the surrounding tissues of the body, the motion of the patient and the motions of their bloodflow through the brain. No studies are currently available which detail findings on post-mortem MRI examined through analysis of the electronic data.

The difficulties of identifying patients with the disease was described in Chapter 2 and the process by which the post-mortem data used in this study was generated, collected, prepared and processed is fully explained and illustrated in Chapter 3.

Three main Regions Of Interest (ROIs) within the brain were selected based upon the published findings investigating in-vivo data. These ROIs were then subjected to a series of tests to investigate whether or not the reported findings for the in-vivo data might translate to the post-mortem data. These tests are fully described, reported, analysed and discussed in Chapter 4.

Additional tests to further investigate the properties of the MRI dataset were described, reported, analysed and discussed in Chapter 5.

6.2 The findings of this thesis

From the work carried out here, a successful method of manual segmentation of post-mortem electronic MRI scan data has been used to allow the intensity characteristics that relate most to

those used by clinical radiologists to be examined statistically. From these analyses, it has been shown that the Putamen region of the brain is a reliable and consistent indicator of condition for Creutzfeld-Jakob disease with many tests reporting a statistical significance level of 99% with respect to the clustering of cases of CJD within the gross population of a given dataset.

The Thalamus and Posterior Thalamus regions have not demonstrated such reliability or consistency in their ability to predict the condition of CJD and therefore are not supported or recommended by the work done here for consideration when conducting similar tests to those used here.

The inclusion and consideration of a contrast region of a neighbouring white-matter structure, in this case a section of the Inner Capsule, was shown to be of benefit to the classification process in most tests where it was available and its use in future tests would be recommended.

The differentiation of CJD from other similar disorders is also an issue and it was demonstrated that additional ROIs may yield helpful results toward achieving this goal. In this case, a region called the Centrum Semiovale which represents the white-matter tissues of the Cerebral cortex was found to be both a better region for indicating CJD than both the Thalamus and Posterior Thalamus, themselves considered to be often indicative by in-vivo studies, and also potentially able to help differentiate CJD from other disorders which may present with a similar set of clinical symptoms.

The differences between the characteristic responses from the left and right hemispheres of the brain were investigated jointly and separately to allow a determination to be made as to the validity of results that are produced when only a single hemisphere of the brain has been made available for scanning. It was found that the single-hemisphere scans are similarly demonstrative of the same properties in a given test thus allowing their results to be considered alongside those of dual-hemisphere scans and although dual-hemisphere scans are almost always preferable, single-hemisphere scans are equally acceptable where necessary.

6.3 Contribution

This work has demonstrated novel results by applying standard methods of image analysis to electronic copies of post-mortem MRI data of the Human brain with a view to determining the potential for such data to be used, in the future, as an indicator for the condition.

This is the first such study of post-mortem MRI data and the findings here that the MRI data can identify clustering of CJD cases within a population of data that includes non-CJD cases to a statistically significant level will be of use to other researchers in this field that are seeking by alternative means to find other indicators for this disorder. Furthermore, the identification of additional ROIs within the brain that may also provide indicator potential will be valuable to any future work.

The tests to assess the bilateral symmetry of the brain's response to CJD to ensure that the tests conducted on half-organs are comparable to those conducted on whole-organs should be useful to anyone that has concerns now that the trend of supplying only a half-organ for scanning is becoming an increasingly common occurance.

In addition, due to the hazards involved in dealing with infected CJD tissues such mechanisms of using MRI for diagnostic purposes may be preferable routes for diagnosis in the future due to the manner in which a scan can be performed.

6.4 Future Work

The nature of a Human brain is that it is, in-vivo, encased in a skull and that it contains a high proportion of water and is constantly fed by a supply of oxygen-rich blood. Post-mortem brains are removed from the skull cavity introducing deformations and are then fixed in a formalin solution to preserve the tissues. This process may characteristically alter the response the brain then gives in an MRI scanner and therefore the results from analysing a series of post-mortem brain MRI scans may not translate to the same findings as the results of performing the same scans on in-vivo brains. Therefore, the natural extension and continuation of this work would be to perform similar tests and analyses on data from in-vivo scans to see if this might lead to the possibility of in-vivo diagnosis.

In addition, further ROIs within the brain might be worthy of investigation based upon the success reported here with the Centrum Semiovale. It may transpire that this form of analysis provides a more subtle level of detection than the current clincial practice of visually inspecting hard-copy data on a lightbox.

Another avenue of investigation which time did not allow to be pursued here but which may offer a means of improving the diagnostic ability of the post-mortem MRI for cases of CJD is combinatorial statistical analysis. Each of the tests conducted in this work were considered separately and their results were analysed separately. However, it may be possible to increase the overall effectiveness of the individual tests by combining them together to produce a new metric which takes into consideration multiple properties, in this case; the effects on the Putamen, Thalamus, Posterior Thalamus and potentially the effects on the Centrum Semiovale as well. This may then offer a test with improved sensitivity, reliability and perhaps even the potential for the cross-over to in-vivo data.

6.5 Summary

The possibility of using post-mortem MRI data to identify CJD cases has been demonstrated and the promise of future developments of this work has outlined the potential of extending the novel results reported here towards a method of finding an in-vivo diagnostic aid for the condition of CJD. Bilaterally symmetric responses of the brain to CJD have been shown to reassure those that only have access to half-brain scan data that these mechanisms may be applied equally in both cases.

References

[1] W. P. of the National Health Advisory Committee of the National Health and M. R. C. (Australia), "Creutzfeldt-jakob disease and other human transmissible spongiform encephalopathies." WWW Publication: http://www.nhmrc.health.gov.au/publicat/pdf/ic5.pdf, August 1996.

[2] H. G. Creutzfeld, "Über eine eigenartige herdformige erkrankung des zentrainervensystems," *Z ges Neurol Psychiat*, no. 5, pp. 1–18, 1920.

[3] A. Jakob, "Über eigenartige erkrankungen des zentrainervensystems mit bermerkenswertem anatomichen befunde (spastiche pseudosklerose-encephalomyelopathie mit disseminierten degenerations-herden," *Z ges Neurol Psychiat*, no. 64, pp. 147–228, 1921.

[4] N. I. of Neurological Disorders and Stroke, "Fact sheet: Creutzfeldt-jakob disease." WWW Publication: http://www.nhmrc.health.gov.au/publicat/pdf/ic5.pdf, June 2000.

[5] A. M. Gajdusek DC, Gibbs CJ, "Experimental transmission of a kuru-like syndrome to chimpanzees.," *Nature*, no. 209, pp. 794–796, 1966.

[6] M. L. Maneuldis EE, "Experiments on maternal transmission of Creutzfeldt-Jakob disease in guinea pigs.," in *Proc Soc Exp Biol Med*, 1979.

[7] R. G. Will, J. W. Ironside, S. Cousens, K. Esteberio, A. Alperovitch, S. Poser, M. Pocchiari, A. Hofman, and P. G. Smith, "A new variant of Creutzfeldt-Jakob disease in the UK," *Lancet*, no. 347, pp. 921–925, 1996.

[8] J. W. Ironside and J. E. Bell, "Florid plaques and new variant Creutzfeldt-Jakob disease," *Lancet*, vol. 350, p. 1475, 1997.

[9] M. E. Bruce, R. G. Will, J. W. Ironside, I. McConnell, D. Drummond, A. Suttie, L. McCardle, A. Chree, J. Hope, and C. Birkett et al, "Transmissions to mice may indicate that 'new variant' CJD is caused by the BSE agent.," *Nature*, vol. 389, pp. 498–501, 1997.

[10] L. J. M. van Keulen, B. E. C. Schreuder, R. H. Meloen, G. Mooij-Harkes, M. E. W. Vromans, and J. P. M. Langeveld, "Immunohistochemical detection of prion protein in lymphoid tissues of sheep with natural scrapie.," *J Clin Microbiol*, vol. 34, pp. 1228–1231, 1996.

[11] J. M. G. Santos, J. A. L. Corbalán, J. F. Martínez-Lage, and J. S. Guillen, "CT and MRI in iatrogenic and sporadic creutzfeld-jakob disease: as far as imaging perceives," *Neuroradiology*, vol. 38, pp. 226–231, 1996.

[12] O. S. A Uchino, M Yoshinaga and M. Ohno, "Serial MR imaging in Creutzfeldt-Jakob disease," *Neuroradiology*, vol. 33, pp. 364–367, 1991.

[13] S. Falcone, R. M. Quencer, B. Bowen, J. H. Bruce, and T. P. Naidich, "Creutzfeldt-Jakob disease: Focal symmetrical cortical involvement demonstrated by MR imaging.," *American Journal of Roentgenology*, vol. 13, pp. 403–406, 1991.

[14] W. G. Bradley and G. Bydder, *MRI Atlas of the Brain*, ch. 1, pp. 1–6. 154 Camden High Street, London. NW1 0NE. United Kingdom: Martin Dunitz, 1st ed., 1990.

[15] M. Fisher MD, C. H. Sotok Ph.D., K. Minematsu MD, and L. Li Ph.D., "New magnetic resonance techniques for evaluating cerebrovascular disease.," *Ann Neurol*, vol. 32, pp. 115–122, 1992.

[16] M. Onofrj, T. Fulgente, D. Gambi, and G. Macchi, "Early MRI findings in Creutzfeldt-Jakob disease," *Neurology*, vol. 240, pp. 423–426, 1993.

[17] H.-J. Gertz, H. Henkes MD, and J. Cervos-Navarro MD, "Creutzfeldt-Jakob disease : Correlation of MRI and neuropathologic findings.," *Neurology*, vol. 38, no. 1481-1482, 1988.

[18] G. S. Pearl MD Ph.D. and R. E. Anderson MD, "Creutzfeldt-Jakob disease: High caudate signal on magnetic resonance imaging.," *Southern Medical Journal*, vol. 82, pp. 1177–1180, 1989.

[19] J. Roether, A. Schwartz, M. Haerle, K. Ulrich Wentz, P. Berlit, and M. Hennerici, "Magnetic resonance imaging follow-up in Creutzfeldt-Jakob disease.," *Journal of Neurology*, vol. 239, pp. 404–406, 1992.

[20] D. P. Barboriak, J. M. Provenzale, and O. B. Boyko, "MR diagnosis of Creutzfeldt-Jakob disease: Significance of high signal intensity of the basal ganglia," *AJR*, vol. 162, pp. 137–140, 1994.

[21] A. Di Rocco, S. Molinari, A. L. Stollman, and M. D. Yahr, "MRI abnormalities in Creutzfeldt-Jakob disease," *Neuroradiology*, vol. 35, pp. 584–585, 1993.

[22] M. Michael Gold, P. Amyn Rojiani, MD, and M. Reed Murtaugh, "A 66-year-old woman with a rapidly progressing dementia and basal ganglia involvement.," *J Neuroimaging*, vol. 7, pp. 171–175, July 1997.

[23] S. S. Yoon MD, S. Chan MD, S. Chin MD, K. Lee MD, and R. R. Goodman MD PhD, "MRI of Creutzfeldt-Jakob disease: Asymmetric high signal intensity of the basal ganglia.," *Neurology*, vol. 45, pp. 1932–1933, 1995.

[24] H.-H. Liou, H.-c. Chiu, and H.-M. Liu, "Abnormal enhancement of the left putamen on brain MRI in a case of proven Creutzfeldt-Jakob disease.," *European Neurology*, vol. 36, pp. 107–108, 1996.

[25] Y. Iwasaki, K. Ikeda, N. Tagaya, and M. Kinoshita, "Magnetic resonance imaging and neuropathological findings in two patients with Creutzfeldt-Jakob disease.," *Journal of Neurological Sciences*, vol. 126, pp. 228–231, 1994.

[26] W.-C. Shyu, C.-C. Lee, Y.-D. Hsu, J.-C. Lin, J.-T. Lee, W.-H. Lee, and W.-L. Tsao, "Panencephalitic Creutzfeldt-Jakob disease: Unusual presentation of mangentic resonance imaging and proton magnetic resonance spectroscopy.," *Journal of Neurological Sciences*, vol. 138, pp. 157–160, 1996.

[27] M. Finkenstaedt MD, A. Szudra MD, I. Zerr MD, S. Poser MD, J. H. Hise MD, J. M. Stoebner MD, and T. Weber MD, "MR Imaging of Creutzfeldt-Jakob disease," *Radiology*, vol. 199, pp. 793–798, 1996.

[28] P. Sahoo, S. Soltani, A. Wong, and Y. Chen, "Survey of thresholding techniques," *Computer Vision, Graphics and Image Processing*, vol. 41, no. 2, pp. 233–260, 1988.

[29] A. Kundu and S. Mitra, "A new algorithm for image edge extraction using a statistical classifier approach," *IEEE Trans. Patt. Anal. and Machine Intelligence*, vol. 9, no. 4, pp. 569–577, 1987.

[30] E. Hancock and J. Kittler, "Edge-labeling using dictionary based relaxation," *IEEE Trans. Patt. Anal. and Machine Intelligence*, vol. 12, no. 2, pp. 165–181, 1990.

[31] Haralick and Shapiro, "Image segmentation techniques.," *Computer Vision, Graphics and Image Processing*, vol. 29, pp. 100–132, 1985.

[32] L. Clarke, R. Velthuizen, M. Camacho, J. Heine, M. Vaidyanathan, L. Hall, R. Thatcher, and M. Silbiger, "MRI segmentation: methods and applications," *Magn. Reson. Imag.*, vol. 13, no. 3, pp. 343–368, 1995.

[33] M. Atkins and B. Mackiewich, "Fully automatic segmentation of the brain in MRI," *IEEE Trans. Med. Imaging*, vol. 17, no. 1, pp. 98–107, 1998.

[34] M. Puvaneswary, D. Floate, and C. Harper, "Creutzfeldt-Jakob disease: Magnetic resonance imaging findings.," *Australasian Radiology*, vol. 43, pp. 91–94, 1999.

[35] R. Haralick, K. Shanmugam, and I. Dinstein, "Textural features for image classification," *IEEE Trans. on Systems, Man and Cybernetics*, vol. 3, pp. 610–621, 1973.

[36] M. Galloway, "Texture analysis using gray-level run lengths," *Computer Graphics and Image Processing*, vol. 4, pp. 172–179, 1975.

[37] J. Keller, S. Chen, and R. Crownover, "Texture description and segmentation through fractal geometry," *Computer Vision, Graphics and Image Processing*, vol. 45, no. 2, pp. 150–166, 1989.

[38] H. Peitgen and D. Saupe, *The Science of Fractal Images*. New York: Springer Verlag, 1988.

[39] A. Penn and M. Loew, "Estimating fractal dimension of medical images with fractal interpolation function models," *Internal Publication, The George Washington University, Washington, DC 20052*, 1990.

[40] G. Matheron, *Random sets and integral geometry.* New York (USA): Wiley, 1975.

[41] J. Serra, *Image Analysis and Mathematical Morphology*. London (UK): Academic Press, 1982.

[42] Giardina and Dougherty, *Morphological Methods in Image and Signal Processing*. Englewood Cliffs, NJ (USA): Prentice-Hall, 1988.

[43] E. Kreyszig, *Advanced Engineering Mathematics*, ch. 24.10, pp. 1255–1257. New York (USA): John Wileys & Sons, Inc, 7th ed., 1993.

Appendix A
Bespoke Project Software

The attached CD-ROM contains the collection of bespoke software that was developed for this project.

- **Commontools.pm** - Common toolkit of library functions. (Screen display, interaction and system routines.)
- **Data_manipulation.pm** - Library of data manipulation functions. (Data extraction, sorting, basic histogramming and format conversion.)
- **Fileops.pm** - File read and write (import/export) filter library.
- **Pnm_toolbox.pm** - Library of functions for handling PNM (Portable Anymap) image data. (Read/Write Ascii/Raw, Single band to triple band conversion.)
- **Statistics.pm** - Library of basic statistical functions. (Mean, Variance, Standard variation.)
- **analyse_info.pl** - Reads ANALYZE header file and reports the information contained within.
- **analyse2ppm.pl** - Converts and ANALYZE format image database file into a sequence of PPM images.
- **rename_city2wgh.pl** - Renames a data-file produced by the City Hospital to conform with the naming standard used in the Western General Hospital.
- **unarchive.pl** - Unpacks a tape-archived dataset into the component ANALYZE format files.
- **bp_hwm.pl** - Batch processes a sequence of images, creating histograms based upon applying simple mask images to the MRI scans.

- **bp_hwm_contrast.pl** - Batch processes a sequence of images, creating histograms based upon applying contrast mask images to the MRI scans.
- **hwm.pl** - Performs the actual histogramming operation required by bp_hwm.pl.
- **hwm_contrast.pl** - Performs the actual histogramming operation required by bp_hwm_contrast.pl.

A number of other related files are also included on the CD-ROM including automation scripts for the Paint Shop Pro packages used and a number of programs similar to those described above but with minor variations that are fully described in the program's in-line comments.